ABSTRACT

LIN, ZHAN. Platinum and Platinum Alloy-Carbon Nanofiber Composites for Use as Electrodes in Direct Methanol Fuel Cells. (Under the direction of Professors Xiangwu Zhang and Wendy E. Krause.)

In response to the energy needs of modern society and emerging ecological concerns, the pursuit of novel, low-cost, and environmentally friendly energy conversion and storage systems has raised significant interest. Among various energy conversion and storage systems, fuel cells have become a primary research focus since they convert chemical energy directly into electrical energy with high efficiency and low pollutant emissions. For example, direct methanol fuel cells (DMFCs), which supply the electrical energy by converting methanol to energy, are an ideal fuel cell system for applications in electric vehicles and electronic portable devices due to their relatively quick start-up, rapid response to catalyst loading, and low operating temperature. However, the wide commercial use of DMFCs in advanced hybrid electric vehicles and electronic portable devices is hampered by their high cost, poor durability, and relatively low energy and power densities. In order to address these problems, their research focuses on the development of highly active electrode catalysts coupled with a suitable electrode structure for the oxidation of methanol at the anode and the reduction of oxygen at the cathode to attain high efficiency of DMFCs, and subsequently lowering the cost. In this dissertation, the fabrication of novel platinum and platinum alloy nanoparticle-loaded carbon nanofibers (CNFs) for use as electrodes in DMFCs is demonstrated through electrospinning, carbonization, and deposition. The resulting CNF-based electrodes possess the properties of high electroactive surface area, good catalytic

abilities towards the oxidation of methanol and the reduction of oxygen, and great long-time stability. As a result, DMFCs using these CNFs-supported platinum and platinum alloy nanoparticles as electrodes offer many advantages, such as improved electrocatalytic abilities, long-term stability, easy fabrication, low cost, and environmental benignity. Therefore, this new technology opens up new opportunities to develop high-performance electrode materials in the future for high-performance DMFCs, which are one of the promising power sources for consumer devices and electric vehicles, and play a critical role in solving the worldwide critical energy issue.

Platinum and Platinum Alloy-Carbon Nanofiber Composites for Use as Electrodes in Direct Methanol Fuel Cells

by
Zhan Lin

A dissertation or thesis submitted to the Graduate Faculty of
North Carolina State University
in partial fulfillment of the
requirements for the Degree of
Doctor of Philosophy

Fiber and Polymer Science

Raleigh, North Carolina

March 31, 2010

APPROVED BY:

_____	_____
Prof. Xiangwu Zhang Chair of Advisory Committee	Prof. Wendy E. Krause Co-Chair of Advisory Committee
_____	_____
Prof. Saad A. Khan	Prof. Samuel M. Hudson

DEDICATION

To

my respected parents,

Fa Lin and Yun Lin,

who made all of this possible,

for feeding, teaching, and supporting me.

And also to

my two elder sisters,

Xiangming Lin and Xiangling Lin,

for their advice and help.

Thank you for the love from my family,

I really appreciate all that you have done.

BIOGRAPHY

Zhan Lin was born in Fuqing City, Fujian, P. R. China. He completed his middle school and high school education in Fuqing No.1 Middel School, and then attended Hefei University of Technology in September 1999, and graduated with a batchelor's degree in Polymer Science and Engineering in July 2003. After that, he went to University of Science and Technology of China as a graduate student majoring in Applied Chemistry and obtained his Master Degree in July 2006. After graduation, he obtained a researcher scientist position in Functional Membrane Lab in Hefei, where he did one year of research on the fabrication and design of functional polymer materials.

In July 2007, Zhan Lin came to the U.S. and started working toward his Ph.D. degree majoring in Fiber and Polymer Science in the Department of Textile Engineering, Chemistry and Science at North Carolina State University. His research activities ranged from the preparation and characterization of nanostructured carbon or carbon-composite materials and their application in energy conversion and storage systems, to the fabrication and functionlization of polymer or polymer composite materials for specific utilization.

In addition to his research, Zhan Lin also has many hobbies in his spare time, such as working out, swimming, travelling, and hiking.

ACKNOWLEDGMENTS

The author would like to offer his sincerest appreciation to respected advisors: Professors Xiangwu Zhang and Wendy E. Krause, for supervising, supporting, and helping him grow during his Ph.D. studies; to his other committee members: Professors Saad A. Khan and Samuel M. Hudson, for their wise counsel, advice, and support; and also to the Graduate School representative Professor Orlin D. Velev, for his encouragement and communication.

The author also acknowledges funding supports from the National Textile Center, U.S. National Science Foundation, and ACS Petroleum Research Fund.

Moreover, the author would like to thank Mr. Liwen Ji, Mr. Quan Shi, Mr. Bingkun Guo, Mr. Christopher Bonino, Mr. Yingfang Yao, Mr. Ozan Toprakci, Mr. Narendiran Vitchuli, Mr. Guanjie Xu, Mr. Mataz Alcoutlabi, Mr. Andrew J. Medford, Ms. Mariah D. Woodroof, Ms. Kyung-Hye Jung, Ms. Bohyung Kim, Ms. Shuli Li, Ms. Yinzheng Liang, Ms. Shu Zhang, Ms. Ying Li, Ms. Samantha Shintay, Ms. Jinmei Du, and Ms. Lu Liu at North Carolina State University for their earnest cooperation and warmhearted help during his Ph.D. study.

The author also deeply appreciates Mr. Chuck Mooney and Mr. Roberto Garcia in Analytical Instrumentation Facility, Mr. Dzung Nguyen and Ms. Birgit Andersen in the College of Textiles at North Carolina State University, and Dr. Mark D. Walters in the Shared Materials Instrumentation Facility at Duke University for their help in sample characterization.

TABLE OF CONTENTS

LIST OF TABLES

LIST OF FIGURES

ABBREVIATIONS

DMFCs	Direct methanol fuel cells
Pt	Platinum
Ru	Ruthenium
Pd	Palladium
CNFs	Carbon nanofibers
CNTs	Carbon nanotubes
MWCNT	Multi-walled carbon nanotubes
SWCNT	Single-walled carbon nanotube
PAN	Polyacrylonitrile
PMMA	Poly(methyl methacrylate)
PVP	Poly (vinyl pyrrolidone)
PEO	Poly (ethylene oxide)
PVC	Polyvinylchloride
PI	Polyimide
PE	Polyethylene
PS	Polystyrene
PVA	Polyvinyl alcohol
PVB	Polyvinylbutyral
PC	Propylene carbonate
PBI	Polybenzimidazole

SBS	Stryrene-butadiene-styrene
DMF	N,N-dimethylformamide
THF	Tetrahydrofuran
LIBs	Lithium-ion batteries
CV	Cyclic voltammogram
SHE	Standard hygroden electrode
MEA	Membrane electrode assembly
GDL	Gas diffusion layer
MOR	Methanol oxidation reaction
ORR	Oxygen reduction reaction
1D	One-dimensional
2D	Two-dimensional
3D	Three-dimensional
Co	Cobalt
Fe	Iron
Ni	Nickle
Cr	Chromium
Os	Osmium
Sn	Tin
Cu	Copper
Rh	Rhodium
HNO_3	Nitric acid

H_2SO_4	Sulfuric acid
EG	Ethylene glycol
HCHO	Methanal
H_2PtCl_6	Chloroplatinic acid
$RuCl_3$	Ruthenium chloride
$(NH_4)_2PdCl_6$	Ammonium hexachloropalladate
1-AP	1-aminopyrene
$K_4[Fe(CN)_6$	Potassium hexacyanoferrate (II)
CH_3OH	Methanol
$HClO_4$	Perchloric acid
ATR-FTIR	Attenuated total reflection fourier transform infrared
XRD	X-ray diffraction
FESEM	Field emission scanning electron microscopy
TEM	Transmission electron microscopy
EDS	Energy dispersive X-ray spectroscopy
EASA	Electrochemically active surface area
KCl	Potassium chloride
Sodium borohydride	$NaBH_4$
1-AP-CNFs	1-aminopyrene functionalized CNFs
AO-CNFs	Acid-treated CNFs
UT-CNFs	Un-treated CNFs

CHAPTER 1. INTRODUCTION

1.1. Overview of electrospinning

1.1.1. Introduction of electrospining

One-dimensional (1D) nanostructrues with a variety of forms, such as nanotubes, nanowires, nanobelts, and nanofibers, have attracted much attention in recent years because of their

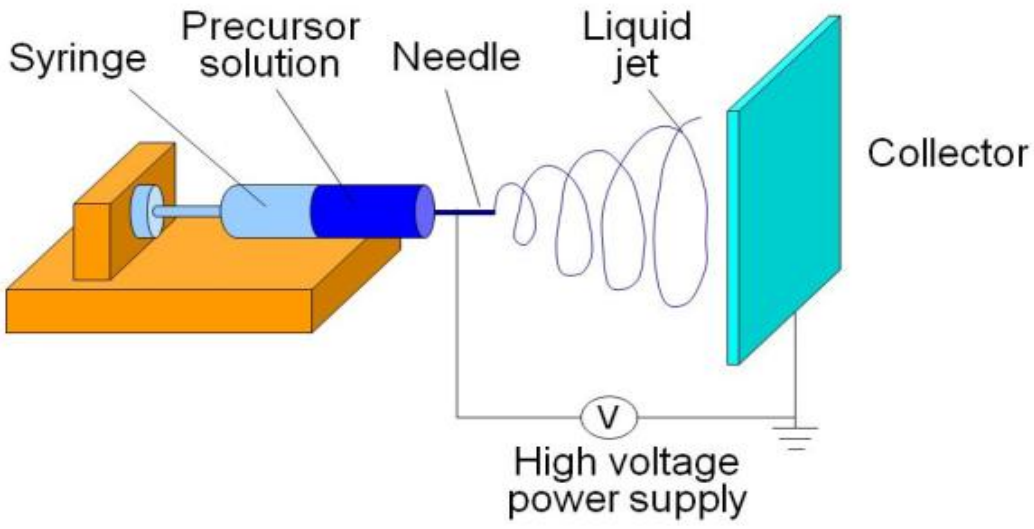

Figure 1.1. Schematic illustration of a typical setup for the electrospinning.

novel structures, interesting properties, and fascinating potential applications in many areas.[1-3] Among various 1D nanostructures, nanofibers, with diameters ranging from tens of nanometers to several micrometers, have been a subject of intensive research for various applications, such as composite systems, thin filters, and biomedical applications.[4-7] Many methods have been developed to fabricate nanofibers, such as templating,[8, 9] self-assembly,[10, 11] phase separation,[12] and electrospinning.[13-16] Among them, electrospinning, which produces continuous nanofibers through the action of an external electric field imposed on a solution or melt, has been considered as a simple and effective method to produce nanofibers.

Figure 1.1 shows the schematic illustration of a typical setup of electrospinning equipment. Generally, the electrospinning equipment consists of three components: a high-voltage power supply, a spinneret, and a collector. Direct current power supply is typically used in the electrospinning, though the use of alternating current power supply is also possible.[17, 18] The spinneret was connected to a syringe filled with polymer solution or melt, which was pushed by a syringe pump. Under the external high voltage, a pendent droplet of polymer solution or melt at the nozzle of the spinneret became highly electrified, and the induced charges on the surface made the droplet deformed into a Taylor cone. When the applied electric field overcomes the surface tension of the droplet, a charged stream of polymer solution or melt was ejected. The stream grows longer and thinner because of bending instabilities or splitting until it was deposited on the collector in the form of nanofibers. A typical diameter of electrospun nanofibers is ranging from tens of nanometers to a few

micrometers,[17, 19] as shown in Figure 1.2.

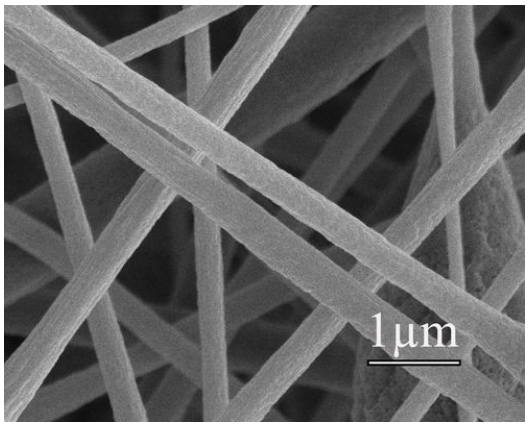

Figure 1.2. SEM image of typical electrospun nanofibers.

The origin of electrospinning can be traced back to the early 1930s, when Formhals patented his first invention relating to an apparatus for producing artificial filaments using electric charges.[20, 21] However, it was difficult to completely dry the fibers after spinning because of the short distance between the spinning and collection zones, and a less aggregated web structure. In the 1960s, fundamental studies on the jet forming process were initiated by Taylor, who studied the shape of the polymer droplet produced at the tip of the needle when an electric field is applied.[22] The shape is a cone and the jets are ejected from the vertices of the cone, which was referred as the "Taylor Cone." In the 1970s, Baumgarten reported the electrospinning of acrylic fibers with nanoscale diameters.[23] However, at that time, the focus of this technology was shifted to studying the structural morphology of nanofibers, this technology has not received much more academic attention after a decade. In the 1990s, a

major upsurge in research on the electrospinning took place due to increased knowledge on the potential applications of nanofibers in various areas, such as high efficiency filter media, catalyst substrates, protective clothing, and adsorbent materials.[21]

1.1.2. Types of nanofibers

The electrospinning has demonstrated the fabrication of a broad range of thin fibers, such as polymer nanofibers, composite nanofibers, and ceramic nanofibers, which have charming applications in various fields due to their unique features and properties, such as high surface area, complex porous structure, and extremely long fiber length.[3, 16, 24, 25] The scope of possibilities presented by electrospinning encompasses a multitude of new and interesting concepts, which are developed at breakneck speed. The following subsections show several types of electrospun nanofibers reflected by the skyrocketing numbers of scientific publications and patents.

1.1.2.1. Polymer nanofibers

Research activities on the electrospinning of polymer nanofibers have been conducted with different polymeric solutions and melts. Polymers with attractive chemical, mechanical, and

Table 1.1. Electrospun Polymers and Corresponding Literature.[21]

No	Polymer	Solvent	Comments
1	Polyethylene oxide	Water/chloroform	Jaeger *et al.* studied the morphological characteristics of electrospun polymeric fibers in the diameter range of 200–800 nm.[26]
2	Polyethylene terephthalate	Mixture of dichloromethane and trifluoroacetic acid.	Reneker and Chun demonstrated the spinning of polyethylene terephthalate fibers of 300 nm in diameter with cylindrical structures.[19]
3	Polyaniline/PEO blends	Chloroform	Norris *et al.* produced fine fibers with desired conductivity by using Polyaniline/PEO polymeric blends. The fiber diameters were in the range of 950 nm to 2.1 μm.[27]
4	Polystyrene	Tetrahydrofuran (THF)	MacDiarmid *et al.* have electrospun polystyrene using THF as a solvent to produce nanofibers with a minimum diameter of 16 nm and an average diameter of 30.5 nm.[28]
5	Polybenzimidazole (PBI)	N,N-Dimethyl Acetamide	Kim and Reneker electrospun aromatic heterocyclic PBI polymer by electrospinning and produced birefringent fibers of approximately 300 nm in diameter.[29]
6	Nylon 6 and Nylon 6-montmorillonite (NLS)	1,1,1,3,3,3-hexa fluoro-2-Propanol (HFIP) and DMF	Fong *et al.* experimented with the spinning of NLS with HFIP and DMF and observed cylindrical fibers along with some ribbon shaped fibers with thickness of 100–200 nm and width of 10 μm.[30]

Table 1.1. *Continued*

No	Polymer	Solvent	Comments
7	Polyvinyl chloride	THF, DMF	Lee *et al.* studied the effect of volume ratio of mixed solvents on the structure and morphology of electrospun fibers.[31]
8	Polyurethane	DMF	Demir *et al.* prepared polyurethane urea copolymer solution in DMF and observed that the average fiber diameter (AFD) increases with the solution concentration.[32]
9	Polycaprolactone	Acetone	Reneker *et al.* studied the onset of the bending instability during spinning and observed the formation of a closed single and double loop fiber structure called "Garland".[33]
10	Styrene-Butadiene-Styrene (SBS) triblock copolymer	75% THF and 25% DMF	Fong and Reneker examined the morphology of fibers with respect to micro phase separation and experimented with annealing for accelerating the ordering process and stress relaxation.[34]
11	Poly-L-Lactide	Dichloromethane	Zeng Jun *et al.* electrospun PLA fibers and observed the cylindrical morphology of fibers with diameters ranging from 800 nm-2400 nm.[35]

electrical properties like high conductivity, high chemical resistance, and high tensile strength have been spun into ultrafine fibers by the electrospinning process and their potential applications in many areas like drug delivery, membrane filtration, optical fibers,

tissue scaffolds, sensors, and energy storage have been examined.[36-39] Some types of the polymers, including synthetic and biodegradable polymer, are summarized in Table 1.1 for a quick and cursory review according to their corresponding literature.

1.1.2.2. Composite nanofibers

Composite nanofibers, consisted of nanoscale polymer matrix and inorganic fillers, can combine both the advantages of the polymer materials such as light weight, excellent flexibility, and good moldability, and of inorganic materials such as high strength, good heat stability, and high chemical resistance.[25, 38] As a result, these composite nanofibers have improved the mechanical, electrical, optical, thermal, and magnetic properties of materials, and hence they can be excellent candidates for multi-functional applications that include tissue engineering, biomedical devices, semiconductor nanowire synthesis, membrane filtration, and energy conversion and storage systems.[3, 39]

In tissue engineering, the biomedical role of nanofibers has extended into various specific applications. For example, biodegradable polymers can be directly electrospun onto an injured location of skin to form a fibrous mat dressing. The further introduction of composite materials into the electrospun mats can amplify their functionality by strategic incorporation of specific species. For example, Fujihara *et al.,* synthesized a new type of guided bone regeneration membranes by electrospinning polycaprolactone (PCL) and PCL/$CaCO_3$

composite nanofibers.[40] They concluded that membranes rich in PCL had better cell attachment and proliferation than those of $CaCO_3$ rich membranes. Another example is that, synthetic polymer/DNA composite scaffolds for therapeutic application in gene delivery were electrospun from poly(lactide-co-glycolide) (PLGA) and poly(D,L-lactide)-poly(ethylene glycol) (PLA-PEG).[41] Variations in the PLGA to PLA-PEG ratio were observed to vastly affect the overall structural morphology, rate and efficiency of DNA release from 68 to 80% of the initially loading. The synthetic tensile moduli and strain resemble those of skin and cartilage.

Semiconductor nanowire is the next category of electrospun composites, which has also expanded possible applications for nanofibers. For example, 1D metal oxides have been extensively researched due to their improved electro-optical, electro-chromic, ferroelectric, catalytic, and gas sensing properties. The first report of electrospinning metal oxide composite fibers was made by Dai *et al.,* in 2002.[42] Alumina borate solution, which was mixed with polyvinyl alcohol (PVA) to form a viscous gel, was electrospun. Composite nanofibers were calcinated above 1000 ^{o}C to form pure $Al_4B_2O_9$, $Al_{18}B_4O_{33}$, and stable phase of α-Al_2O_3. Titanium dioxide (TiO_2) was the next metal oxide electrospun into composite nanofibers by Li et al. in 2003.[43] Titania sol-gel was directly added to an alcohol solution containing polyvinylpyrrolidone (PVP) and electrospun to form composite nanofibers. Pure metal oxide nanofibers were achieved by a heat treatment at 500 ^{o}C in air for 3 hours. Moreover, many other metal oxides, such as MoO_3/WO_3,[44] Co_3O_4,[45] and SiO_2,[46] have also been reported on the preparation of composite nanofibers through electrospinning.

Moreover, composite nanofibers have also been widely used in other topics of nanofiber research, such as membrane filtration application and structural-strengthening composite synthesis. For example, Hsu et al. reported that composite nanofibers have an advantage of being electrostatically charged to modify the ability of electrostatic attraction of particles without increasing pressure drop to further improve filtration efficiency.[47] In order to prepare composite nanofibers with desirable mechanical and electrical properties, carbon nanotubes (CNT) and other materials are arguably the most fascinating materials to be dispersed in a nanofiber matrix to form composite materials. The electrospinning process was used by Ayutsede et al. to prepare CNT-reinforced spider silk.[48] With strengths approaching 4GPa and a strain-to-failure exceeding 35%, spider silk has been recognized as a model of a strong, tough fiber. Single wall carbon nanotubes (SWCNTs) were successfully dispersed in transgenic spider silk with various combinations of silk proteins to form spinning dope for electrospinning. The mechanical properties of the SWNT-reinforced fibers show an increase in Young's modulus up to 460% in comparison with the un-reinforced aligned fiber with only 0.5-5 wt% of SWNT in a silk matrix. Moreover, Reneker *et al.,* observed for the first time that the orientation of the CNTs within the nanofibers was much higher than that of the PAN polymer crystal matrix.[49] This suggests that not only surface tension and jet elongation but also slow relaxation of the CNTs in the nanofibers is a determining factor in the orientation of CNTs.

1.1.2.3. Carbon nanofibers

To date, many polymers have been electrospun to form ultrafine fibers as precursors for carbon nanofibers (CNFs), including polyethylene oxide, nylon, polyethylene glycol, polyethylene terephthalate, and polyacrylonitrile.[26, 27, 50, 51] Among these polymers, polyacrylonitrile (PAN) is a relatively tough, insoluble, and high-melting temperature polymer with good resistance to aging, chemicals, water, and cleaning solvents, which make it widely used in many applications such as engineering plastics, ultrafiltration membranes, and sensors.[52-56] Most importantly, PAN becomes an excellent precursor for producing carbon fibers because of its high dielectric constant and high carbon yield, and the resultant carbon fibers are suitable for a wide range of applications ranging from lithium ion batteries, fuel cells, to biological/chemical sensors.[57-60] Thererfore, compared with other polymer carbon precursors, such as pitch and rayon, PAN-based fibers are the most suitable precursors for producing high-performance carbon fibers.

1.1.2.3.1. Electrospun CNFs based on PAN precusor

CNFs can be produced by thermally treating electrospun PAN nanofibers. The process of converting PAN nanofibers to CNFs is typically achieved by chemically modifying its structure through two heat treatment steps, the oxidation of PAN at 250-300 ^{o}C in air environment and subsequent carbonization at 600-1300^{o}C in inert atmosphere (Figure 1.3).

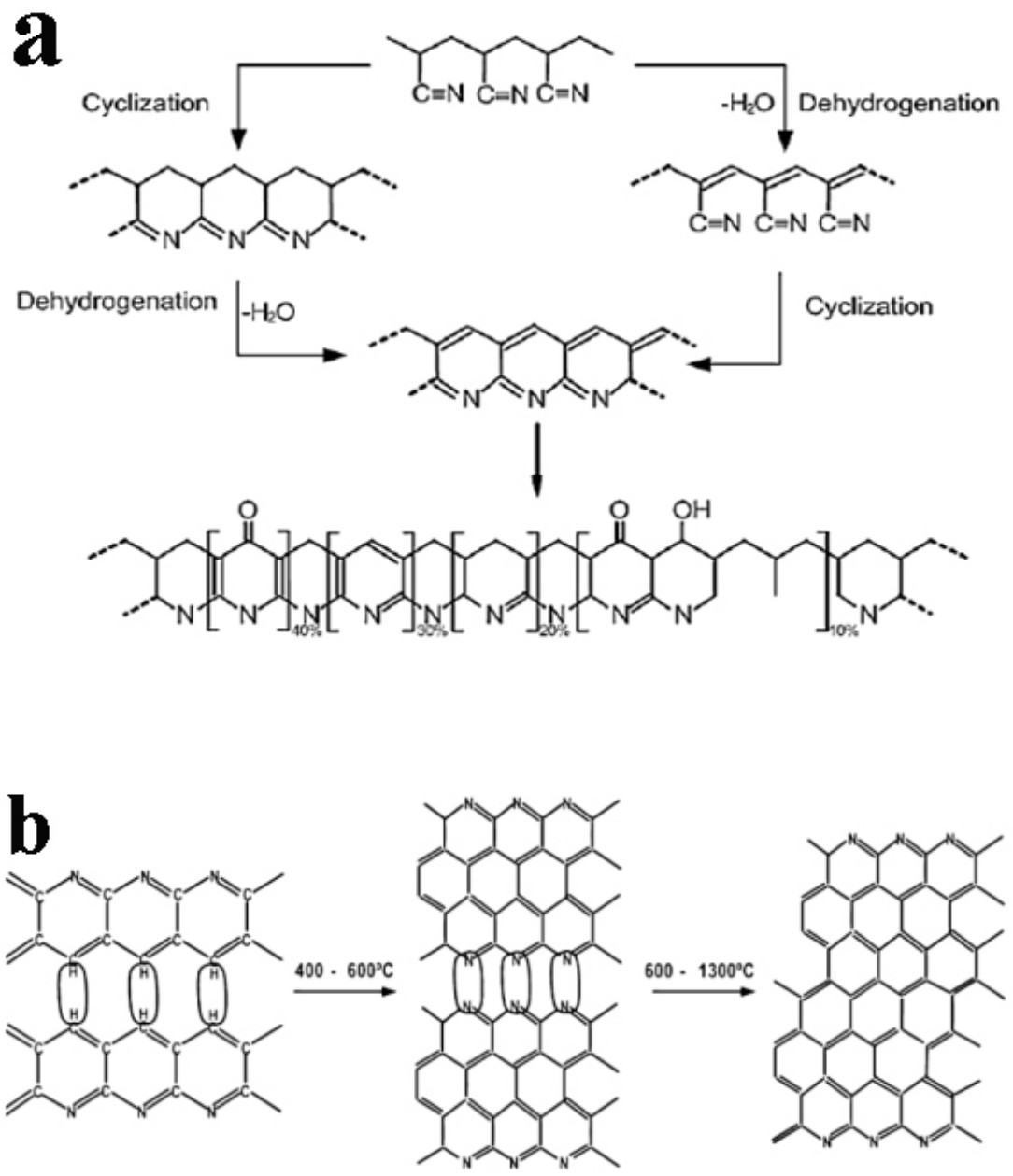

Figure 1.3. Schematic illustration of the oxidation of PAN nanofibers at 250-300 ^{o}C in air environment (a), and the subsequent carbonization at 600-1300 ^{o}C in inert atmosphere (b).

As shown in Figure 1.3a, PAN becomes a crosslinked structure through dehydrogenation and cyclization reactions, and the resultant fibers are called as oxidized PAN nanofibers.[54] The oxidized PAN nanofibers are then heat treated in an inert atmosphere, such as nitrogen or argon, at 600-1300 ^{o}C (Figure 1.3b). During this process, the non-carbon elements are removed in the forms of methane, hydrogen, hydrogen cyanide, water, carbon dioxide, and ammonia etc.,[54] which result in the formation of CNFs. The resultant CNFs have higher density, reduced diameter, and 40-50 % of their original weight compared to the original PAN nanofibers.[61, 62] The CNFs can be directly used in this state, or can undergo additional heat treatments up to 3000 ^{o}C to yield graphitic structures.[63]

1.1.2.3.2. The applications of CNFs

CNFs have been used in various areas, such as reinforced composites, biosensor, and rechargeable lithium-ion batteries (LIBs), due to their special physical and chemical properties (*e.g.,* high conductivity, large surface area, inherent and induced chemical functionalities, and good biocompatibility).

In the case of CNF-reinforced composites, Tandon et al. enhanced the thermomechanical properties of conventional aerospace materials IM7 by making carbon nanofiber-reinforced composites (IM7/CNFs) using the filament winding technique.[64] Finegan et al. improved the strength and stiffness of polypropylene (PP) by incorporating CNFs in a PP matrix.[65]

Prolongo et al. synthesized epoxy/CNF composites with different proportions of CNFs functionalized with amino group.[66] It was found that the CNF dispersion is enhanced with the functionalization process up to nanofibers contents of 1 wt%, and the addition of CNFs causes increases in the coefficient of thermal expansion and the glassy storage modulus of composites.

Potentially, CNF-based biosensors have extensive applications, *e.g.,* glucose and hydrogen peroxide biosensors. Wu et al. reported a CNF-based amperometric glucose sensor with excellent catalytic activity of soluble CNFs, which was obtained with a simple nitric-acid treatment and with electro-reduction of dissolved oxygen at a low operating potential.[67] Li et al. studied the effect of CNF microstructure on the electrochemical sensing of hydrogen peroxide.[68] Three types of CNFs, *e.g.,* platelet-like CNFs (PCNFs), fish-bone-like CNFs (FCNFs), and tube-shaped CNFs (TCNFs), were investigated, and the results revealed significant diversity of electrocatalytic activity of these CNFs toward the oxidation of hydrogen peroxide, which could have resulted from differences of the CNFs in morphology, texture, and crystalline structure.

To increase energy and power densities as well as other electrochemical performance of rechargeable lithium-ion batteries (LIBs), novel carbon nanomaterials as CNFs, have been considered as promising candidates for anode materials in rechargeable LIBs.[69-71] For example, Kim et al. reported the fabrication of electrospun CNFs, which have a capacity of 450 mAh g^{-1},[72] however, this capacity is still relatively low. Many approaches to improve

the electrochemical performance of CNFs have been used to incorporate them with higher-capacity anode materials. For examples, Fan et al. reported an ordered, nanostructured SnO_2/carbon composite, which displayed better cycling performance than that of nanosized counterparts without carbon matrix.[73] These hybrid materials delivered an initial charge capacity of 1347 mAh g^{-1} and a subsequent capacity of more than 500 mAh g^{-1}. Wu et al. electrochemically synthesized manganese oxide electrodes composed of interconnected nanowires from manganese acetate solution at room temperature without any template and catalyst.[74, 75] The reversible capacity of such materials is about 600 mAh g^{-1} after annealing at 100 °C, and the electrodes' reversible capacity reaches 800 mAh g^{-1}after annealing at 300 °C, which remains nearly constant even after 100 cycles.

In addition to the applications mentioned above, CNF-based materials are playing an increasingly important role in many other fields, *e.g.,* catalysis, electrical and optical systems, fuel cells, solar cells, and supercapacitors.[39, 76, 77]

1.2. Overview of DMFCs

1.2.1. The history of fuel cells

The concept of fuel cell has existed for more than a hundred years and has attracted more and

more attention in recent decades due to high-energy demands, fossil fuel depletions, and environmental pollution throughout the world. The first fuel cell was reported in 1838 by William Robert Grove, who discovered that when arranging two platinum electrodes with one end of each immersed in a container of sulfuric acid and the other ends separately sealed in containers of oxygen and hydrogen, a constant current would flow between the electrodes. Then he combined several of these cells in a series circuit and called it a "gas battery".[78] In the 1880s, designs for workable gas batteries began to emerge from laboratories in Europe and the US. In 1889, Mond and Carl Langer described their experiments with a fuel cell using coal-derived 'Mond-gas' and attained 6.45 mA cm^{-2} at 0.73 V *vs.* SHE.[79] However, the poisons caused by the impurities of hydrogen and the high cost of Pt catalyst made the fuel cell impractical. It should be noted that these challenges are still faced by the present fuel cell industry. Despite these challenges, there were still many researchers worked on the possibility of converting coal or coal gas directly into electricity by use of the 'gas battery'. It wasn't until 1933 that direct coal fuel cells were principally abandoned in favor of alkali electrolyte fuel cells, also named "Bacon Cell" now. In 1939, Bacon built a cell that used nickel gauze electrodes and operated it under pressure as high as 3000 psi, and in 1958 he also demonstrated an alkali fuel cell in a stack of 10-inch diameter electrodes using alkali electrolytes, which was settling on potassium hydroxide instead of using acid electrolytes.[80, 81] Though expensive, Bacon's fuel cell proved reliable enough to attract the attention of the U.S. space program of National Aeronautics and Space Administration (NASA) in the 1960s. The space program gave fuel cells a kick-off development and successfully used them in supplying energy for space vehicles. Currently, researchers, who are developing various fuel

cells for automobiles, buses, and cell phone towers etc., are expecting to see that fuel cells could play a practical and realistic role in the generators of power for all manner of electrical devices in a clean, quiet and petroleum-free way.[82, 83]

1.2.2. Types of Fuel Cells

Table 1.2. Different fuel cells that have been realized and are currently in use or development.[84]

	AFC	PEMFC	DMFC	PAFC	MCFC	SOFC
Operating temp.[85]	**<100**	**60-120**	**60-120**	**160-220**	**600-800**	**800-1000**
Anode reaction	**$H_2+2OH^-\rightarrow 2H_2O+2e^-$**	**$H_2\rightarrow 2H^++2e^-$**	**$CH_3OH+H_2O\rightarrow CO_2+6H^++6e^-$**	**$H_2\rightarrow 2H^++2e^-$**	**$H_2+CO_3^{2-}\rightarrow H_2O+CO_2+2e^-$**	**$H_2+O^{2-}\rightarrow H_2O+2e^-$**
Cathode reaction	**$1/2O_2+H_2O+2e^-\rightarrow 2OH^-$**	**$1/2O_2+H^++2e^-\rightarrow H_2O$**	**$3/2O_2+6H^+ + 6e^-\rightarrow 3H_2O$**	**$1/2O_2+2H^++2e^-\rightarrow H_2O$**	**$1/2O_2+CO_2+2e^-\rightarrow CO_3^{2-}$**	**$1/2O_2+2e^-\rightarrow O^{2-}$**
Applications	**Transportation Space Military Energy storage systems**			**Combined heat and power for decentralized stationary power systems**	**Combined heat and power for stationary decentralized systems for transportation**	
Realized Power	**Small plants 5-150kW**	**Small plants 5-250kW**	**Small plants 5kW**	**Small-medium plants 50kW-11MW**	**Small plants 100kW-2MW**	**Small plants 100-250kW**
Charge Carrier in Electrolyte	**OH^-**	**H^+**	**H^+**	**H^+**	**CO_3^{2-}**	**O^{2-}**

The fuel cells can be classified according to the operating temperatures, which include low-temperature and high-temperature fuel cells. Low-temperature fuel cells are alkaline fuel cell (AFC), polymer electrolyte fuel cell (PEMFC), direct methanol fuel cell (DMFC) and phosphoric acid fuel cell (PAFC). The high-temperature fuel cells are operated at temperatures 600-1000 ^{o}C and two different types have been developed: molten carbonate fuel cell (MCFC) and solid oxide fuel cell (SOFC). An overview of different fuel cell types is given in Table 1.2 in order of increasing operating temperature.[84]

1.2.3. Applications of Fuel Cells

Fuel cells have been used extensively and successfully in the U.S. space program and now efforts are made to commercialize them in other applications. Possible applications of fuel cells are listed below.[86]

- Transportation:
  - Buses and cars
  - Other vehicles
- Portable electronics:
  - Laptops
  - Cell phones
  - Other portable electronics
- Stationary power:

- Power generating stations
- Auxiliary units
- Distributed power generations
- Combined heat and power generation systems

1.2.4. Working Principle

A fuel cell is an electrochemical cell where electrochemical reactions are characterized by the thermodynamic equilibrium potential described by the Nernst equation. Due to mixed potential formation and other parasitic processes, a fuel cell is always lowering in the thermodynamic value even under no-current conditions. When current flows, a deviation from the open circuit voltage, the overpotential, occurs corresponding to the electrical work performed by the cell. One limiting factor for the overpotential is the finite rate of reactions at the electrodes; others reasons, *i.e.,* mass transport hindrance, are also present in the systems and are described in terms of potential losses.[84]

For a redox reaction at one electrode, the current density (j) is given by the Butler-Volmer equation:

$$j = j_O\{\exp(\alpha_A F\eta/RT) - \exp(-\alpha_C F\eta/RT)\} \qquad (1.1)$$

where j_O is the exchange current density, α_A and α_C the transfer coefficients for the anodic and cathodic reaction, respectively, F the Faraday constant, η the overpotential, R the molar, and T the temperature.

The anode overpotential (η_a) and cathode overpotential (η_c) are:

$$\eta_a = U_a(j) - U_{o,a} \quad \text{with } \eta_a > 0 \text{ (the oxidation of fuel)} \qquad (1.2)$$

$$\eta_c = U_c(j) - U_{o,c} \quad \text{with } \eta_c < 0 \text{ (the reduction of oxygen)} \qquad (1.3)$$

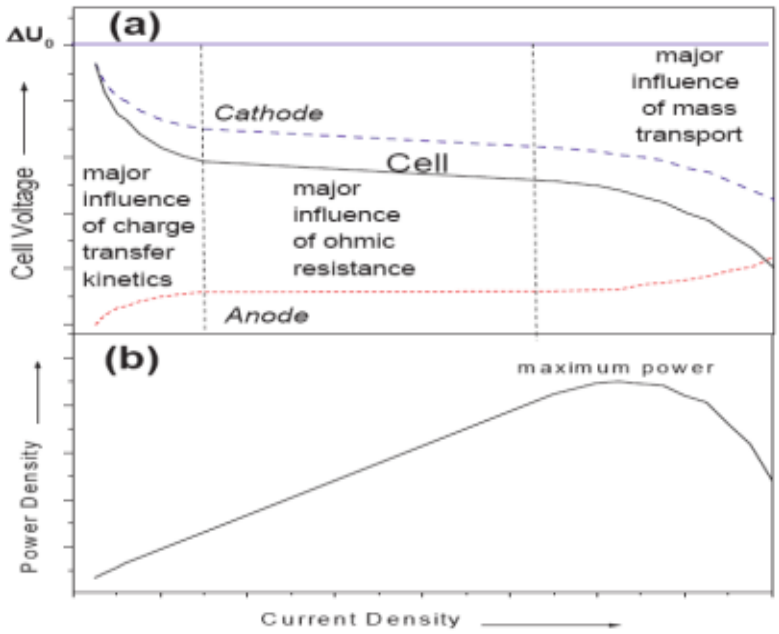

Figure 1.4. Schematic of the fuel cell voltage versus current density (a) and the power density versus current density (b).

where $U_a(j)$ and $U_c(j)$ are the exchange potentials of the anode and cathode, and $U_{o,a}$ and $U_{o,c}$ the thermodynamic equilibrium potentials of the anode and cathode, respectively.[87] The fuel cell voltage is the difference between the two half cell potentials, which is showed in Figure 1.4a. Due to the losses in both half cell reactions, the cell voltage is also not ideal and decreases with increasing current density. A typical graph of power density *vs.* current density plot is seen in Figure 1.4b, which is a useful representation in comparing the performance of different fuel cells.

1.2.5. Comparison of PEMFCs and DMFCs

Among low-temperature fuel cells, Proton Exchange Membrane Fuel Cells (PEMFCs) and Direct Methanol Fuel Cells (DMFCs) have been considered to be the most effective energy conversion devices in supplying reliable clean energy. PEMFCs transform the chemical energy liberated during the electrochemical reaction of hydrogen and oxygen to electrical energy. However, the production, storage, and transportation of hydrogen and the cost, reliability and durability issues have prevented PEMFCs from commercially available at the current technological stage.[88] DMFCs, using liquid and renewable methanol fuel, have been considered to be a good candidate of an effective energy conversion device in terms of fuel usage and feed strategies.[89, 90] Compared with PEMFCs, the capacity of the methanol storage and the magnitude of power density in DMFCs are much higher. Moreover, the liquid methanol fuel is easily stored and transported because it does not need high pressure or low

temperature since methanol is a liquid from -97.0 °C to 64.7 °C (-142.9 °F to 148.4 °F),[91] which simplifies the fuel cell system.

1.2.6. Membrane Electrode Assembly of DMFCs

A DMFC is an electrochemical device, in which methanol and oxygen are converted into waste products carbon dioxide and water, producing electricity and heat in the process. A typical DMFC consists of three basic components, *e.g.,* electrodes, polymer electrolyte membrane, and gas diffusion layer (GDL), which are assembled into a Membrane Electrode Assembly (MEA) shown in Figure 1.5.[92]

1.2.6.1. Electrodes

The porous structure with catalyst at both the anode and cathode electrodes in DMFCs are always needed to ensure the reactant liquid and gas to reach the active zones where the catalyst is in contact with the ionic and electronic conductor. The catalyst is usually made of Pt particles dispersed in carbon materials, which allows for the oxidation of methanol and the reduction of oxygen.

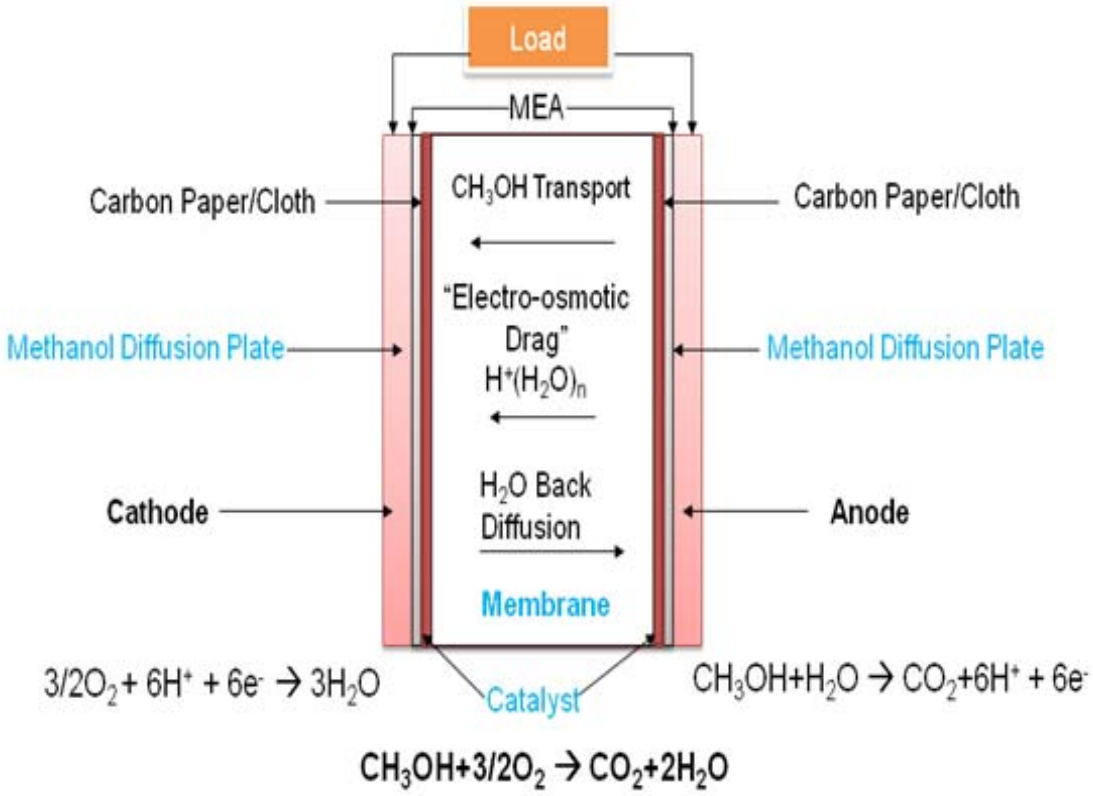

Figure 1.5. Schematic illustration of the Membrane Electrode Assembly (MEA) in a DMFC.

The requirement of a good electrode in a MEA is a three-phase boundary, where the reactant liquid and gas, the catalyst particles, and the ionic conductor have good contact with each other, which is showed in Figure 1.6. The catalyst particles always face the electrolyte and must be in direct contact with an electronic conductor to ensure effective electrons transfer during reactions. Carbon materials, which supply good electronic conductivity, are usually used as the supporter for the catalyst particles. Moreover, in order to ensure good contact of most catalyst particles with electrolyte as Nafion^{TM}, the three-phase boundary is always made

by impregnating the catalyst-support powder with a ionomeric binder (usually Nafion^{TM} solution) before assembling the electrodes onto the MEA.

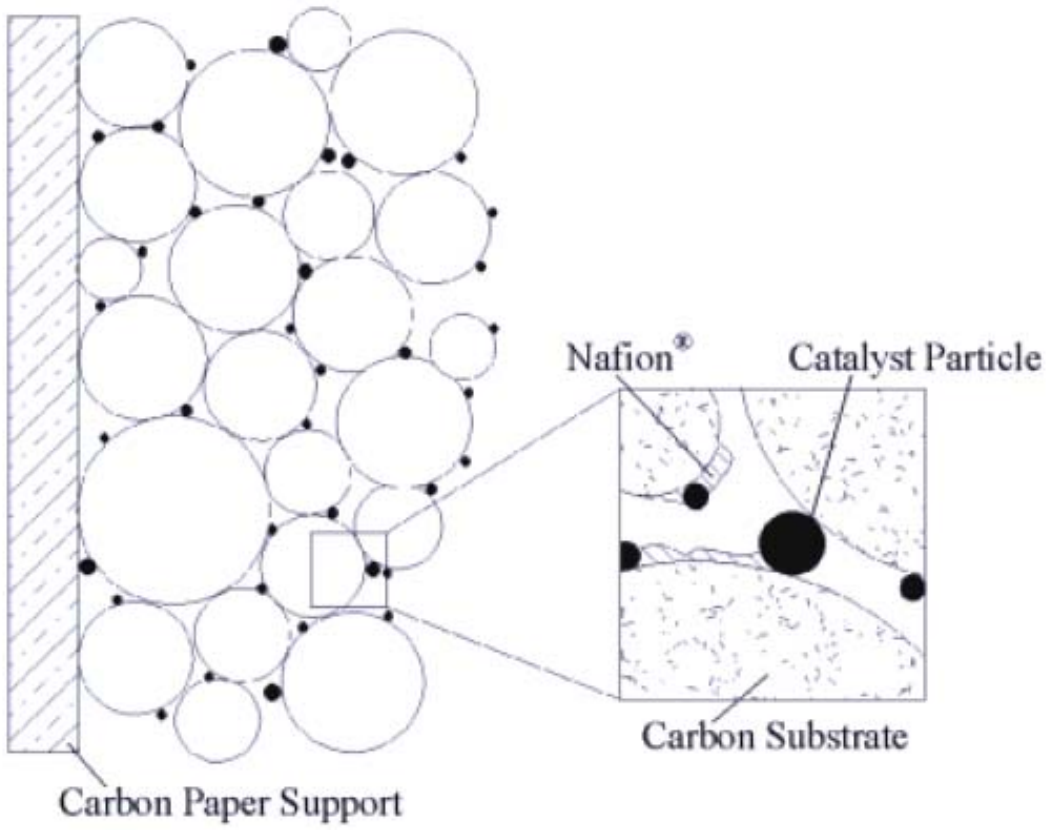

Figure 1.6. Schematic illustration of the three-phase boundary formed by the reactant liquid and gas, the catalyst particle, and the ionic conductor in a porous electrodes of a MEA.

The anode in the MEA is a negatively charged electrode with the catalyst (*e.g.,* Pt) dispersed. When methanol is fed into the electrode, it is oxidized on the surface of the catalyst to form protons and electrons, which is known as the Methanol Oxidation Reaction (MOR) . The

protons flow through the electrolyte to reach the cathode; at the same time, the electrons flow through the electrical circuit and reach the cathode, during which the electricity is produced.

However, the major problem related to the anode electrode is CO poison, which occurs due to adsorption of the species to the active sites of the Pt catalyst particles so that no sites are available for further reaction with methanol.[93, 94] In order to reactivate the surface of Pt catalyst particles, CO needs to be further oxidized to CO_2.

In order to solve the problem of the CO poison, numerous research activities on different areas, such as new catalyst structure and catalyst support, have been conducted to develop novel CO-tolerant catalysts.[95-99] Among various CO-tolerant catalysts, the catalysts based on Pt-Ru alloys have been widely studied.[100-105] The mechanism of CO oxidation and CO tolerance on the surface of Pt-Ru catalysts has been investigated and clarified by several groups, which will be further discussed in detail in the following chapters. Among various catalyst supports, CNTs and CNFs have been widely investigated as the promising support materials in place of carbon black for catalysts in DMFCs, due to their unique 1-dimensional structure, high electronic and thermal conductivities, and good electrochemical stability.[106, 107]

The cathode in the MEA is a positively charged terminal, in which the electrons are conducted from the external circuit to meet with the protons and oxygen to form water molecules, which is known as Oxygen reduction reaction (ORR). This reaction, or

combination, is also realized on the surface of dispersed catalyst (*e.g.,* Pt).

ORR is fundamentally complex and very sensitive to electrode surfaces and the presence of other adsorbed species. The biggest issue associated with the ORR is its high over-potential during reaction, which subsequently results in the sluggish reaction kinetics. Until now, Pt-based catalysts are the superior material for the ORR, though a huge variety of catalysts have been investigated.[108-110] Moreover, many other factors, such as the composition and structure of Pt-based catalysts, catalyst particle size, and the support materials, can greatly influence the kinetics of the ORR at the cathode electrode. For example, Pt dispersed on carbon or other small Pt particles (such as colloids) exhibit a good performance toward the ORR.[111] Furthermore, due to the low operating temperature in DMFCs, the catalyst loadings for the ORR are significant to compensate for the slow reaction kinetics. Since pure oxygen is rarely available, air is often used in DMFCs as the cathode gas supply. As a result, the lower oxygen partial pressure in air leads to a decrease in activity compared to pure oxygen. More information on the ORR and its kinetics has been discussed in many literature papers, which will be further discussed in detail in the following chapters.

1.2.6.2. Electrolyte

In DMFC, the electrolyte is also known as the proton exchange membrane, which separates the anode from the cathode, and allows only the ionic flow and resists the electronic flow in

the cell.

Until now, the most commercially available electrolyte is Nafion™ membrane, which is produced by DuPont™. However, one major problem related to the Nafion™ membrane is the methanol crossover during reactions in DMFCs. Since the proton movement in the membrane is associated with the water content of the membrane, methanol molecules as well as water molecules are transported to the cathode by the electro-osmotic drag as well as diffusion due to the similar properties of methanol as compared to water (*e.g.,* dipolemoment). At the cathode, methanol causes a mixed potential due to the interference of methanol oxidation with the oxygen reduction reaction. Methanol that crosses over reacts directly with oxygen at the cathode. Electrons are transferred directly from the anode to the cathode along with methanol, which results in an internal short-circuiting and consequently a loss of current (Figure 1.7). As a consequence, this results in a decrease in cell performance.

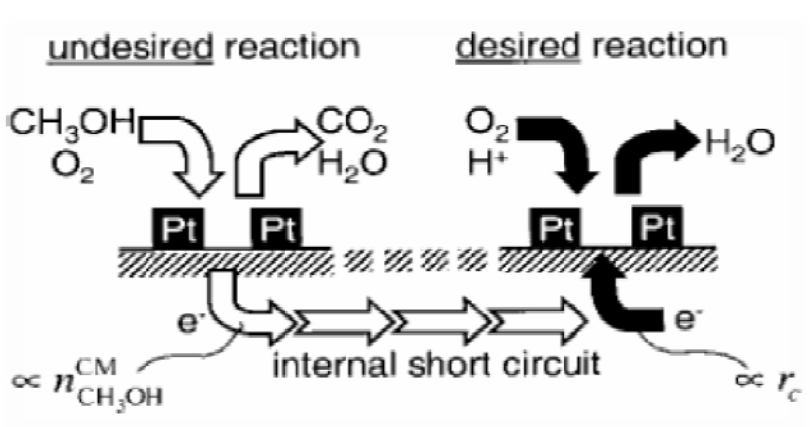

Figure 1.7. Oxygen reduction and undesired methanol oxidation with internal short circuit created by crossover at the cathode.

Methanol crossover is related to a number of factors, such as the types of membranes, the membrane permeability/thickness, the concentration of methanol in the fuel feed, the operating temperature, and the performance of the anode itself.[112-114] In order to decrease methanol crossover and improve the performance of DMFCs, many types of novel membranes, fluorinated and non-fluorinated membranes such as polybenzimidazole (PBI), sulfonated poly(ether-ether) ketone (sPEEK), and polystyrene [115], have been synthesized by various research groups.[116-119] For example, the XUS^{TM} membrane is prepared by the co-polymerisation of tetrafluoroethylene and vinylene monomers by Dow^{TM}, which is 50 μm thinner in thickness and has less methanol crossover than Nafion^{TM} 117.[120]

1.2.6.3. Gas diffusion Layer

A gas diffusion layer (GDL), which is between the flow field of the bipolar plate and the reaction zone of the electrode active layer, is the place where direct and uniform access of fuel and oxidant to the catalyst layers occurs. In DMFCs, an effective mass transport of reactants to as well as of products from the reaction zone is always required to achieve high reaction rates, which stimulate each half reaction with minimal efficiency losses. Accordingly, the GDL is always designed to be porous to ensure a homogeneous and efficient mass transport over the whole active area of the cell. For example, Thangamuthu et al. reported the preparation of porous gas diffusion electrodes using poly(ethylene glycol)/SiO_2 hybrid materials, which were combined with the carbon-supported Pt catalyst

layers through sol-gel processes.[121] They found that there is a optimum composition of poly(ethylene glycol)/SiO_2 hybrid material, beyond which the cell performance decreased continuously due to excess hybrid materials in the catalyst layer blocking the gas diffusion channels. However, most of research activities have been conducted on the modeling of the complicated two-phase mass transport in the GDL in the electrodes, such as the influence of the porosity, the tortuosity, and the thickness of the GDL.[122-124] For examples, Bernardi et al. developed one-dimensional (1D) model to the direction of membrane thickness, and examined concentration distribution and water management in the GDL; and Yu et al. further developed the model from 1D to two-dimension (2D).[125-127] Yi et al. developed heat and water transport models that accounted for various operation and membrane hydration conditions in the GDL.[128]

1.2.6.4. Fabrication of the MEA

The fabrication of a MEA is an intricate procedure, in which all details of the structure and preparation are important since that the function of the electrodes is far more than just catalyzing a reaction. Generally, two model procedures, *i.e.,* 1) the application of the catalyst layer to the GDL followed by membrane addition, and 2) to the membrane followed by GDL addition, are always used to fabricate the MEA, both procedures are showed in Figure 1.8.[129]

Model 1: Application of the catalyst layer to the GDL.

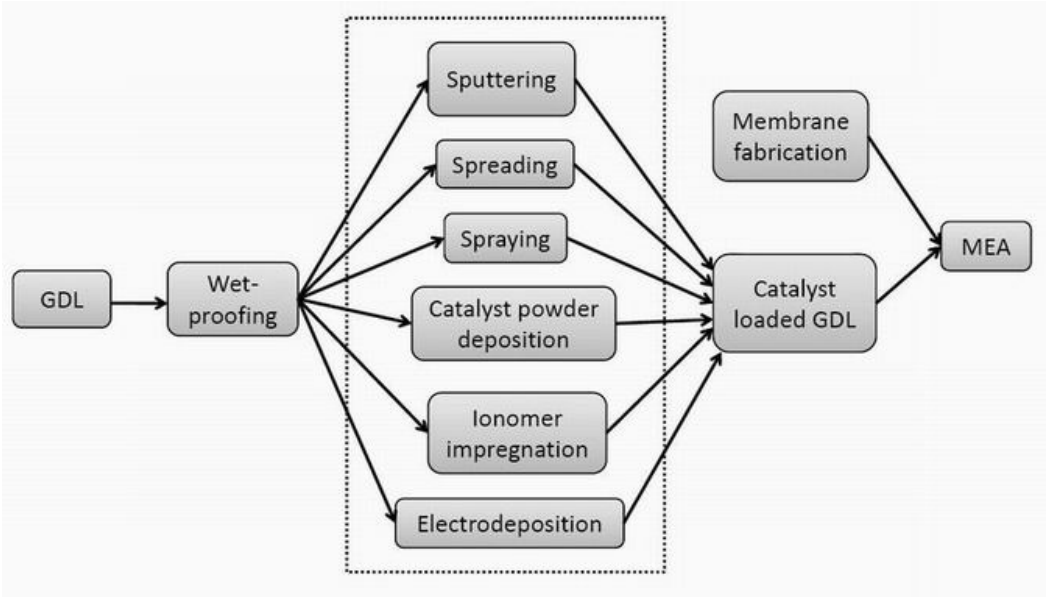

Model 2: Application of the catalyst layer to the Membrane.

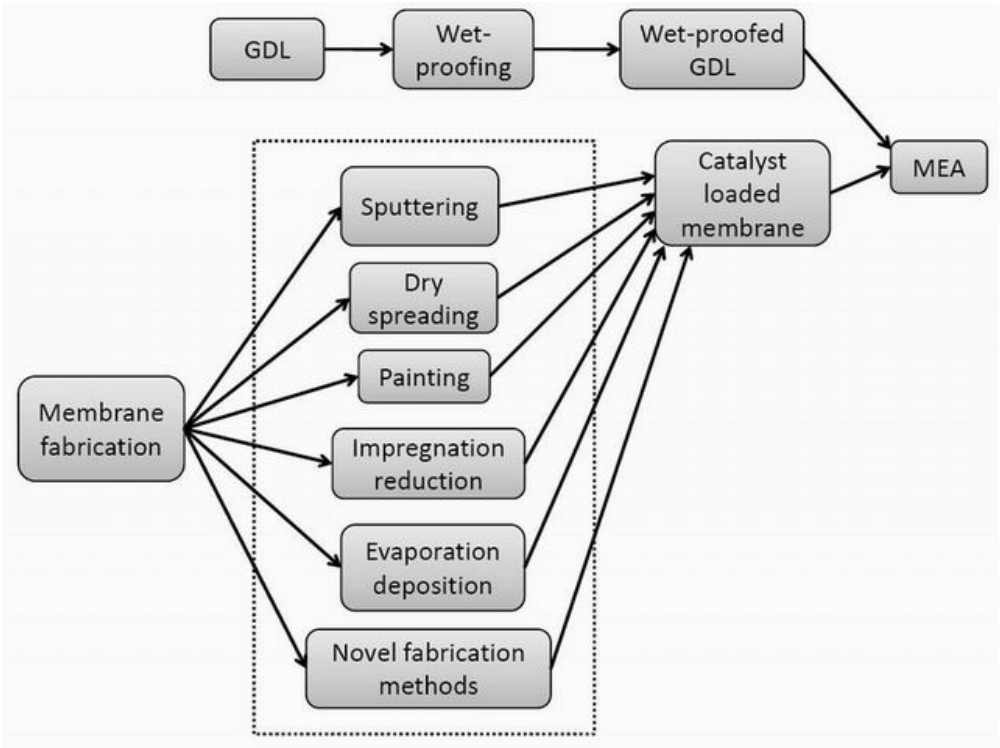

Figure 1.8. The model procedures of the MEA fabrication.

For the model procedure 1, six manufacturing methods, *e.g.,* sputtering, spreading, spraying, catalyst powder deposition, ionomer impregnation, and electrodeposition, have been used for the catalyst preparation and application to prepare MEAs.[130-132] For example, Srinivasan et al. prepared a catalyzed carbon and PTFE dough using the spreading method, which leads to a thin and uniform active layer on the GDL/catalyst assembly for the direct loading of Pt catalyst.[133]

For the model procedure 2, six fabrication methods have been developed so far, including sputtering, dry spreading, painting, impregnation reduction, evaporative deposition, and novel fabrication method.[134-136] For example, Fedkiw et al. deposited $(NH_3)_4PtCl_2$ onto a membrane from an aqueous solution using evaporation method.[137] After the deposiotn of the Pt salt, the metallic Pt was produced by immersion of the entire membrane in a $NaBH_4$ solution, which results in a small loading of Pt catalyst, *i.e.,* $\leq$0.1 mg Pt/cm^2, with good performance.

1.2.7. Reactions in DMFCs

How does a DMFC work? The whole procedure of reactions in the MEA of the DMFC is showed in Figure 1.2. Generally, the reactions include the methanol oxidation at the anode and the oxygen reduction at the cathode, and the overall reaction is the sum of the anodic and cathodic reactions to produce the carbon dioxide and water (Equation 1.4).

$$CH_3OH + H_2O \rightarrow CO_2 + 2H_2O \qquad (1.4)$$

1.2.7.1. Methanol oxidation reaction (MOR)

At the anode, methanol is oxidized with water on a catalyst layer (*e.g.,* Pt) to form carbon dioxide, protons and electrons:

$$CH_3OH + H_2O \rightarrow CO_2 + 6H^+ + 6e^- \qquad E^o = 0.02\ V\ vs.\ SHE \qquad (1.5)$$

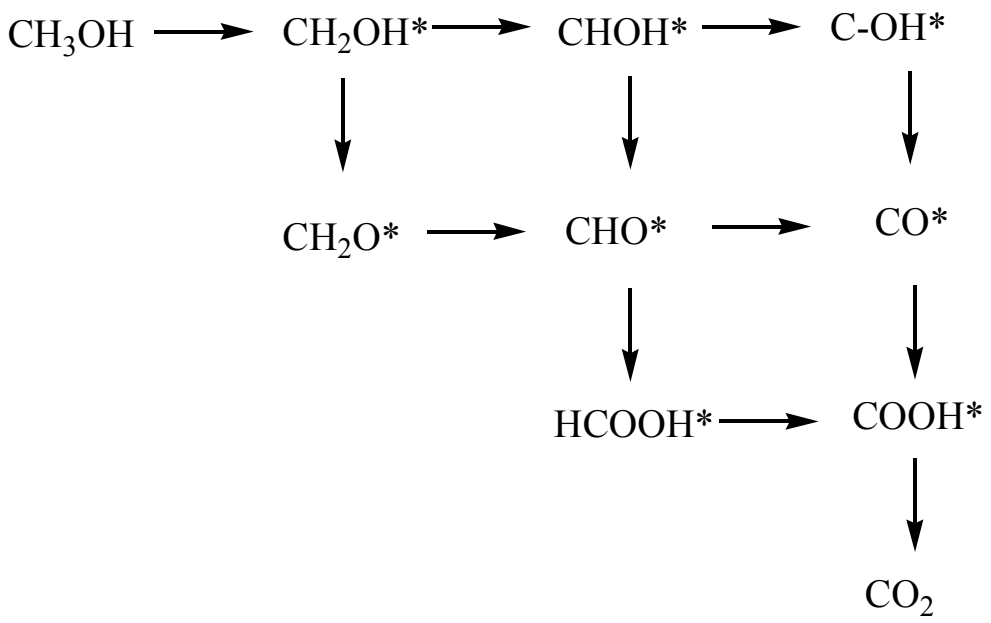

Figure 1.9. Schematic illustration of possible reaction paths and possible reaction products for the methanol oxidation (″*″ indicates the intermediate product).

The thermodynamic potential of methanol reaction in Equation 1.5 is very close to the equilibrium potential of hydrogen, however, the procedure is much more complicated. The possible reaction paths and reaction products for methanol oxidation are shown in Figure 1.9.

In General, the methanol oxidation includes five steps: (1) methanol adsorption, (2) C-H bond activation, (3) water adsorption, (4) water activation, and (5) CO oxidation. The procedure begins in the methanol adsorption and then undergoes successive dehydrogenation steps.[138]

$$CH_3OH \rightarrow (CH_3O)_{ads} + H^+ + e^- \quad (1.6)$$

$$(CH_3O)_{ads} \rightarrow (CH_2O)_{ads} + H^+ + e^- \quad (1.7)$$

$$(CH_2O)_{ads} \rightarrow (CHO)_{ads} + H^+ + e^- \quad (1.8)$$

$$(CHO)_{ads} \rightarrow (CO)_{ads} + H^+ + e^- \quad (1.9)$$

The adsorption of methanol in Equation 1.6 requires multiple active sites on the surface of the catalyst, thus a relatively higher potential (*i.e.,* 0.2 V *vs.* SHE for Pt catalyst) is needed for neighboring catalyst sites to become free of protons. Once methanol is adsorbed, the removal of the first four protons is quick (Equation 1.6-1.9).[139, 140] However, the successive oxidation of CO, which includes the dehydrogenation of water molecule and the combination of the oxygen group of water molecule with the adsorbed CO to form of CO_2, is much slower.

$$(H_2O)_{ads} \rightarrow (OH)_{ads} + H^+ + e^- \quad (1.10)$$

$$(HO)_{ads} \rightarrow O_{ads} + H^+ + e^- \quad (1.11)$$

$$(CO)_{ads} + O_{ads} \rightarrow CO_2 \quad (1.12)$$

Moreover, it should be noted that the formation of OH by water activation in Equation 1.10 on the Pt catalyst, which is a necessary step for the oxidative removal of adsorbed CO, requires a high potential, which limits the use of a pure Pt catalyst in DMFCs. Thus, a second metal (*i.e.,* Ru) that can provide oxygenated species at lower potentials for the oxidative removal of adsorbed CO is definitely needed. The bi-functional mechanism, which involves the adsorption of oxygen containing species on Ru at lower potentials thereby promoting the oxidation of CO to CO_2, is summarized as follows.[140, 141]

$$Pt + CH_3OH \rightarrow Pt(CO)_{ads} + 4H^+ + 4e^- \quad (1.13)$$

$$Ru + H_2O \rightarrow Ru(OH)_{ads} + H^+ + e^- \quad (1.14)$$

$$Pt(CO)_{ads} + Ru(OH)_{ads} \rightarrow CO_2 + Pt + Ru + H^+ + e^- \quad (1.15)$$

The catalytic activity of the Pt-Ru catalyst is strongly dependent on the composition, structure, morphology, particle size, and alloyed degree.

1.2.7.2. Oxygen reduction reaction (ORR)

At the cathode, the oxygen reacts with protons, which are conducted through the proton exchange membrane, and electrons, which are conducted at the anode to an external electric circuit, to produce water:

$$3/2O_2 + 6H^+ + 6e^- \rightarrow 3H_2O \qquad E^o = 1.23 \text{ V } \textit{vs.} \text{ SHE} \qquad (1.16)$$

Oxygen reduction is much complex and sensitive to electrode surfaces and the presence of other adsorbed species. Figure 1.10 shows the possible intermediates and their chemical potentials during the ORR.[142]

However, in most literature papers, the oxygen reduction mechanism has been separated into two parallel paths: the oxygen is reduced to hydrogen peroxide, and then further reduced to water.[143-146]

$$3/2O_2 + 3H^+ + 3e^- \rightarrow 3/2H_2O_2 \qquad E^o = 0.67 \text{ V } \textit{vs.} \text{ SHE} \qquad (1.17)$$

$$3/2H_2O_2 + 3H^+ + 3e^- \rightarrow 3H_2O \qquad E^o = 1.77 \text{ V } \textit{vs.} \text{ SHE} \qquad (1.18)$$

For DMFCs, many noble metals such as Pt, Pd, Ag, and Au have been considered as feasible catalysts for the reduction of oxygen. The most thoroughly studied oxygen reducing catalyst

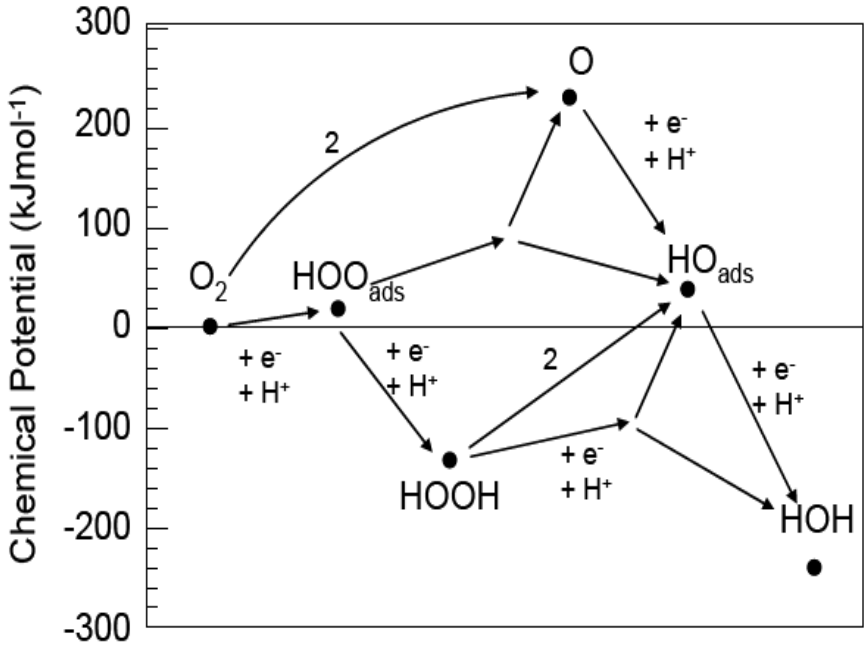

Figure 1.10. Schematic illustration of possible intermediates and their chemical potentials for the ORR.

is Pt, and the oxygen reduction reaction is very sensitive to the Pt surface. A model for the oxygen reduction reaction based on the simplified version of the parallel paths is showed in the following.[147]

$$1/2O_2 + Pt \rightarrow Pt - O \qquad (1.19)$$

$$Pt - O + H^+ + e^- \rightarrow Pt - OH \qquad (1.20)$$

$$Pt - OH + H^+ + e^- \rightarrow H_2O + Pt \qquad (1.21)$$

Since the reactions (1.19) and (1.20) are endothermic, the oxygen reduction is slowed by those adsorbed oxygen and hydroxide. In order to improve the performance of the oxygen reduction, a second element or third has been alloyed into Pt. Fundamentally, the second (or third) element can alter Pt's interatomic spacing and increase the Pt 5d orbital vacancies, thus enhance the efficiency of the oxygen reduction.[148-151]

1.2.8. Challenges of DMFCs

The success of a fuel cell greatly depends on two key materials: the membrane and the catalyst at the electrodes. These two key materials are also directly linked to the major challenges in DMFCs, which include the methanol crossover, the slow kinetics of methanol oxidation caused by CO poison at the anode, and the kinetically limited oxygen reduction at the cathode.[152-155] Recently, some significant progresses, such as cheap and durable proton exchange membranes with low methanol crossover, have been made in the development of new polymer electrolyte membranes for DMFCs in terms of cost reduction and functionality improvement, together with other associated technology advancements.[156-161] However, with regard to new DMFC catalysts, there are still two major challenges, the relatively poor performance such as low activity, poor reliability and unsatisfactory durability, and the high cost. In order to improve the performance of catalysts in DMFCs, noble and non-noble metals are often utilized at the electrodes. Pt alloys and carbon supported nanoparticle catalysts are believed to be the most promising materials for

catalysis at both the anode and the cathode in DMFCs.[89, 129, 162]

1.2.8.1. Pt alloy catalysts

Pt-based alloys, bi-metallic catalyst such as Pt-Ru, Pt-Pd, Pt-Co, Pt-Fe, and Pt-Ni, and tri-metallic catalyst, such as Pt-Ru-Cr, Pt-Ru-Ni, Pt-Pd-Co, and Pt-Co-Cr, have been investigated in order to improve the electro-catalytic ability for the oxidation of methanol at the anode and the reduction of oxygen at the cathode in DMFCs.

1.2.8.1.1. Pt-Ru

Pt-Ru alloy has been found to be the most active bi-metal as the catalyst at the anode of DMFCs. The enhanced activity of the Pt-Ru catalyst when compared with Pt for methanol oxidation has been attributed to both a bi-functional mechanism[141, 163, 164] and a ligand effect.[165] Several factors, such as the composition of Pt-Ru and the particle size, play important roles in the catalytic ability toward the oxidation of methanol. As reviewed by Dillon et al.,[166] many researchers have been devoted to the performance optimization of Pt-Ru catalyst towards methanol oxidation. The current consensus is that the optimal Pt/Ru ratio is 1:1, for example, tests on carbon supported high surface area catalyst nanoparticles tend to show $Pt_{50}Ru_{50}$ as the best composition. However, the good catalytic ability of Pt-Ru alloys with a Pt rich optimum composition between $Pt_{90}Ru_{10}$-$Pt_{80}Ru_{20}$ has been also reported,

which is showed in Figure 1.11.[167-171]

In order to improve the catalytic ability of Pt-Ru alloys, the third element, such as Os, Co, and Sn, has been alloyed into Pt-Ru to test their catalytic ability in DMFCs.[172-174] For

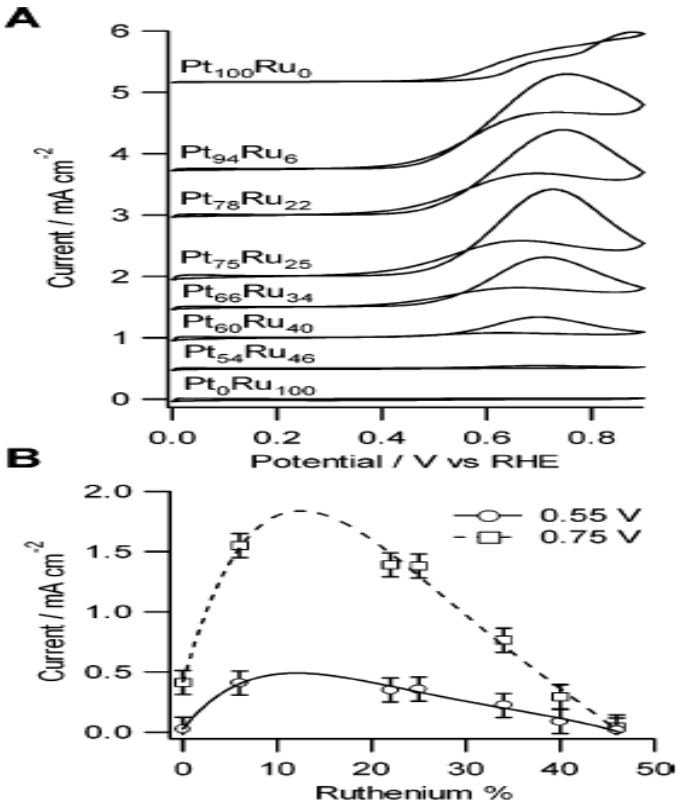

Figure 1.11. Cyclic voltammetry of Pt*x*Ru*y* electrodes in a 1.0 M CH_3OH + 0.5 M H_2SO_4 solution at 25 °C (A). Scan rate is 0.01 V s^{-1}. Plot (B) of current from (A) versus Ru composition at substrate potentials of 0.55 and 0.75 V.

example, Ley et al. studied the MOR on arc-melted Pt-Ru-Os alloys prepared by the $NaBH_4$

reduction of metal chloride salts.[175] Hydrogen adsorption/desorption measurements on the polished alloy electrodes, in the presence of adsorbed CO at 25°C, showed that selected ternary alloys have significant hydrogen adsorption/desorption integrals at adsorption potentials, where $Pt_{50}Ru_{50}$ was fully blocked and higher integrals at all adsorption potentials up to 400 mV *vs.* RHE. Fuel cell performance of the arc-melted alloys confirmed that $Pt_{65}Ru_{25}Os_{10}$ is more active than $Pt_{50}Ru_{50}$.

1.2.8.1.2. Pt-Pd

Until now, there are no experimental reports of using Pt-Pd alloy to oxidize methanol. Kua et al. performed a simulation and found that Pd can absorb and dehydrogenate methanol, however, it would be poor at dehydrogenating water to complete the methanol oxidation. Theoretically the second element Pt can be alloyed with Pd to strengthen the dehydrogenation of water and accomplish the reaction, but there are still no experiments to confirm this.

Generally, the Pt-Pd alloy can be an effective catalyst to facilitate the oxygen reduction at the cathode of DMFCs by engineering its morphology and/or composition. For example, recently Xia et al. reported the synthesis of a Pt-Pd bimetallic nanodendrite catalyst consisting of a dense array of Pt branches on a Pd core, which show five times more active ability toward the oxygen reduction than that of the first-generation supportless Pt/C catalyst (Figure

1.12).[176] Li et al. also reported the synthesis of a novel carbon-supported palladium-rich $Pt_{25}Pd_{75}$/C catalyst by a modified polyol process, which showed a better cell performance of the oxygen reduction than the commercial Pt/C catalyst in DMFCs.[177]

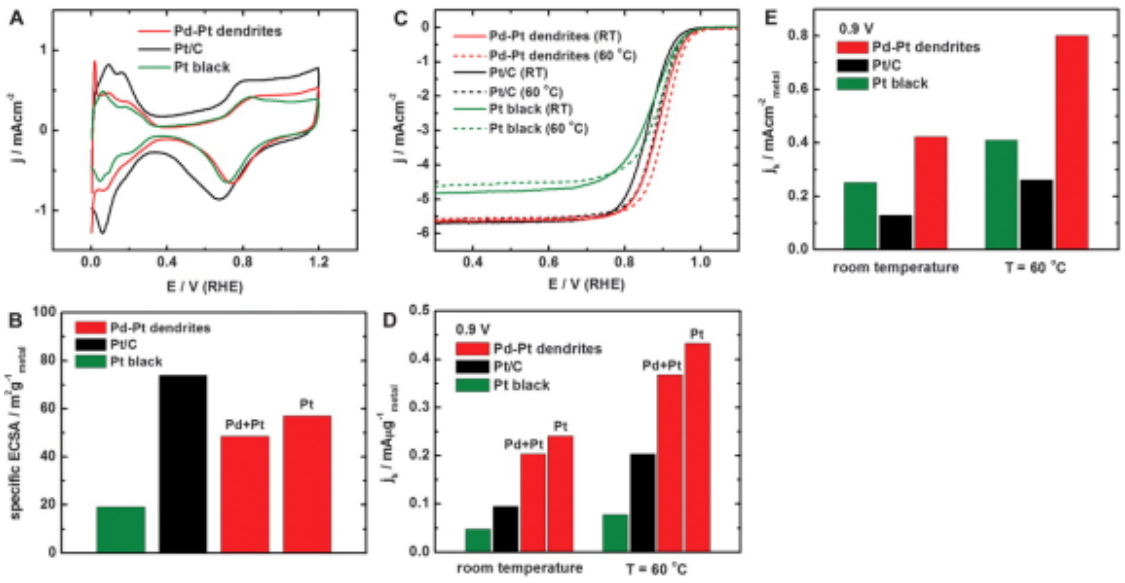

Figure 1.12. Comparison of electrocatalytic properties of the Pd-Pt nanodendrites, Pt/C catalyst (E-TEK), and Pt black (Aldrich).

1.2.8.1.3. Pt-Co

There have been a substantial number of investigations on the synthesis of Pt-Co alloy, some results of which have shown good catalytic ability toward the methanol oxidation. For

example, Zhang et al. reported that $Pt_{41}Co_{59}$ articles, which were made by a micro-emulsion technique, showed catalytic activity 1.6-2.2 times higher than that of pure Pt particles over a wide potential range for the methanol oxidation in an alkaline electrolyte (Figure 1.13).[178] Zeng et al. prepared a $Pt_{50}Co_{50}$ catalyst, which showed enhanced activity for the oxidation of methanol relative to a pure Pt catalyst, with performance being better than twice that for the pure Pt catalyst after four hours' operation.[179] Okada et al. also reported the methanol oxidation activity of different composition of Pt with Co-based organic complexes ($Pt_{60}Co_{40}$, $Pt_{50}Co_{50}$, and $Pt_{40}Co_{60}$) is larger than that of pure Pt.[180] In contrast, Pt-Co alloy has been also reported as a superior catalyst for the oxygen reduction. Mukerjee et al. studied $Pt_{75}Co_{25}$ in single cell tests and found that the alloy had better ORR activity than pure Pt, and they also tested a commercially available Pt-Co catalyst for the oxygen reduction and found its performance is also better than the pure Pt catalyst.[181, 182]

Though bimetallic Pt-Co alloys have showed great catalytic ability toward the MOR or the ORR, the further improvement of the catalytic ability of the Pt-Co alloy have been studied by several research groups. For example, Zhang et al. prepared tri-metallic Pt-Ru-Co nanoparticles by a micro-emulsion process, which shows a homogenous alloy structure with average diameter distribution of 2.7 ± 0.6 nm.[183] The composition of Pt-Ru-Co nanoparticles can be controlled by adjusting the initial metal salt solution and preparation average diameter distribution of 2.7 ± 0.6 nm.[183] The composition of Pt-Ru-Co nanoparticles can be controlled by adjusting the initial metal salt solution and preparation

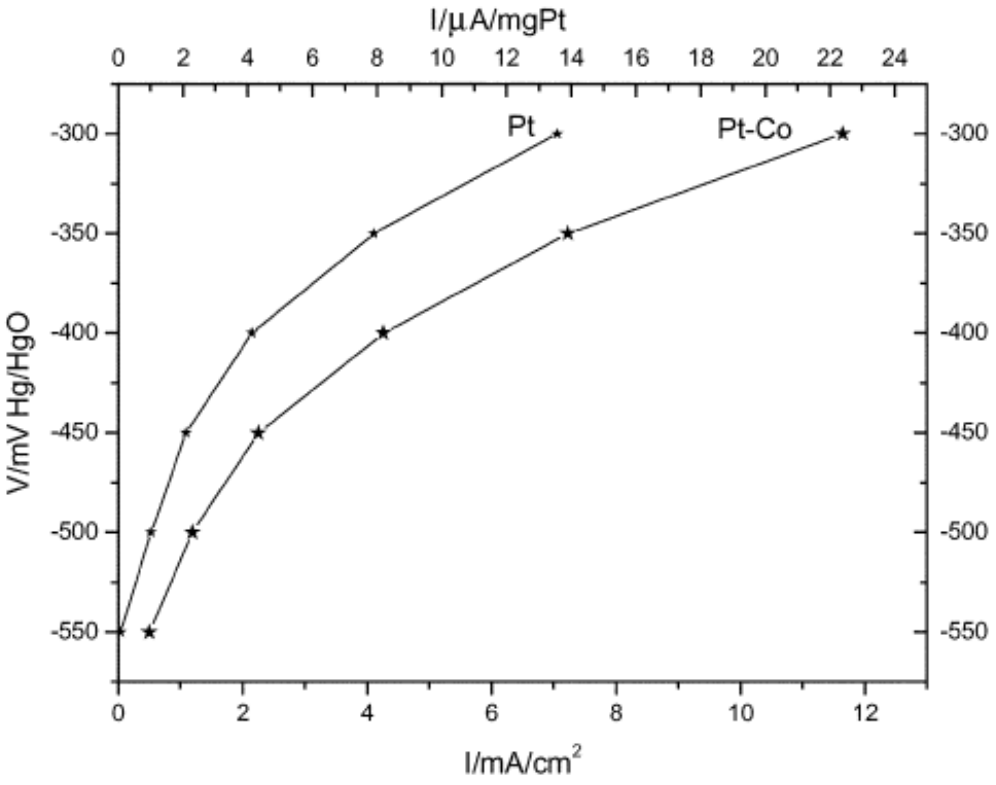

Figure 1.13. Polarization curves for the oxidation of an equal volume mixture of 1 M methanol + 1 M KOH solutions at room temperature by Pt/C and Pt-Co/C.

Bogdanovskaya et al. synthesized a tri-metallic Pt-Co-Cr catalyst dispersed on a carbon black KhS 72, and studied the influence of the structure on electrocatalytic activity toward the ORR in 0.5 M H_2SO_4.[184] Although the mechanisms of the ORR on both Pt and tri-metallic catalyst were similar, a higher activity of the tri-metallic Pt-Co-Cr catalyst was observed (Figure 1.14), which was caused by smaller catalyst surface coverage by oxygen containing particles.

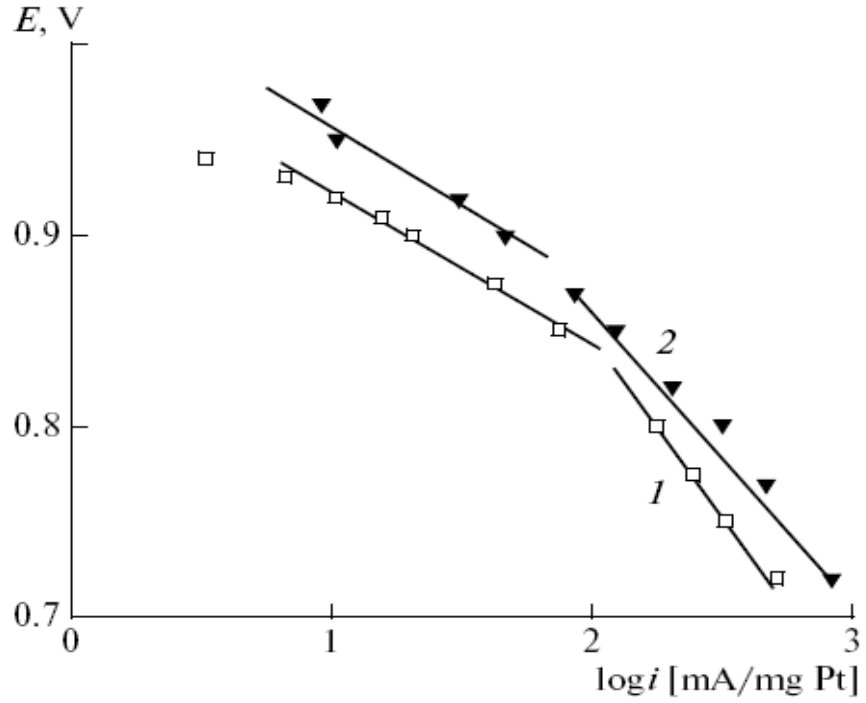

Figure 1.14. Polarization curves of the ORR in Tafel coordinates obtained on a thin layer rotating disk electrode in 0.5 M H_2SO_4, 60°C: HiSPEC(40 wt% Pt, 1), and Pt-Co-Cr (20 wt% Pt, 2).

1.2.8.1.4. Pt-Fe

Page et al. reported a commercially available carbon membrane electrode with a $Pt_{50}Fe_{50}$ catalyst with the loading of 0.5 mg cm^{-2} had an onset potential of 375 mV *vs.* SCE for the methanol oxidation at 25 °C, which is similar to that of the pure Pt carbon membrane electrode under the same condition (385 mV *vs.* SCE).[185] Shukla et al. reported a Pt-Fe

catalyst has a same methanol oxidation onset potential as the pure Pt catalyst but a much weaker peak current density by using cyclic voltammetry.[186] However, the major work on the Pt-Fe alloy is concerned with the oxygen reduction reaction. Toda et al. deposited several Pt-Fe alloys by sputtering and reported that all of the alloys have a better performance than the Pt catalyst in the oxygen reduction reaction; and the Pt-Fe alloy with the best catalyst ability is $Pt_{50}Fe_{50}$.[187, 188] They also postulated that compositions with more Pt than $Pt_{50}Fe_{50}$ had a weak adsorption of O_2 and compositions with less Pt than $Pt_{50}Fe_{50}$ became inactive due to a strong OH bond.

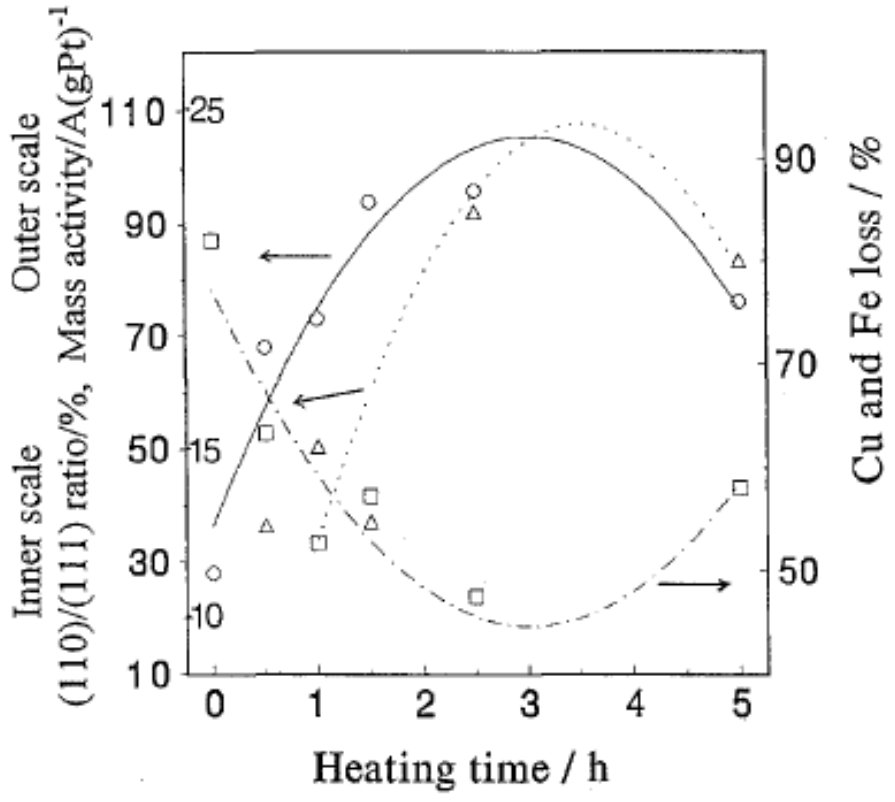

Figure 1.15. Mass activity (□), (110/111) peak ratio (○), and dissolution loss of total Cu and Fe (Δ) plotted against heating time at 900 °C in Pt-Fe-Cu catalysts.

Roh et al. prepared ternary Pt-Fe-Cu alloy catalysts from aqueous media, followed by heat treatment at 900 °C for various heating durations.[189] When the heating duration increases, the formation of an ordered alloy is enhanced and the formation is completed in 2.5 hours, as confirmed by the intensity of super-lattice diffraction lines. For the electrochemical reduction reaction of oxygen in fuel cell operation, ordered alloys have shown improved catalytic activity, which is showed in Figure 1.15. Lee et al. reported the composition optimization of Pt-Ru-Fe catalysts for the MOR via a combinatorial method.[190] High MOR activities were observed in $Pt_{50}Ru_{30}Fe_{20}$ and $Pt_{40}Ru_{30}Fe_{30}$ via quantitative analysis of each catalyst spots, and the fuel cell performances showed the highest MOR activity was observed in the $Pt_{50}Ru_{40}Fe_{10}$, which is 98% higher mass activity than that of commercial Pt-Ru.

1.2.8.1.5. Pt-Ni

Page et al. reported a commercially available carbon membrane electrode with a 0.5 mg cm^{-2} $Pt_{50}Ni_{50}$ catalyst loading has an onset potential of 370 mV *vs.* SCE for the methanol oxidation at 25 °C, which is just 15mV lower than the pure Pt carbon membrane electrode under the same condition.[185] Moreover, Pt-Ni alloys have also been considered as good catalysts toward the oxygen reduction. Xiong et al. performed a study on Pt-Ni alloys for the oxygen reduction reaction, and showed that $Pt_{73}Ni_{27}$ has an 10 mV higher oxygen reduction onset potential than that of pure Pt catalyst though the current density is 10 % poorer.[191]

Mukerjee et al. performed a single cell test on a commercially available Pt-Ni catalyst for the oxygen reduction, and reported that it has better performance than that of pure Pt catalyst under the same situation.[150]

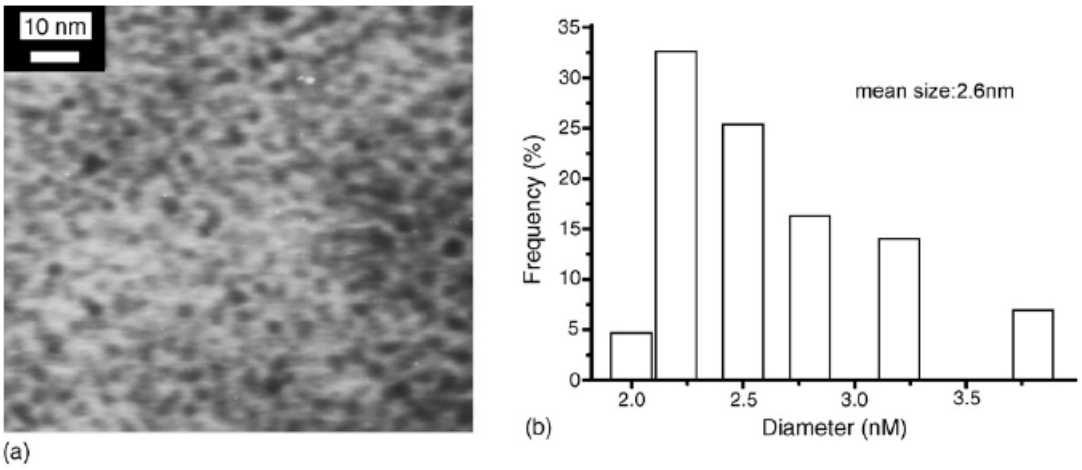

Figure 1.16. TEM images of Pt-Ru-Ni nanoparticles prepared by the water-in-oil microemulsion (a), and histograms of particles (b).

Moreno et al. reported the preparation and characterization of a tri-metallic anode catalyst $Pt_{60}Ru_{30}Ni_{10}$ by using the combustion method.[192] TiO_2 was used as the support material for this anode catalyst, which can exhibit a bi-functional catalytic effect, *i.e.* increasing CO oxidation and promoting hydroxide formation. The obtained catalyst showed a single tri-metallic phase with an average particle size of 8 nm, and the high power density of 107 mW cm^{-2} was obtained. Zhang et al. prepared Pt-Ru-Ni tri-metallic nanoparticles from water-in-oil reverse microemulsions of water/Triton X-100/propanol-2/cyclohexane, and the

resulting particles showed a narrow size distribution with an average diameter of 2.6 ± 0.3 nm, as shown in Figure 1.16.[193] When compared to Pt-Ru bimetallic nanoparticles, Pt-Ru-Ni ternary metallic nanoparticles showed an enhanced catalytic activity towards the MOR. That is because both Ru and Ni atoms have high affinity toward -OH formation and the combination of Ru and Ni promises the formation of -OH as an intermediate, which results in the MOR at more catholic potentials.

1.2.8.1.6. Other Pt-based alloy catalysts

In addition to the bimetallic Pt alloys mentioned above, a number of other Pt alloys, such as Pt-Sn,[194-196] Pt-Cu,[197, 198] and Pt-Rh,[199-201] have been studied for their electro-catalytic abilities toward the methanol oxidation at the anode and the oxygen reduction at the cathode in DMFCs. Moreover, other Pt tri-metallic alloys[202-204] and tetra-metallic Pt alloys[205-209] have also been investigated.

1.2.8.2. Carbon nanotube- and nanofiber-supported catalysts

Carbon nanomaterials are currently being considered as the suitable catalyst supports in DMFCs,[199, 210-214] because of their unique graphite properties combined with three-dimensional flexible structures. Among various carbon nanomaterials, carbon

nanotubes (CNTs) and carbon nanofibers (CNFs), are promising support materials for catalysts in DMFCs, due to their unique 1-dimensional structure, high electronic and thermal conductivities, and good electrochemical stability.[106, 107, 215, 216] Compared with CNTs, CNFs are inexpensive and can be produced with various controlled structures at relatively high speeds. However, both of them are chemically inert, thus it is necessary to activate their graphitic surface because the deposition, distribution and size of Pt or Pt alloy nanoparticles strongly depend on the surface properties of CNTs and CNFs.[217, 218] Until now, efforts have been carried out to use different methods to prepare 1-dimensional carbon-supported catalysts (especially, CNT- and CNF-supported catalysts) for the methanol oxidation and the oxygen reduction in DMFCs.

1.2.8.2.1. Chemical deposition

Chemical deposition, also called electroless deposition, is the most widely used method in preparing highly dispersing Pt nanoparticles on carbon supports for DMFCs. Figure 1.17 shows the typical preparation procedure of the chemical deposition method for Pt/CNT catalysts.[219] First, the aromatic conjugate ring structure of the CNTs is modified by an oxidation process of extremely aggressive reagents (HNO_3 or H_2SO_4 or their mixture), during that process, various surface functional groups such as quinoid (=O), hydroxy (-OH) and carboxyl (-COOH) were produced. These functional groups can supply defect sites for the Pt nanoparticle deposition. After adding Pt salt and a reductive agent such as H_2, HCHO or

ethylene glycol, Pt^{2+} ions can be reduced and deposited on the defect sites created during the acid treatment.

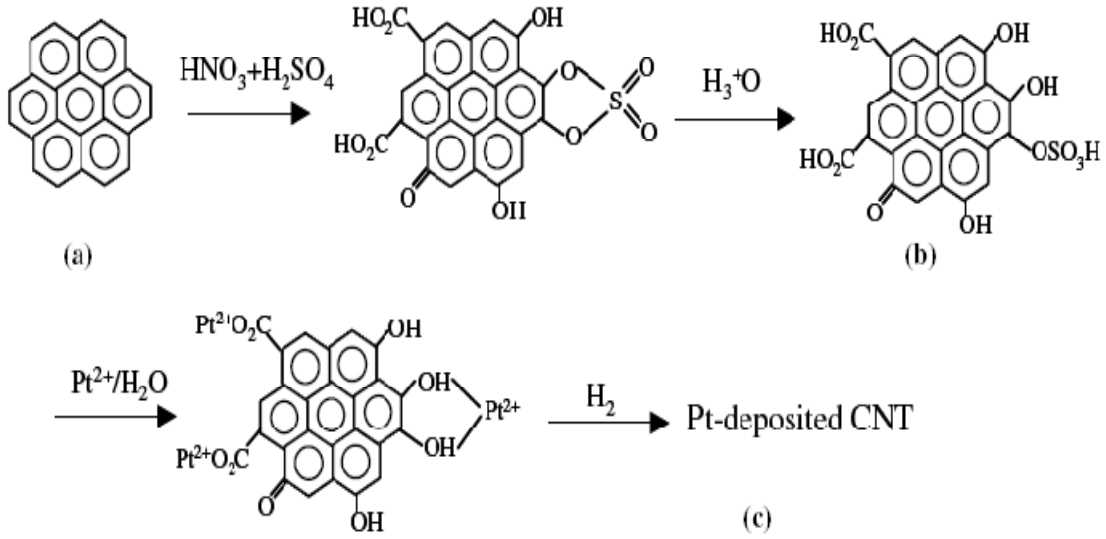

Figure 1.17. Scheme of the mechanism of Pt deposition via the oxidation of HNO_3 + H_2SO_4 on CNTs.

The procedure has been adopted by many scientists working on the preparation of Pt/CNT catalysts. For example, Rajalakshmi et al. investigated the effect of surface oxidation pre-treatment on Pt deposition.[220] Non-oxidized CNTs, sonicated CNTs, and surface-oxidized CNTs using 70% nitric acid were prepared, and Pt particles were deposited on those CNTs through a chemical reduction of H2PtCl6 by NaBH4. The results showed that surface-oxidized CNTs have smaller Pt nanoparticle size (3-5 nm) and more uniform Pt

A.

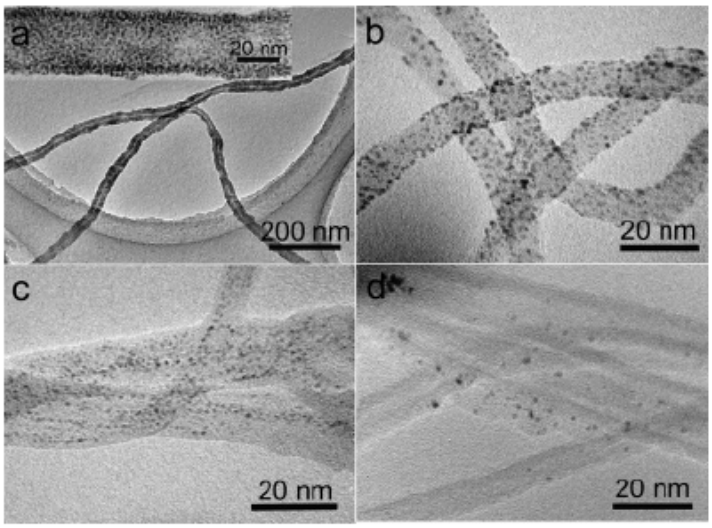

B.

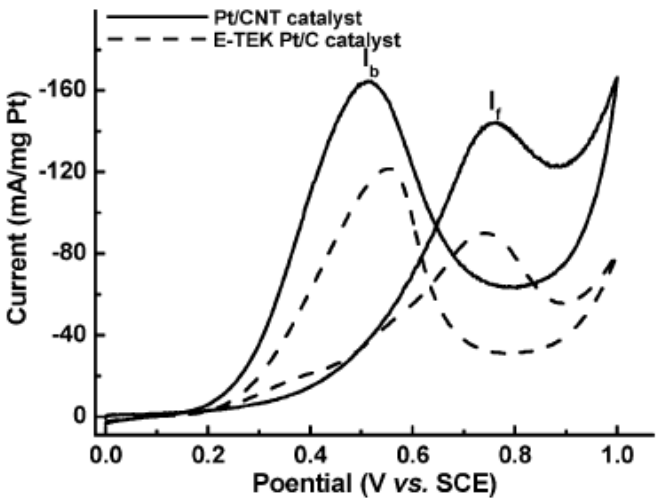

Figure 1.18. A. TEM images of Pt/CNT composite with different Pt content: 40.6 (a, inset: enlarged image of panel a), 24.0 (b), 19.1 (c), and 3.1 wt% (d). B. Cyclic voltammograms of the methanol oxidation on Pt/CNT composites and commercial E-TEK Pt/C catalyst in 2 M CH_3OH + 1 M H_2SO_4 at 20 mV S^{-1} at room temperature.

particle distribution compared with those of nonoxidized CNTs. Mu et al. reported the controllable Pt nanoparticle deposition on CNTs as an anode catalyst in DMFCs with different amount of Pt loading (40.6, 24.0, 19.1, and 3.1 wt%, respectively), which is showed in Figure 1.18A.[221] Figure 1.18B shows that the prepared Pt/CNT composites have higher electrocatalytic activity and better tolerance to poisoning species in the methanol oxidation than the commercial E-TEK catalyst, which can be ascribed to the high dispersion of Pt nanoparticles on the CNT surface.

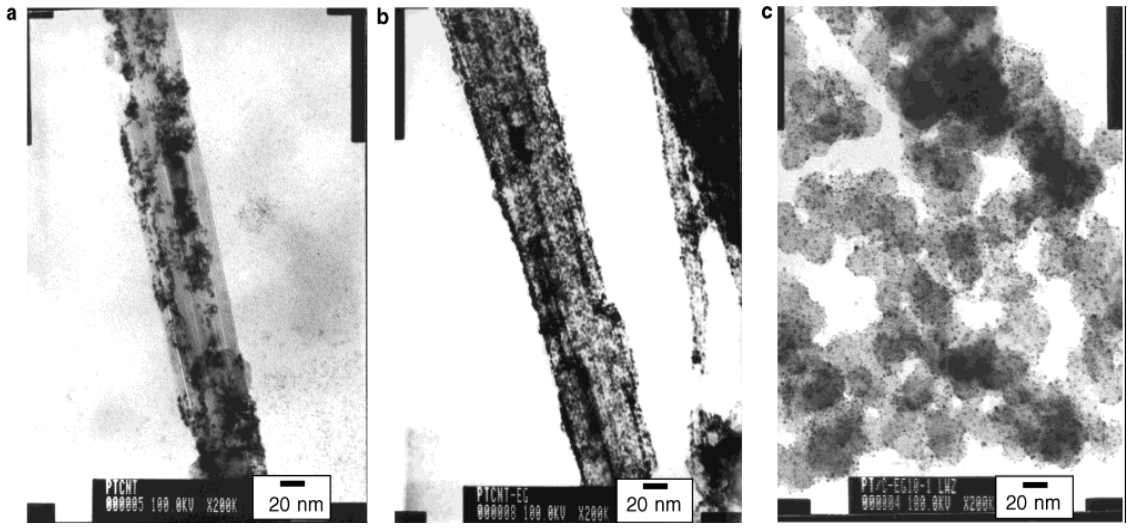

Figure 1.19. TEM micrographs of Pt/CNTs prepared by the HCHO method (a) and the EG method (b), respectively, and Pt/XC-72 prepared by the EG method (c).

Li et al. compared two synthesis methods using different reducting agents, HCHO and ethylene glycol, for Pt deposition on CNTs.[222] The HCHO method could give a Pt particle

size distribution range from 2 to 9 nm with a mean particle size of 3.4 nm, while the ethylene glycol method provided a high and homogeneous dispersion of spherical Pt nanoparticles, which are in the particle size range from 2 to 5 nm with a mean size of 2.6 nm. This means that the ethylene glycol method is better than the HCHO method in terms of the size and distribution uniformity of Pt nanoparticles on the CNTs (Figure 1.19)

For CNFs, Steigerwalt et al. reported a multistep deposition and reactive decomposition of a precursor molecule containing one Pt and one Ru atom on herringbone graphitic carbon nanofibers (GCNFs), which resulted in a Pt-Ru/GCNF nanocomposites containing Pt-Ru alloy nanoclusters widely dispersed on the GCNF surface.[223] The nanocomposites have a total metal content of 42 wt% with a bulk Pt/Ru atomic ratio of 1:1, and metal alloy nanoclusters have average particle sizes of 6-7 nm. Comparative testing of those nanocomposites and unsupported Pt-Ru colloid with similar surface area and catalyst particle size reveals a 50% increase in performance for the Pt-Ru/GCNF nanocomposites. Guo et al. reported CNFs were used as supports to prepare highly dispersed Pt-Ru catalysts for DMFCs.[216] The results show that the diameter of Pt-Ru nanoparticles is around 5 nm in Pt-Ru/CNF composites, and the CNF-supported catalysts give better performance than commercial catalysts when the current density is higher than 50 $mA\,cm^{-2}$ in spite of low methanol oxidation peak current density (Figure 1.20). This improvement can be ascribed to the specific surface and structural properties of CNFs.

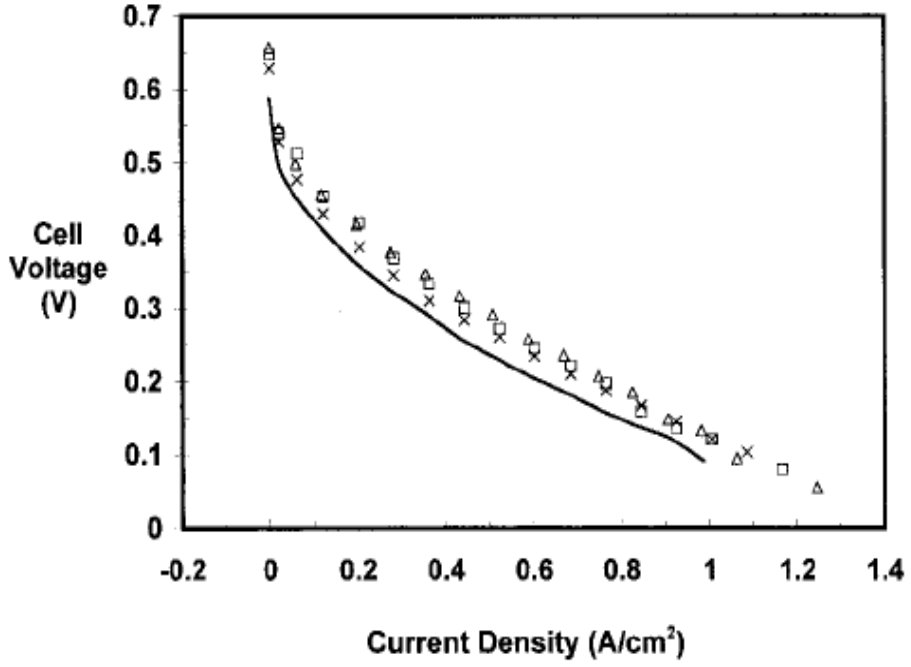

Figure 1.20. *I-V* curves comparing the performance of Pt-Ru nanocomposites at a loading of 1.5 mg cm^{-2} with (triplicate) and without (solid line) CNF supports as anode catalysts in DMFCs.

1.2.8.2.2. Electrodeposition

The electrodeposition method, which is used for attaining Pt particles onto the carbon supports, has been developed by several research groups to improve the Pt utilization and reduce Pt loading.[224-227] The synthesis procedure for Pt/CNT or Pt/CNF catalysts using electrodeposition is showed in Figure 1.21, which is similar to that used in the electroless

deposition.

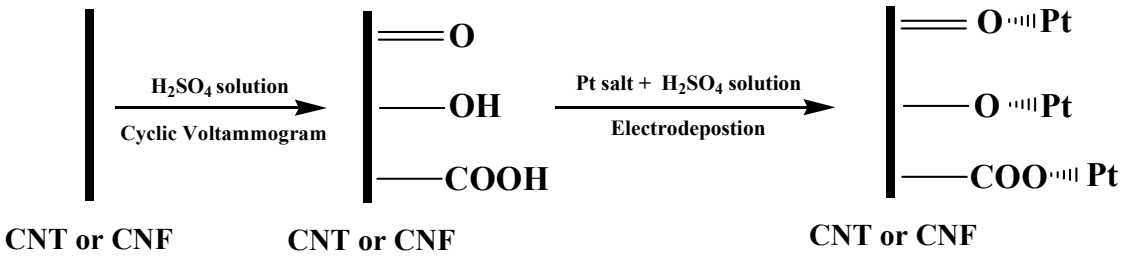

Figure 1.21. Schematic diagram illustrating the procedure of electrodepositing Pt nanoparticles onto a CNT or CNF.

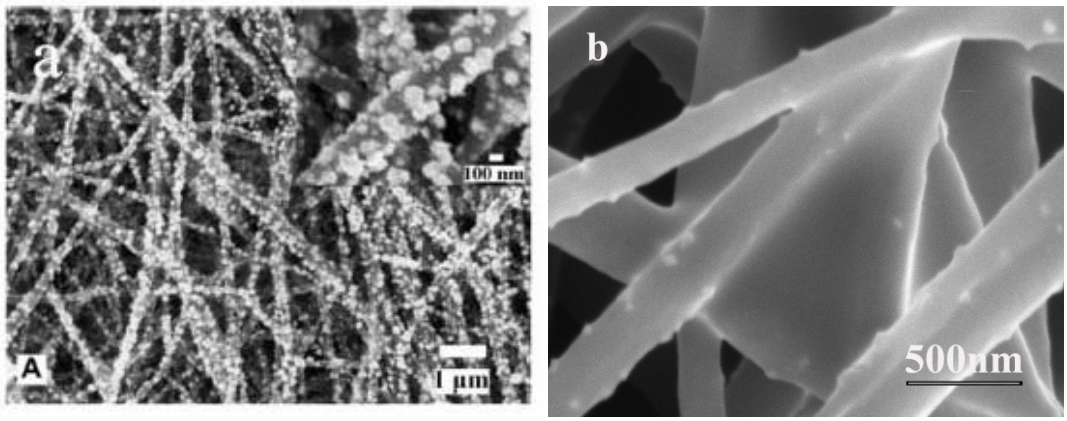

Figure 1.22. SEM images of as prepared Pt/CNF electrode using multi-cycle CVs in 2.0 M H_2PtCl_6 + 0.5 M H_2SO_4 solutions (a), and Pt/CNFs prepared with the electrodeposition potentials -0.2 V (*vs.* Ag/AgCl/4.0 M KCl) in 5.0 mM $H_2PtCl_6 \cdot xH_2O$ + 1.0 M H_2SO_4 solutions (b).

In the electrodeposition, CNTs or CNFs are first cycled in a sulfuric acid solution between -0.7 and +1.2 V to oxidize the surface. During that process, various surface functional groups such as quinoid (=O), hydroxy (-OH) and carboxyl (-COOH) were produced, which can supply defect sites for the Pt nanoparticle deposition.[228] For instance, Wang et al. have successfully prepared Pt/CNT catalysts by electrodepositing Pt nanoparticles on the CNTs in a H_2SO_4 + H_2PtCl_6 solution.[229] The results show that although the Pt loading is 0.2 mg cm^{-2} on the CNT surface, and the average diameter of the Pt particle was much large (*i.e.* 25 nm) compared to the commercially available Pt/C catalysts, and the fuel cell performance was also lower than that of the conventional catalyst at a comparable Pt loading. Li et al. used the cyclic voltammogram method to deposit Pt particles onto CNFs, but the diameters of deposited Pt nanoclusters are too large (50-200 nm) for practical fuel cell applications (Figure 1.22a).[230] In comparision, Lin et al. reported the preparation and characterization of Pt/CNFs by the electrodeposition of smaller Pt nanoparticles (≤ 55 nm) onto electrospun CNFs under different potentials (Figure 1.22b).[231]

1.2.8.2.3. Non-covalent method

In order to anchor and deposit catalyst nanoparticles homogeneously on the surface of CNTs and CNFs, many traditional harsh oxidative methods, such as refluxing in concentrated mixtures of H_2SO_4 and/or HNO_3 and cycling in H_2SO_4 solution using cyclic voltammograms, have been utilized. However, those methods often result in lots of defects on CNTs and

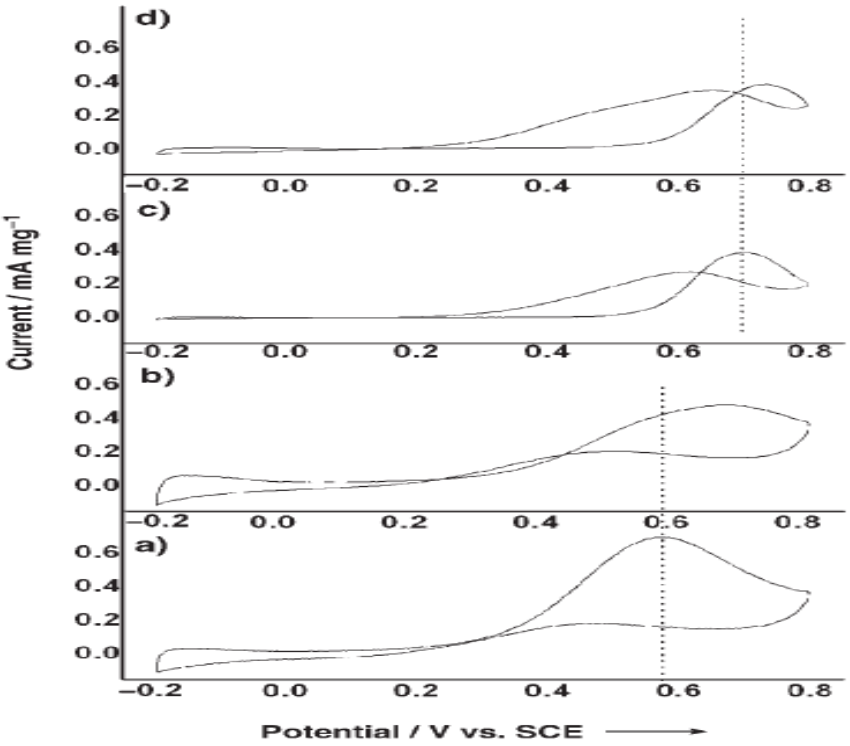

Figure 1.23. Cyclic voltammograms of Pt/$RuO_2{\cdot}xH_2O$/CNT (a), PtRu/Vulcan (b), Pt/CNT (c), and Pt/Vulcan (d).

CNFs, which are harmful to the electrochemical active surface area of Pt or Pt alloy electrocatalysts and their durability during fuel cell operation. Recently, a novel noncovalent functionalization approach of CNTs has attracted particular attention because it enables the surface activation of CNTs without destroying the intrinsic properties of CNTs.[85, 232, 233] For instance, Cao et al. synthesized Pt/$RuO_2{\cdot}xH_2O$/CNT composite catalysts by pre-coating CNTs with 1 % sodium dodecyl sulfate and then depositing Pt using ethylene glycol as a

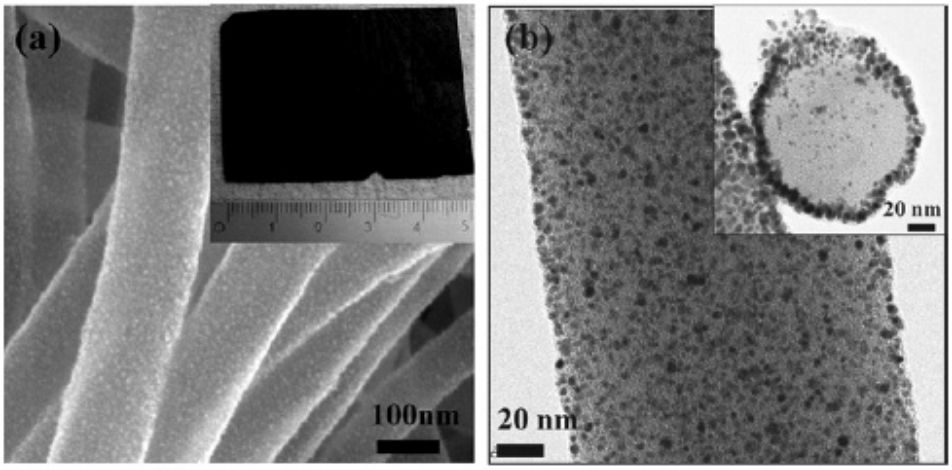

Figure 1. 24. SEM image of a Pt-loaded CNF mat and its optical micrograph in the inset (a), and TEM image of a Pt-loaded CNF and its cross section in the inset (b).

reducing agent in H_2PtCl_6 solution. As shown in Figure 1.23, the Pt/$RuO_2{\cdot}xH_2O$/CNTs had the best activity for the direct electrooxidation of methanol compared with the catalysts Pt-Ru/Vulcan, Pt/CNT, and Pt/Vulcan.[234] Xuyen et al. demonstrated that Pt nanoparticles can be loaded on the surface of polyimide-based (PI) nanofibers via an immobilization process induced by hydrolysis, where the binding of Pt acetylacetonate [$Pt(acac)_2$] on hydrolyzed PI is strong with a binding energy of -4.3 eV, which originates mostly from Pt-O binding and π-stacking between (acac) and poly(amic acid).[235] The uniform distribution and sizes of Pt nanoparticles were controlled further by carbonization, which is showed in Figure 1.24. The cyclic voltammetry demonstrated that this CNF mat can be utilized as the electrodes of fuel cells. Lin et al. prepared Pt/carbon composite nanofibers by depositing Pt

nanoparticles directly onto electrospun CNFs using a polyol processing technique.[236] The morphology and size of Pt nanoparticles were controlled by 1-aminopyrene functionalization. The noncovalent functionalization of CNFs by 1-aminopyrene is simple and can be carried out at ambient temperature without damaging the integrity and electronic structure of CNFs. Results show that Pt/1-aminopyrene-functionalized CNFs possess the properties of high active surface area and improved performance towards the electrocatalytic oxidation of methanol.

1.2.8.2.4. Microwave heating process

Recently, a microwave heated polyol process was employed to synthesize carbon-supported metal catalysts for DMFCs.[237-239] In this process, a polyol (ethylene glycol) solution, which contains catalyst metal precursors, is refluxed at around 393-443 K in order to homogeneously decompose the polyol and create an active reducing agent for the deposition of metal ions. Unlike the conventional heating strategy, the microwave heating process can accelerate the reduction of the metal ions on the surface of carbon supports. Moreover, the homogeneous microwave heating could reduce the temperature and concentration gradients in the solution, resulting in a more uniform environment for the nucleation and growth of metal particles.[240] Therefore, as a rapid, uniform and effective heating method, the microwave heating has become an attractive alternative approach for the synthesis of

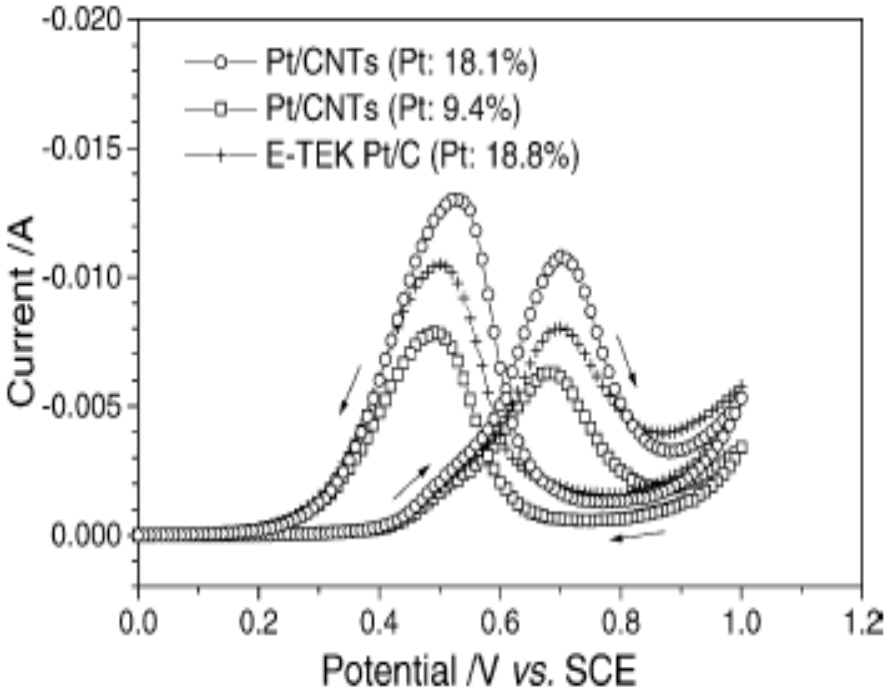

Figure 1.25. CVs of methanol electrooxidation over the microwave synthesized Pt/CNTs and E-TEK Pt/C catalysts in 2 M CH_3OH + 1 M H_2SO_4 at a scan rate of 20 mV s^{-1} at room temperature.

carbon-supported Pt catalysts. For example, Liu et al. employed a microwave heated polyol process for the synthesis of Pt/CNT catalysts.[241] Highly dispersed Pt nanoparticles of 3.6±0.3 nm on CNTs were obtained, which is smaller than that of Pt/Vulcan catalysts (3.8±0.3 nm). In addition, the fuel cell performance showed that the Pt/CNT catalyst has greater catalytic activity towards the oxygen reduction than that of Pt/Vulcan catalysts (Figure 1.25). Steigerwalt et al. reported the preparation of Pt-Ru/graphitic CNF

nanocomposites, using of a bimetallic precursor and microwave heating process.[242] The use of microwave heating permits rapid preparation of these nanocomposites and leads to Pt-Ru nanoclusters of nearly uniform size.

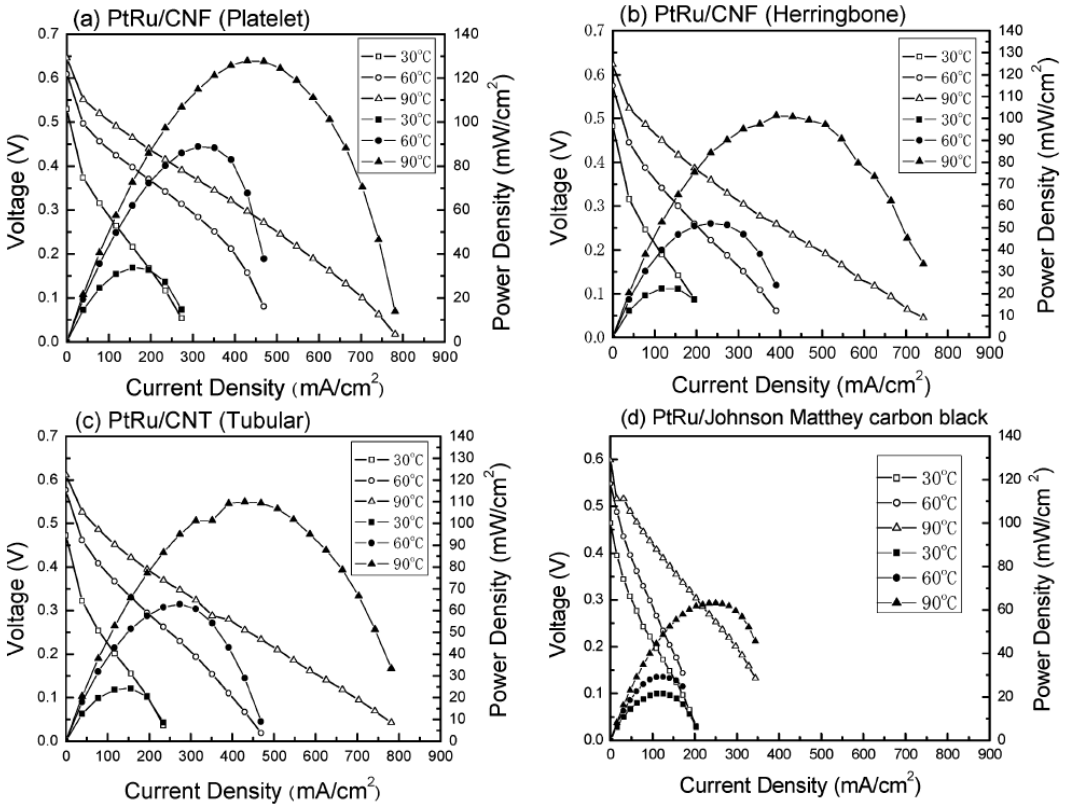

Figure 1.26**.** Electrocatalytic activity of Pt-Ru catalysts loaded on platelet (a), herringbone (b), tubular CNFs (c), and carbon black Vulcan XC72R (d). Open and solid symbols represent voltage and power density, respectively.

Tsuji et al. prepared Pt-Ru alloy nanoparticles supported on CNFs within a few minutes by

using a microwave-polyol method.[243] Three types of CNFs with very different surface structures, such as platelet, herringbone, and tubular ones, were used as carbon supports. It was found that the methanol fuel cell activities of Pt-Ru/CNF catalysts were in the order of platelet, tubular, and herringbone, and the methanol fuel cell activities of PtRu/CNFs measured at 60 °C were 1.7-3.0 times higher than that of a standard Pt-Ru catalyst loaded on carbon black Vulcan XC72R, which is showed in Figure 1.26.

1.2.8.2.5. Other methods

Except the methods mentioned above, many other methods, such as the colloid method,[244-247] sputter-deposition technique,[182, 248] and physical methods,[249-252] have been used to deposit Pt or Pt alloy nanoparticles onto CNTs and CNFs, and their electro-catalytic ability toward the methanol oxidation at the anode and the oxygen reduction at the cathode at DMFCs have also been studied.

CHAPTER 2. OBJECTIVES

Membrane electrode assembly (MEA) is the key component of DMFCs and is consisted of a polymer electrolyte membrane and two catalyst-loaded porous electrodes for methanol oxidation at the anode and oxygen reduction at the cathode. The overall methanol conversion process, typically catalyzed by Pt or Pt alloy in acidic solution, is expressed using the equation (1.4) in Chapter one. For the electrode reactions to occur, the catalyst particles must have simultaneous exposure to the reactants, protons, and electrons. In conventional fuel cell electrodes, catalyst-loaded carbon particles are typically bound (*e.g.,* Vulcan XC-72 carbon black-supported Pt) with Nafion®, in which carbon black facilitates electron transport and Nafion® conducts protons. A high catalyst loading in these electrodes is typically required because they cannot ensure a simultaneous access of all catalyst particles to the fuel, electron-conducting diffusion layer, and proton-conducting electrolyte. Therefore, the high cost of precious Pt and Pt alloy electrocatalysts, one of the most significant barriers here, prevents the commercial applications of DMFCs.

Moreover, methanol should be oxidized spontaneously when the anode potential is above 0.002 V (*vs.* SHE), and oxygen should be reduced spontaneously when the cathode assumes a potential below 1.23 V (*vs.* SHE). However, in practical DMFCs, poor electrode kinetics (kinetic losses) at both the anode and cathode cause the electrode process to deviate from their ideal thermodynamic behavior, thereby resulting in an undesired reduction of the cell

efficiency.

To achieve practical cell efficiency, a conducting material is needed to support particle catalysts for the applications in DMFCs. Carbon nanomaterials are currently being considered as suitable catalyst supports in DMFCs because of their unique graphite properties combined with three-dimensional flexible structures. Among various carbon nanomaterials, carbon nanotubes (CNTs) and carbon nanofibers (CNFs) are promising support materials for catalysts in DMFCs due to their unique 1-dimensional structure, high electronic and thermal conductivities, and good electrochemical stability. Compared with CNTs, CNFs are inexpensive and can be produced with various controlled structures at relatively high speeds.

In our work, we will focus on the development of highly active electrode catalysts coupled with a suitable electrode structure for the oxidation of methanol at the anode and the reduction of oxygen at the cathode to attain the high efficiency of DMFCs, and subsequently lowering the cost. Two approaches, *i.e.,* chemical deposition and electrodeposition, will be used to prepare these catalyst-loaded CNF electrodes. The following objectives will be completed for both methods:

1. At the anode:

    i) To fabricate Pt & Pt-Ru catalyst-loaded CNF electrodes by combining

electrospinning with the electrodeposition or chemical deposition technique;

ii) To evaluate the performance of Pt & Pt-Ru catalyst-loaded CNF electrodes toward the oxidation of methanol;

iii) To obtain optimized Pt & Pt-Ru catalyst-loaded CNF electrodes by selectively adjusting the electrode structures and to utilize such electrodes in DMFCs.

2. At the cathode:

i) To fabricate Pt-Pd catalyst-loaded CNF electrodes by combining electrospinning with the electrodeposition or chemical deposition technique;

ii) To evaluate the performance of Pt-Pd catalyst-loaded CNF electrodes toward the reduction of oxygen;

iii) To obtain optimized Pt-Pd catalyst-loaded CNF electrodes by selectively adjusting the electrode structures and to utilize such electrodes in DMFCs.

CHAPTER 3. OVERALL EXPERIMENTAL

3.1. Chemicals and reagents

Polyacrylonitrile (PAN), N,N-dimethylformamide (DMF), chloroplatinic acid hydrate ($H_2PtCl_6 \cdot xH_2O$), ruthenium chloride ($RuCl_3$), ammonium hexachloropalladate [$(NH_4)_2PdCl_6$], 1-aminopyrene (1-AP), ethylene glycol (EG), nitric acid (HNO_3, 70%), potassium hexacyanoferrate (II) ($K_4[Fe(CN)_6]$), sulfuric acid (H_2SO_4), methanol (CH_3OH), and perchloric acid ($HClO_4$) were purchased from Sigma-Aldrich, and they were used without further purification. Deionized water was used throughout.

3.2. Synthesis of CNFs

A DMF solution of 8 wt% PAN was prepared at 60 ^oC, with mechanical stirring for three hours. The electrospinning was conducted using a Gamma ES40P-20W/DAM variable high voltage power supply under a voltage of 15 kV. Under high voltage, a polymer stream was ejected through a syringe and accelerated toward the nanofiber collector, during which the solvent was rapidly evaporated. Aluminum foil was placed over the collector plate of the

electrospinning apparatus to collect electrospun PAN fibers. These PAN nanofibers were first stabilized in an air atmosphere at 280 ^{o}C for 2 hours at the heating rate 5 min^{-1} and then carbonized at 700 ^{o}C for 1 hour in nitrogen atmosphere at the heating rate 2 ^{o}C min^{-1}. The resultant CNFs formed free-standing porous nonwoven membranes and were directly used as the support in the chemical deposition or electrodeposition of Pt or Pt alloy nanoparticles.

3.3. Structural characterization

X-ray diffraction (XRD) analysis was performed with a Philips XLF ATPS XRD 100 diffractometer using CuKα radiation (λ=1.5405 Å). The operating voltage and current were 40.0 kV and 60.0 mA, respectively. Raman spectra of Pt or Pt alloy/CNFs were obtained using Horiba Jobin Yvon LabRam Aramis Microscope with 633 nm HeNe Laser. Element analysis was studied by using a CHN Elemental Analyzer.

The structure of CNFs and Pt or Pt alloy/CNFs, which were deposited onto 200 mesh carbon-coated Cu grids, was evaluated using a Transmission Electron Microscope (Hitachi HF-2000 TEM) at 200 kV. These CNFs and Pt or Pt alloy/CNFs were also examined using a JEOL JSM-6360LV FESEM at 15 kV. The diameters of Pt or Pt alloy nanoparticles were determined by measuring 80 randomly selected particles using an ImageJ software package.

3.4. Electrochemical performance

The electrochemical measurements of Pt or Pt alloy/CNFs were performed in a three-electrode cell at 25 ^{o}C on an electrochemical workstation (AQ4 Gamry Reference 600, USA). The cell consisted of a working electrode (Pt or Pt alloy/CNFs), a counter electrode (Pt wire), and a reference electrode (Ag/AgCl/4.0 M KCl). Nitrogen was used to bubble the testing solutions for at least 30 minutes before the measurements, and then was used continually to protect the experiment environment. All the electrochemical potentials were measured and reported with respect to Ag/AgCl/4.0 M KCl.

The measurement of hydrogen electrosorption was conducted by cyclic voltammograms (CVs) of Pt or Pt alloy/CNF electrodes in 0.5 M H_2SO_4 at 50 $mV \cdot s^{-1}$ to determine the electrochemically active surface areas (EASAs). The electron transfer properties were determined by CVs of Pt or Pt alloy/CNFs in 5.0 mM $K_4[Fe(CN)]_6$ + 0.50 M KCl at 50.0 $mV \cdot s^{-1}$. CV responses of Pt or Pt alloy/CNFs in 0.125 M CH_3OH + 0.2 M H_2SO_4 at 5 $mV \cdot s^{-1}$ were also measured to study their activities on the methanol oxidation.

CHAPTER 4. ANODE: CARBON NANOFIBER-SUPPORTED PLATINUM BY CHEMICAL DEPOSITION

Abstract

Pt/carbon composite nanofibers were prepared by depositing Pt nanoparticles directly onto electrospun CNFs using a polyol processing technique. The morphology and size of Pt nanoparticles were controlled by 1-aminopyrene functionalization. The noncovalent functionalization of CNFs by 1-aminopyrene is simple and can be carried out at ambient temperature without damaging the integrity and electronic structure of CNFs. The resulting Pt/carbon composite nanofibers were characterized by running cyclic voltammogram in 0.5 M H_2SO_4 and 0.125 M CH_3OH + 0.2 M H_2SO_4 solutions, respectively. Results show that Pt/carbon composite nanofibers with 1-aminopyrene functionalization have Pt nanoparticles with smaller size and better distribution, compared with those treated with conventional acids. Moreover, Pt/1-aminopyrene functionalized CNFs possess the properties of high active surface area, improved performance towards the electrocatalytic oxidation of methanol, and relatively good long-term stability.

4.1. Introduction

Direct methanol fuel cells (DMFCs) have been considered as one of ideal fuel cell systems for applications as electric vehicles and electronic portable devices, due to their high power density, relatively quick start-up, rapid response to varying loading, and low operating temperatures.[90, 107, 129] The methanol conversion is produced in membrane electrode assembly (MEA), which is the key component of DMFCs and is consisted of a polymer electrolyte membrane and catalyst loaded porous electrodes for methanol oxidation at the anode and oxygen reduction at the cathode. The methanol conversion, typically catalyzed by Pt or Pt alloy in acidic solution, can be expressed using the following equation: [253]

$$CH_3OH + H_2O \rightarrow CO_2 + 6H^+ + 6e^- \qquad (4.1)$$

$$E^o\,(\mathrm{MOR}) = 0.016\mathrm{V}\ \textit{vs.}\ \mathrm{SHE\ at\ 25\ ^oC}$$

For the reaction to happen, the catalyst particles must have simultaneous exposure to the reactants, protons, and electrons. Thus nanosized Pt and Pt alloy supported on carbon black are always used as the most important electrocatalysts in DMFCs.[2, 215, 216, 229, 254] However, the high cost of precious Pt and Pt alloy electrocatalysts, one of the most significant barriers here, prevents the commercial applications of DMFCs. Therefore, the development of highly active electrode catalysts coupled with a suitable electrode structure for the oxidation of methanol is an important subject for attaining the high efficiency in DMFCs, and subsequently lowering the cost.

Carbon nanomaterials are currently being considered as the suitable catalyst supports in DMFCs,[115, 215, 255] because of their unique graphite properties combined with three-dimensional flexible structures. Among various carbon nanomaterials, carbon nanotubes (CNTs) and carbon nanofibers (CNFs), are promising support materials for catalysts in direct methanol fuel cells, due to their unique 1-dimensional structure, high electronic and thermal conductivities, and good electrochemical stability.[256, 257] Compared with CNTs, CNFs are inexpensive and can be produced with various controlled structures at relatively high speeds. However, both of them are chemically inert, thus it is necessary to activate their graphitic surface because the deposition, distribution and size of Pt or Pt alloy nanoparticles strongly depend on the surface properties of CNTs and CNFs.[106]

In order to anchor and deposit catalyst nanoparticles well on the surface of CNTs and CNFs, many traditional harsh oxidative methods, such as refluxing in concentrated mixtures of H_2SO_4 and HNO_3 and cycling in H_2SO_4 solution using cyclic voltammogram, have been widely utilized. However, those methods result in lots of defects on CNTs and CNFs, which are harmful to the electrochemical active surface area of Pt or Pt alloy electrocatalysts and their durability during fuel cell operation. Recently, a novel noncovalent functionalization approach of CNTs has attracted particular attention because it enables the surface activation of CNTs without destroying the intrinsic properties of CNTs.[85, 233] For instance, Cao et al. synthesized Pt/$RuO_2{\cdot}xH_2O$/CNT composite catalysts by pre-coating carbon nanotubes with 1 % sodium dodecyl sulfate and then depositing Pt using ethylene glycol as a reducing agent in H_2PtCl_6 solution. These Pt/$RuO_2{\cdot}xH_2O$/CNTs show good activity for the direct

electrooxidation of methanol.[234]

In this chapter, we report the preparation and characterization of Pt/carbon composite nanofibers (Pt/CNFs) by the combination of 1-aminopyrene functionalization and a polyol processing technique, *i.e.*, functionalizing electrospun CNFs with 1-aminopyrene, followed by the deposition of Pt using ethylene glycol as a reducing agent. Compared with the conventional acid-treated CNFs, the most important advantage of this approach is that the 1-aminopyrene functionalization treatment preserves the integrity and the electronic structure of CNFs. Moreover, Pt nanoparticles with smaller diameter and better distribution can be obtained on CNFs and the resultant Pt/carbon composite nanofibers have high electrochemically active surface area and good activity toward the methanol oxidation.

4.2. Experimental

4.2.1. Chemicals and reagents

Polyacrylonitrile (PAN), N,N-dimethylformamide (DMF), chloroplatinic acid hydrate ($H_2PtCl_6 \cdot xH_2O$), 1-aminopyrene (1-AP), ethylene glycol (EG), nitric acid (HNO_3, 70%), sulfuric acid (H_2SO_4), and methanol (CH_3OH) were purchased from Sigma-Aldrich, and they were used without further purification. Deionized water was used throughout.

4.2.2. Synthesis of CNFs

A DMF solution of 8 wt% PAN was prepared at 60 ^{o}C, with mechanical stirring for three hours. The electrospinning was conducted using a Gamma ES40P-20W/DAM variable high voltage power supply under a voltage of 15 kV. Under high voltage, a polymer stream was ejected through a syringe and accelerated toward the nanofiber collector, during which the solvent was rapidly evaporated. Aluminum foil was placed over the collector plate of the electrospinning apparatus to collect electrospun PAN fibers. These PAN nanofibers were first stabilized in an air atmosphere at 280 ^{o}C for 2 hours at the heating rate 5 min^{-1} and then carbonized at 700 ^{o}C for 1 hour in nitrogen atmosphere at the heating rate 2 ^{o}C min^{-1}. The resultant CNFs formed free-standing porous nonwoven membranes and were directly used as a support in the chemical deposition of Pt nanoparticles.

4.2.3. 1-AP functionalization and acid treatment of CNFs

The procedure of the noncovalent functionalization of CNFs using 1-AP is described as follows. CNFs (0.2 g) and 1-AP (0.2 g) were added into an ethanol solution (30 ml), which was stirred mechanically for 1 hour and stored at room temperature for 24 hours. The solution was then filtered and washed for several times, and the treated CNFs were dried in a vacuum oven at 70 °C for 5 hours and were collected as 1-aminopyrene functionalized CNFs

(1-AP-CNFs). For comparison, CNFs were also functionalized by a conventional acid treatment, *i.e.*, CNFs (0.2 g) were refluxed in a mixed strong acid solution (50 ml H_2SO_4:HNO_3 in 3:1 v/v ratio) at 80 ^oC for 3 hours. The acid-treated CNFs are denoted as AO-CNFs. In addition, un-treated CNFs (UT-CNFs) were also used in the work as a control.

4.2.4. Synthesis of Pt/CNFs

To deposit Pt nanoparticles on 1-AP-CNFs, 1-AP-CNFs (0.3 g) was mixed with approximate amount of $H_2PtCl_6 \cdot xH_2O$ in 50 ml EG solution under ultrasonication in a three-neck flask. The solution was then refluxed in 70 ^oC for almost 6.0 hr until the solution changed from light yellow to dark brown, indicating the reduction and formation of Pt nanoparticles on CNFs. The above solution was filtered and washed for several times, and the resulting Pt/1-AP-CNFs (with metal loading of 20, 40, and 60 wt%) were dried in vacuum oven at 140 °C for a day. Pt/acid-functionalized CNFs (Pt/AO-CNFs) and Pt/untreated CNFs (Pt/UT-CNFs) with Pt loading amount of 20 wt% were also prepared using the procedure described above. The metal loadings were confirmed using a CHN Elemental Analyzer.

4.2.5. Structural characterization of Pt/CNFs

X-ray diffraction (XRD) analysis was performed with a Philips XLF ATPS XRD 100

diffractometer using CuKα radiation (λ=1.5405 Å). The operating voltage and current were 40.0 kV and 60.0 mA, respectively. Raman spectra of Pt/CNFs were obtained using Horiba Jobin Yvon LabRam Aramis Microscope with 633 nm HeNe Laser.

The structure of CNFs and Pt/CNFs, which were deposited onto 200 mesh carbon-coated Cu grids, was evaluated using a Transmission Electron Microscope (Hitachi HF-2000 TEM) at 200 kV. The diameters of Pt nanoparticles were determined by measuring 80 randomly selected particles using an ImageJ software package.

4.2.6. Electrochemical properties of Pt/CNFs

The electrochemical measurements of Pt/CNFs were performed in a three-electrode cell at 25 ^{o}C on an electrochemical workstation (AQ4 Gamry Reference 600, USA). The cell consisted of a working electrode (Pt/CNFs), a counter electrode (Pt wire), and a reference electrode (*Ag*/*AgCl*/4.0 M KCl). Nitrogen was used to bubble the testing solutions for at least 30 minutes before the measurements, and then was used continually to protect the experiment environment. All the electrochemical potentials were measured and reported with respect to Ag/AgCl/4.0 M KCl.

The measurement of hydrogen electrosorption was conducted by cyclic voltammograms (CVs) of Pt/CNF electrodes in 0.5 M H_2SO_4 at 50 $mV \cdot s^{-1}$ to determine the electrochemically

active surface areas (EASAs). CV responses of Pt/CNFs in 0.125 M CH_3OH + 0.2 M H_2SO_4 at 5 $mV \cdot s^{-1}$ were also measured to study their activities on the methanol oxidation.

4.3. Results and Discussion

4.3.1. CNF treatment and Pt deposition

Figure 4.1 shows schematic diagram of the synthesis of Pt/UT-CNFs, Pt/AO-CNFs and Pt/1-AP-CNFs, respectively. The surface of UT-CNFs is chemically inert and does not have any functional groups, which makes the Pt deposition on UT-CNF surface relatively un-controlled.

The Pt deposition process is changed when CNFs are pre-treated with H_2SO_4 + HNO_3 solution. During the treatment, various surface functional groups such as quinoid (=O), hydroxy (-OH) and carboxyl (-COOH) are produced, which can supply defect sites for chemical reaction.[258] After adding $H_2PtCl_6 \cdot xH_2O$ and EG, $PtCl_6^{2-}$ ions can be reduced by EG and deposited on the defect sites created during the acid treatment.

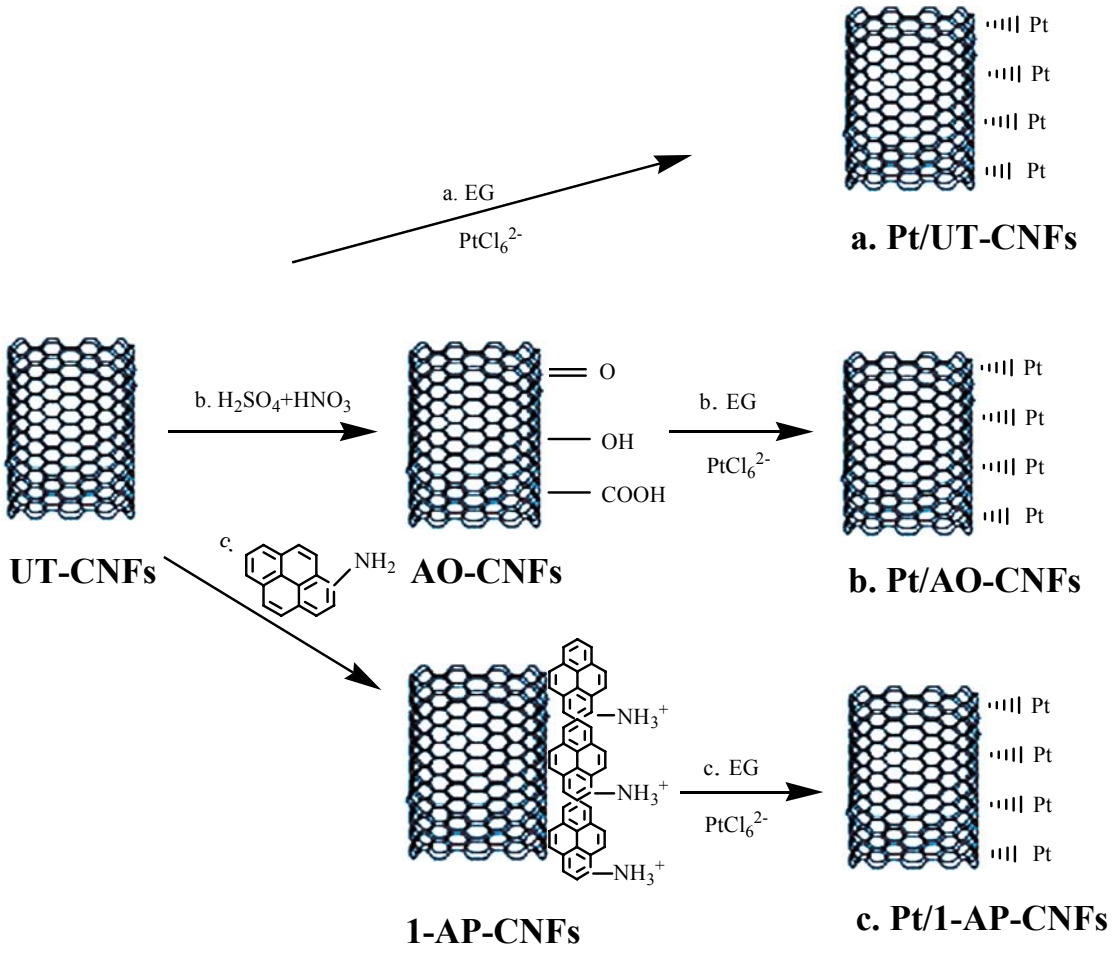

Figure 4.1. Schematic diagram of the synthesis of Pt/UT-CNFs (a), Pt/AO-CNFs (b), and Pt/1-AP-CNFs (c).

Unlike H_2SO_4 + HNO_3 solution that reacts with CNFs, the reagent 1-AP, a bifunctional molecule with a pyrenyl group and an amino functional group, does not have chemical reaction with CNFs and hence are used to carry out the noncovalent functionalization of CNF surface. Typically, the pyrenyl group of 1-AP can be attached onto the basal plane of graphite

via π-stacking.[259] As a result, 1-AP can be immobilized on CNFs through the adsorption of pyrenyl groups onto the inherently hydrophobic surface of CNFs. The introduction of $H_2PtCl_6 \cdot xH_2O$ results in a solution with a pH value of around 6.0 (*i.e.*, slightly acidic). At the same time, the amino groups of immobilized 1-AP molecules become weakly positively charged, which leads to the self-assembly of negatively charged Pt precursor, $PtCl_6^{2-}$ ions. After that, the chemical deposition in the presence of EG reduces the self-assembled Pt precursor, forming Pt nanoparticles on the CNF surface. Therefore, in the case of 1-AP-CNFs, the $PtCl_6^{2-}$ ions are attached onto CNF surface first, and then are reduced to Pt nanoparticles. The Pt deposition processes on UT-CNFs, AO-CNFs, and 1-AP-CNFs are different, and hence the resultant composite nanofibers have different Pt deposition structures, as discussed below.

4.3.2. TEM images of Pt/CNFs

Figure 4.2 shows TEM images of UT-CNFs and three different Pt/CNFs. In Figure 4.2a, UT-CNFs exhibit long and straight fibrous morphology with relatively uniform diameters ranging from 100 to 300 nm. It is also seen that before deposition, CNF surface is smooth and there are no particles loaded. However, Pt nanoparticles are observed on the surface of CNFs after Pt deposition (Figure 4.2b-d). In Pt/UT-CNFs (Figure 4.2b), there are just a few relatively-large Pt particles on the surface of UT-CNFs. For surface-treated CNFs, smaller Pt particles are shown on both AO-CNFs and 1-AP-CNFs (Figures 4.2c-d). However, a large

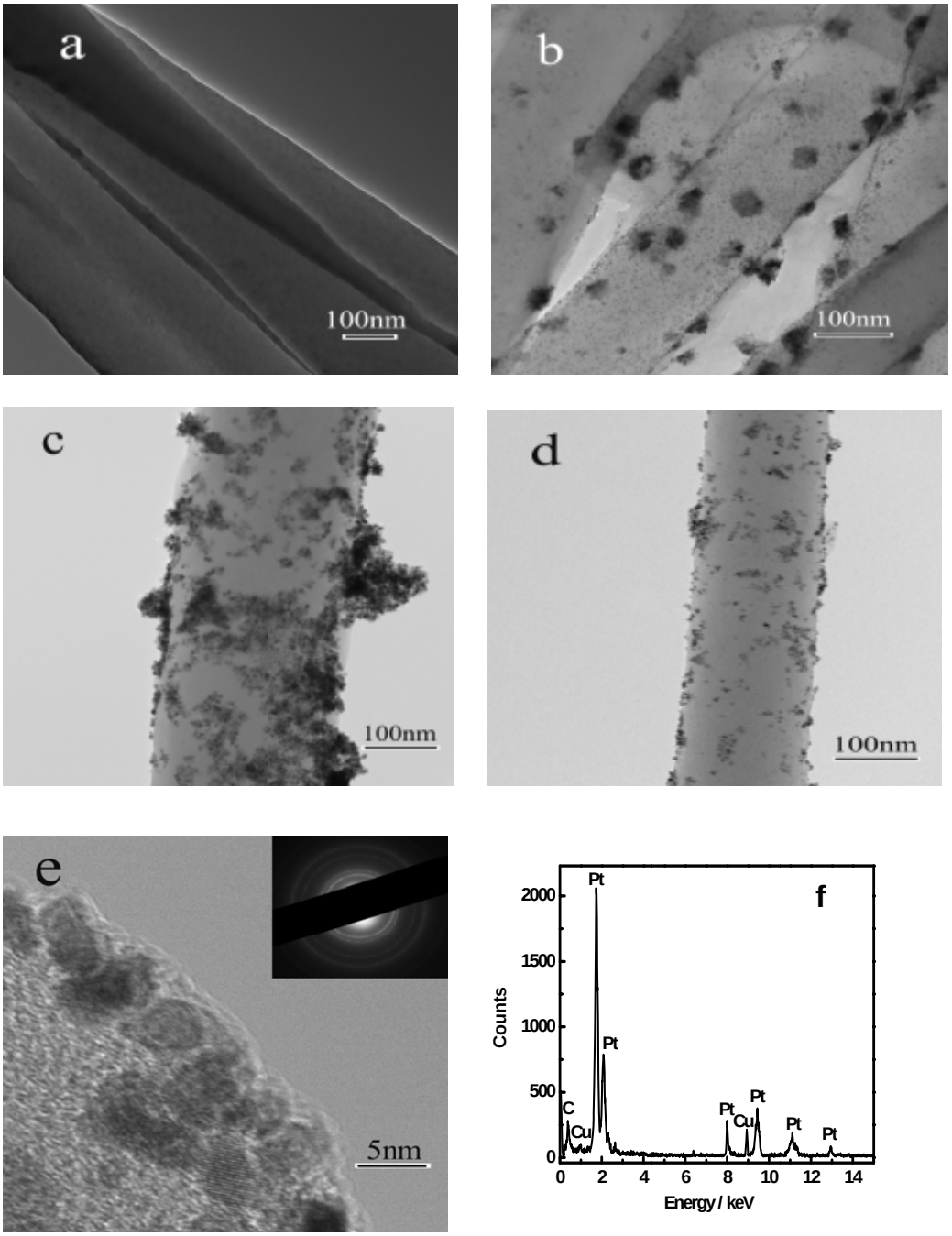

Figure 4.2. TEM images of UT-CNFs (a), Pt/UT-CNFs (b), Pt/AO-CNFs (c), Pt/1-AP-CNFs (d), and high resolution TEM image (e) and EDS spectrum (f) of Pt/1-AP-CNFs. Inset in (e) is the electron diffraction pattern. The Pt loading amount is 20 wt %.

amount of Pt aggregates are found on the surface AO-CNFs, which are caused by the defect sites of CNFs randomly produced during acid treatment. Compared with Pt/AO-CNFs, fewer Pt agglomerates can be seen on the surface of Pt/1-AP-CNFs because of the immobilization of bi-functional 1-AP molecules, which offer uniformly distributed active sites for anchoring metal ions and metal nanopartciles. Figures 4.2e and f shows the high resolution TEM image and energy dispersive X-ray spectroscopy (EDS) of Pt/1-AP-CNFs, respectively. Both confirm the presence of Pt particles on the surface of 1-AP-CNFs. The copper peaks in Figure 4.2f belong to the TEM grid background.

4.3.3. Pt diameter distributions of Pt/CNFs

Figure 4.3 shows the diameter distributions of Pt nanoparticles on Pt/UT-CNFs, Pt/AO-CNFs, and Pt/1-AP-CNFs, respectively. The Pt loading amount is the same, *i.e.*, 20 wt%, for all three Pt/CNFs. As shown in Figure 4.3a, when Pt particles are deposited onto UT-CNFs, the average diameter of Pt nanoparticles is around 21 nm and the diameter distribution is abroad. On one hand, Pt particles as small as 2.0 nm in diameter can be found, but on the other hand, the agglomeration of Pt particles is also severe. However, when the surface of CNFs is oxidized, the diameter of Pt nanoparticles decreases to around 4.2 nm (Figure 4.3b). The distribution of Pt nanoparticles also become narrower, and the agglomeration problem became less severe. When the surface of CNFs is functionalized by1-AP, Pt nanoparticles are uniformly distributed without much agglomeration and the average diameter became smaller,

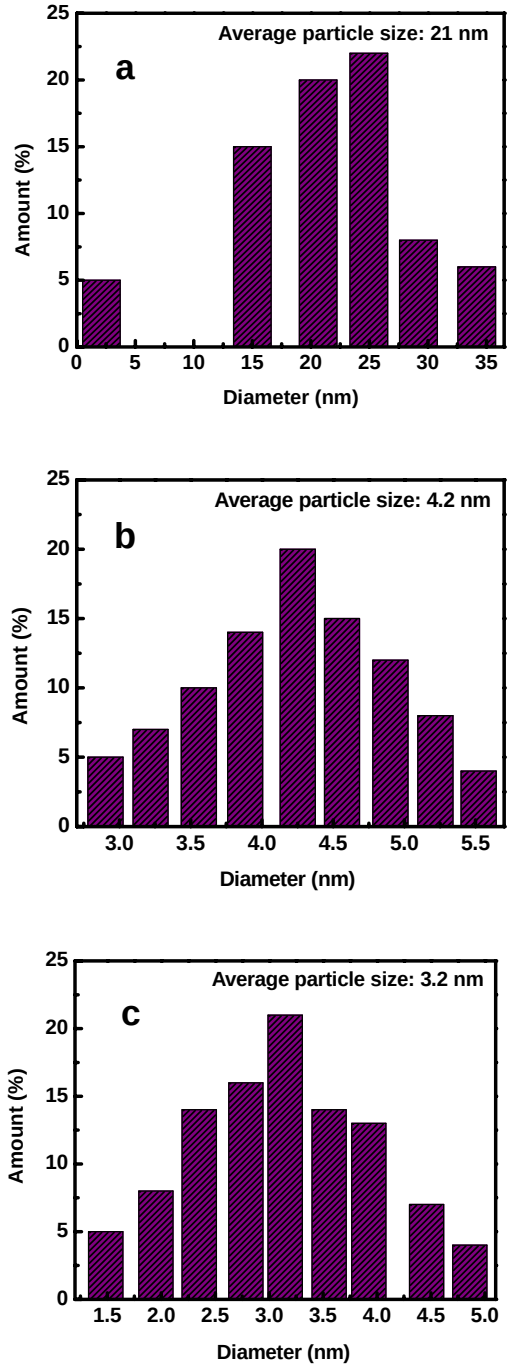

Figure 4.3. Diameter distributions of Pt nanoparticles on Pt/UT-CNFs (a), Pt/AO-CNFs (b), and Pt/1-AP-CNFs (c). The Pt loading amount is 20 wt%.

i.e., 3.2 nm (Figure 4.3c). The small diameter and relatively narrow diameter distribution of Pt nanoparticles on 1-AP-CNFs is clearly due to the immobilization of bifunctional 1-AP, which offers uniformly-distributed active sites for anchoring metal ions and metal nanoparticles. Thus, 1-AP-functionalized CNFs are more effective supports than the conventional acid-oxidized CNFs.

4.3.4. TEM images of Pt/1-AP-CNFs

Figure 4.4 shows TEM images and diameter distributions of Pt/1-AP-CNFs with different Pt loadings (40 and 60 wt%). Compared with Pt/1-AP-CNFs with a Pt loading of 20 wt% (Figure 4.2), more Pt nanoparticles are evenly distributed on the surface of 1-AP-CNFs when the Pt loading amount is 40 wt%. However, when the Pt loading amount is more than 40 wt% (*i.e.,* 60 wt%), the surface of 1-AP-CNFs is almost fully covered by Pt nanoparticles, and significant amount of Pt particle aggregates are also found. The relatively small Pt nanoparticles and their uniform distribution (especially, at loadings below 40 wt%) should be caused by the immobilization of bi-functional 1-AP molecules, which offer large and uniform distributed active sites for anchoring Pt ions and Pt nanoparticles.[260] Comparing Figures 4.3 and 4.4, it is also seen that the particle size of Pt electrocatalysts increases slightly with increase in Pt loading.

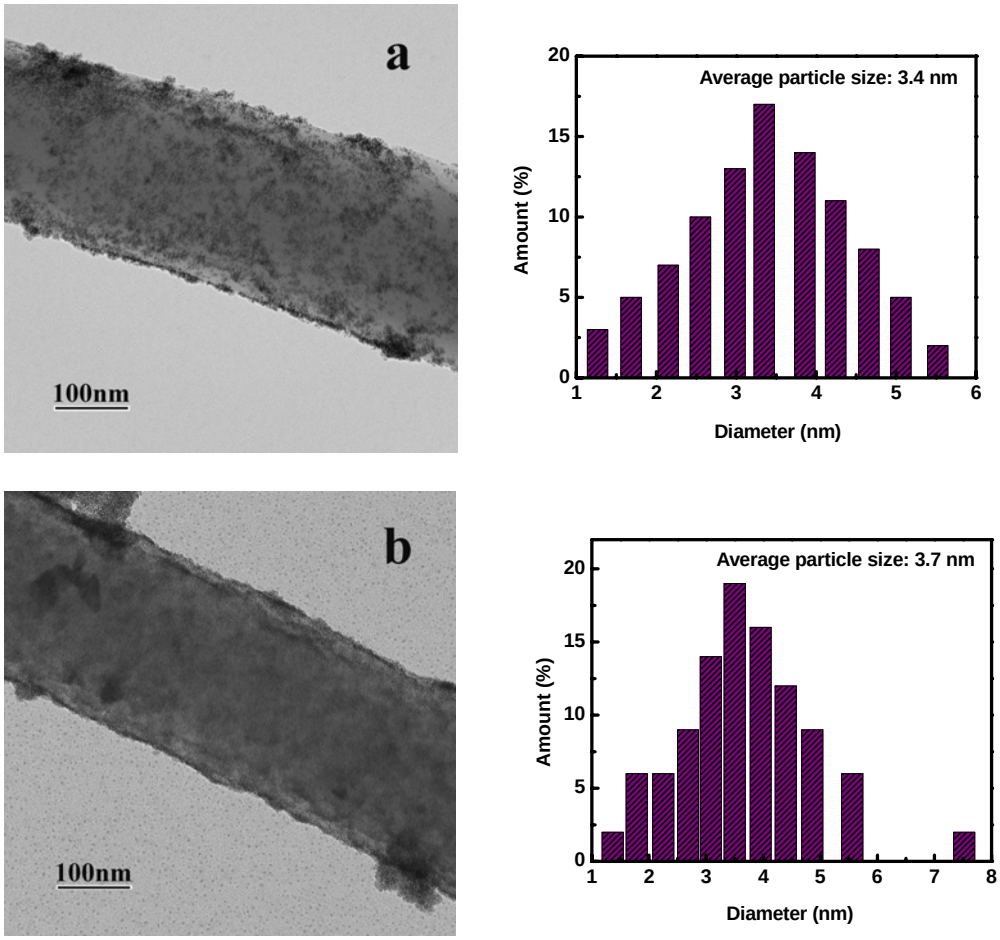

Figure 4.4. TEM images and Pt diameter distributions of Pt/1-AP-CNFs with Pt loading amount of 40 (a) and 60 (b) wt%, respectively.

4.3.5. XRD patterns of Pt/CNFs

X-ray diffraction (XRD) profiles of Pt/CNFs obtained from AO-CNFs and 1-AP-CNFs are

presented in Figure 4.5. The diffraction peak at 25.5° of CNFs can be assigned to the diffraction of the (002) plane of graphite layers in CNFs. The XRD profiles of Pt/AO-CNFs and Pt/1-AP-CNFs also confirm that the Pt phase is indeed formed on both nanofibers and can be indexed to the reflections of face-centered cubic Pt at 39.8° (111), 46.6° (200), 68.2° (220), and 82.2 ° (311), respectively. The diffraction peaks of Pt/1-AP-CNFs are greater than those of Pt/AO-CNFs due to the smaller Pt particle size on Pt/1-AP-CNFs.

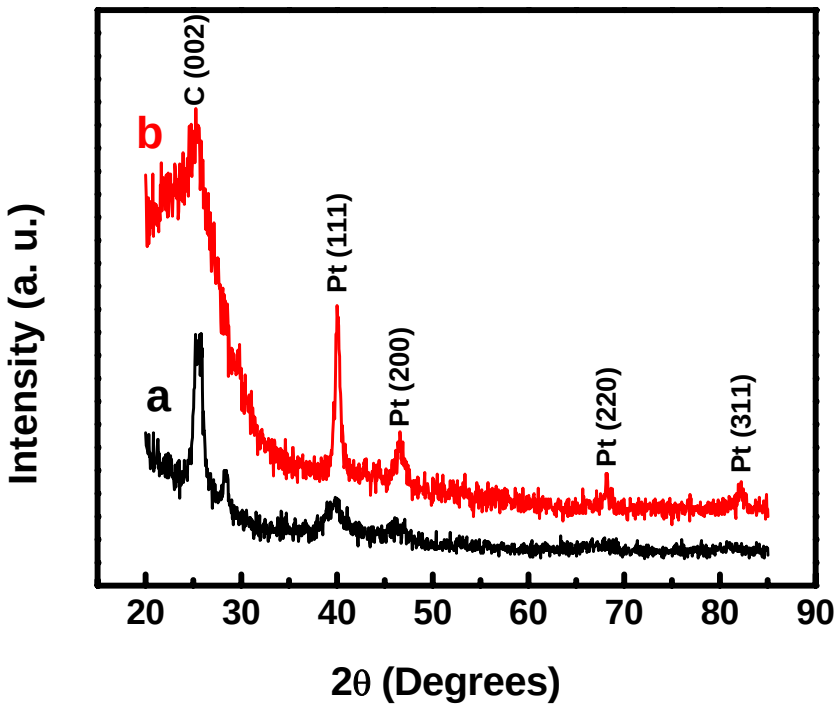

Figure 4.5. XRD profiles of Pt/AO-CNFs (a) and Pt/1-AP-CNFs (b).

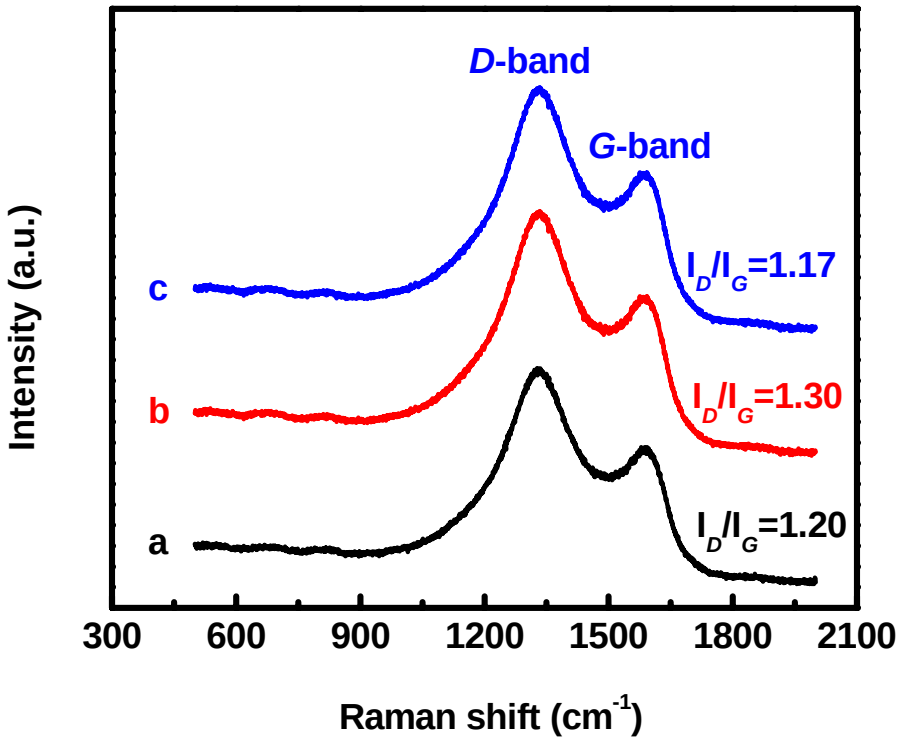

Figure 4.6. Raman spectra of Pt/UT-CNFs (a), Pt/AO-CNFs (b), and Pt/1-AP-CNFs (c).

4.3.6. Raman spectra of Pt/CNFs

The structure of Pt/CNFs prepared from UT-CNFs, AO-CNFs, and 1-AP-CNFs was studied by Raman spectroscopy and the results are shown in Figure 4.6. All three types of Pt/CNFs have similar Raman scattering patterns. Raman spectra of carbon materials reflect their electronic structure and electron-phonon interactions and allow clear identification of

graphite layers.[261] The peak at near 1335 cm^{-1} is assigned to the disordered graphite structure (*D*-band), and the frequency peak near 1587 cm^{-1} (*G*-band) corresponds to a splitting of the E_{2g} stretching mode of graphite, which reflects the structural intensity of the sp^2-hybridized carbon atoms.[262] Therefore, the intensity ratio of *D*- and *G*-bands (I_D/I_G) can be used to evaluate the extent of the modification or defects on CNF surface and a higher I_D/I_G ratio typically indicates a higher degree of disorder. From Figure 4.6, it is seen that, compared to Pt/UT-CNFs, the I_D/I_G ratio of Pt/AO-CNFs increases from 1.20 to 1.30. This indicates that the harsh acid treatment produces carboxylic acid sites on the surface, causing significant structural damage on the ordered structure of CNF surface. From Figure 4.6, it is also seen that Pt/1-AP-CNFs have slightly lower I_D/I_G ratio (*i.e.*, 1.17) than Pt/UT-CNFs, which indicates that the immobilization or wrapping of 1-AP on the surface of CNFs via π-stacking has no detrimental effect on the ordered structure in CNFs. Rather, the slightly decreased ratio may suggest the coverage of the original defect sites by 1-AP molecules.

4.3.7. Electrochemical characterization of Pt/CNFs

CV measurements of Pt/AO-CNFs and Pt/1-AP-CNFs between -0.2 and +1.0 V at 50 $mV \cdot s^{-1}$ in 0.5 M H_2SO_4 were employed to examine whether Pt particles on CNF surface are electrochemically active (Figure 4.7). It is seen that redox current density peaks can be observed, which are due to the adsorption and desorption of hydrogen at the surface of Pt nanoparticles on CNFs. The integration of CV curves from hydrogen desorption peaks from

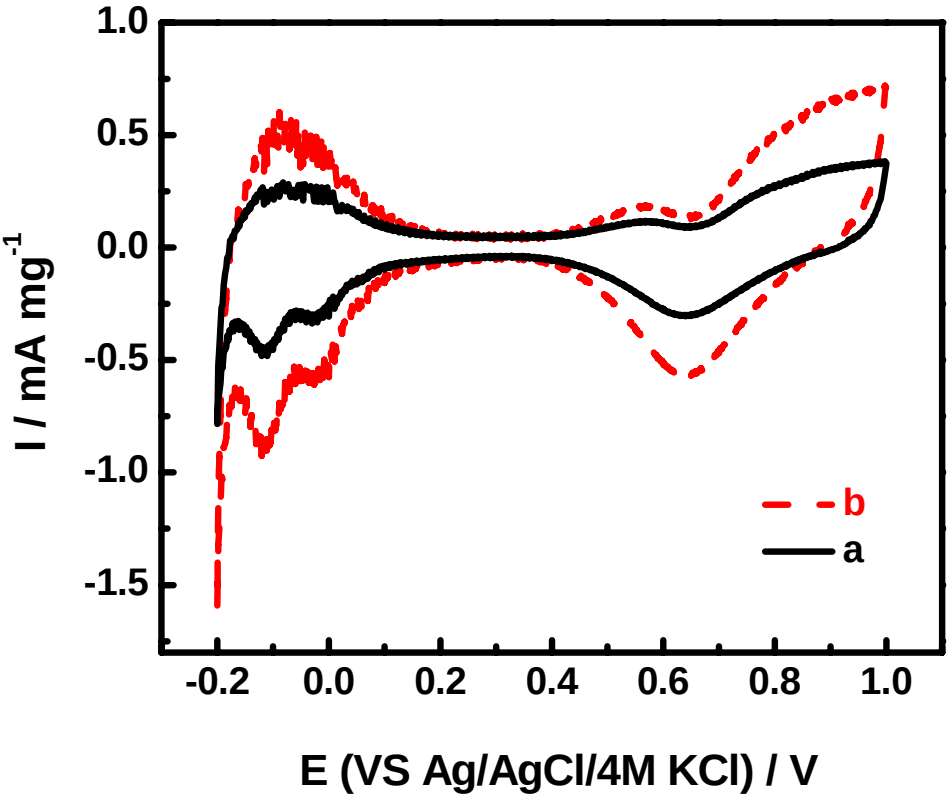

Figure 4.7. Current-potential curves of Pt/AO-CNFs (a) and Pt/1-AP-CNFs (b) in 0.5 M H_2SO_4 at 50 mV·s^{-1}.

-0.2 to +0.2 V gives electrochemical active surface area (EASA), which can be calculated according to the following formula:[263]

$$\text{EASA} = Q(mC\ mg^{-1})/0.22mC\ cm^{-2} \quad (4.2)$$

where Q is the electric charge for hydrogen desorption and 0.22 mC cm^{-2} the hydrogen adsorption constant for Pt. Table 4.1 shows the calculated EASA values for both

Pt/AO-CNFs and Pt/1-AP-CNFs. It is seen that the EASA for Pt/1-AP-CNFs is 409 cm^2/mg of Pt, much higher than that of Pt/AO-CNFs (227 cm^2/mg of Pt), which is due to the smaller Pt particle size and less agglomerate formation on the surface of 1-AP-CNFs. This result demonstrates that Pt nanoparticles deposited on 1-AP-CNFs are electrochemically more accessible, which is very important for electrocatalyst applications in fuel cells.

4.3.8. Electro-oxidation of methanol on Pt/CNFs

Table 4.1. Electrochemical characteristics of Pt/AO-CNFs and Pt/1-AP-CNFs. Solution: 0.5 M H_2SO_4 for EASA and 0.125 M CH_3OH + 0.2 M H_2SO_4 for other characteristics. Scanning rate: 5 $mV \cdot s^{-1}$.

Catalysts	Average particle size (nm)	EASA (cm^2 mg^{-1} Pt)	Onset Potential (V *vs* Ag/AgCl/4.0 M KCl)	Forward peak potential (V *vs* Ag/AgCl/4.0 M KCl)	Forward peak current density (I_f, mA mg^{-1})	Reverse peak current density (Ir, mA mg^{-1})	I_f/I_r
Pt/AO-CNFs	4.2	227	0.41	+ 0.73	1.11	0.77	1.44
Pt/1-AP-CNFs	3.2	409	0.39	+ 0.72	2.32	0.98	2.37

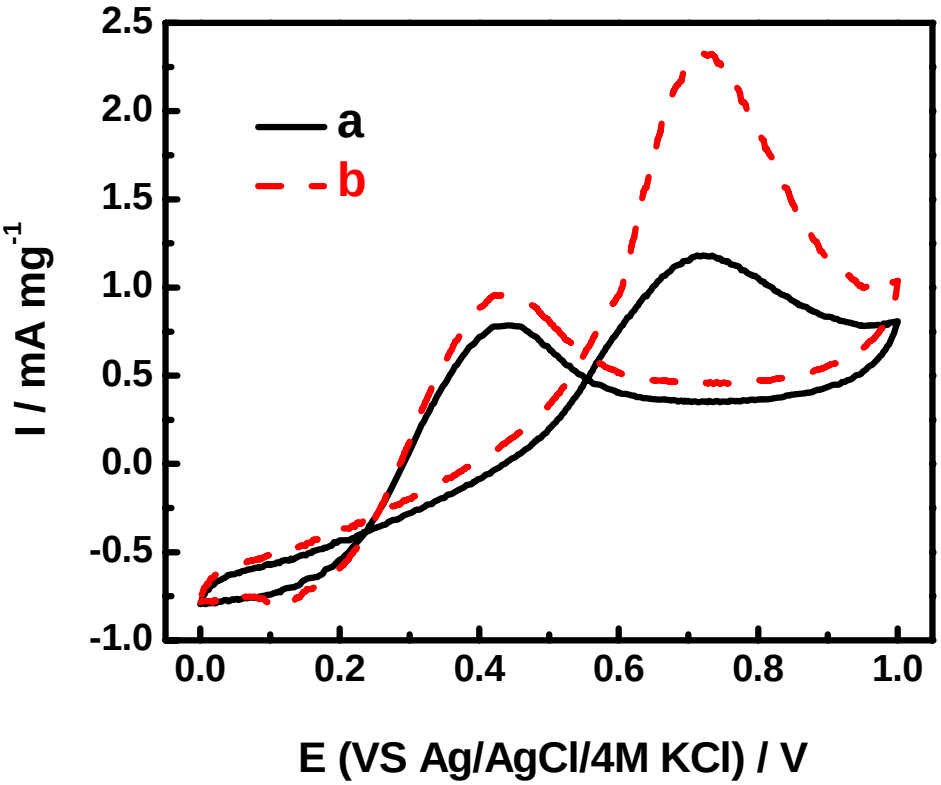

Figure 4.8. Current-potential curves of Pt/AO-CNFs (a) and Pt/1-AP-CNFs (b) in 0.125 M CH_3OH + 0.2 M H_2SO_4 at 5 $mV \cdot s^{-1}$. The Pt loading amount is 20 wt %.

Figure 4.8 shows the current density-potential curves of Pt/AO-CNFs and Pt/1-AP-CNFs in 0.125 M CH_3OH + 0.2 M H_2SO_4 solution at 5 $mV \cdot s^{-1}$. In both curves, Pt/AO-CNFs and Pt/1-AP-CNFs present the electro-oxidation of methanol, which starts at around +0.42 V and then the current density increases to a maximum at +0.63 V; moreover, another current peak is found at about +0.55 V when scanning back. The mechanism for the methanol reaction is:

first, methanol is adsorbed on the surface of Pt nanoparticles, and then transformed to different reactive intermediates, such as $(CH_2O)_{ads}$ and $(CHO)_{ads}$, and poisoning species $(CO)_{ads}$. Both the reactive and poisoning species can be further oxidized to CO_2, however, a relatively high potential is required to oxidize the poisoning species $(CO)_{ads}$.[170, 264, 265]

In order to study the efficiency of methanol oxidation, the electrochemical characteristic data of Pt/AO-CNFs and Pt/1-AP-CNFs are also summarized in the Table 4.1. The efficiencies of methanol oxidation were compared in items of forward onset potential, forward peak current density, reverse peak current density, and the ratio of forward to reverse peak current densities (I_f/I_r). From Table 4.1, the onset potentials of both Pt/AO-CNFs and Pt/1-AP-CNFs are around 0.40 V, which is close to that reported by Wang et al.[260] It is also seen that compared with Pt/AO-CNFs, Pt/1-AP-CNFs have larger forward and reverse peak current densities due to increased amount of available Pt catalysts. The I_f/I_r ratio of Pt/1-AP-CNFs is also larger than that of Pt/AO-CNFs, which may be related to the smaller Pt particles in Pt/1-AP-CNFs. In addition, a smaller forward peak potential is obtained at Pt/1-AP-CNFs, indicating the better catalytic activity of Pt/1-AP-CNFs than Pt/AO-CNFs.

4.3.9. Stability of Pt/CNFs

The stability of the Pt electrocatalysts is an important factor for the development of advanced DMFCs. In order to study the long-term stability of Pt/CNFs, the forward peak current

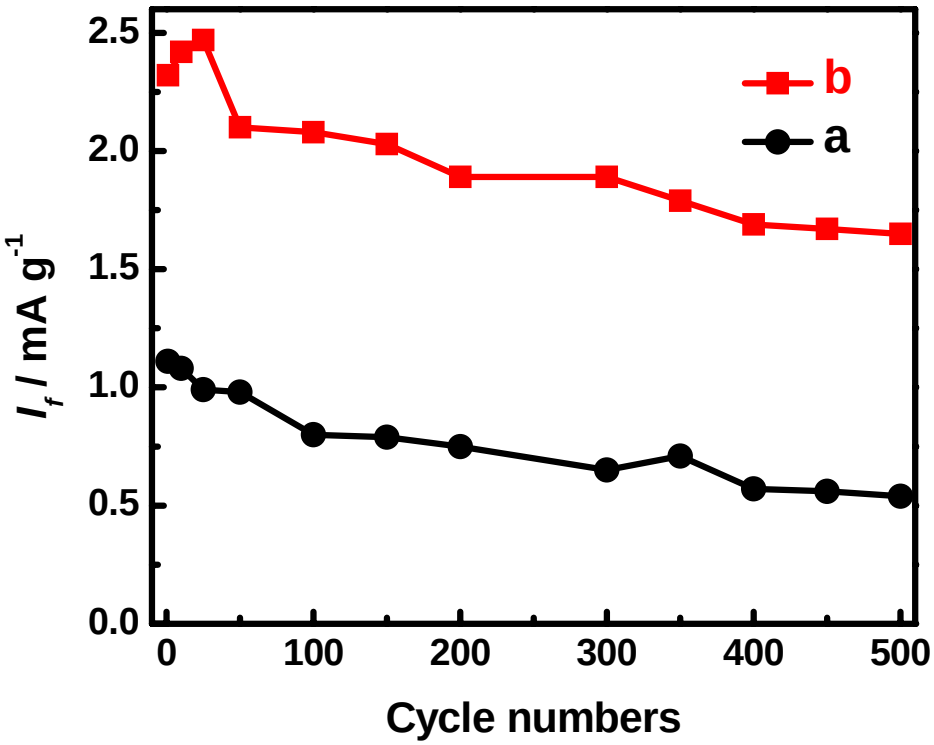

Figure 4.9. Stability of Pt/AO-CNFs (a) and Pt/1-AP-CNFs (b) in 0.125 M CH_3OH + 0.2 M H_2SO_4 at 5 mV·s^{-1} from 0.0 to 1.0 V (*vs.* Ag/AgCl/4.0 M KCl). The Pt loading amount is 20 wt %.

density (I_f) was measured as a function of cycle number in 0.125 M CH_3OH + 0.2 M H_2SO_4 on Pt/AO-CNFs and Pt/1-AP-CNFs, respectively, and the results are shown in Figure 4.9. It is seen that the I_f of Pt/AO-CNFs decreases when the cycle number increases. After 500 cycles, the I_f of Pt/AO-CNFs is about 0.54 mA g^{-1}, which is 49 % of the initial I_f of

Pt/AO-CNFs. In comparison, the I_f of Pt/1-AP-CNFs increases first, and then decreases. The final I_f of Pt/1-AP-CNFs is around 1.65 mA g^{-1}after 500 cycles, which is 71 % of the initial I_f. In general, the gradual decrease of the catalytic activity after successive cycling should be due to the slow degradation of Pt nanoparticles on the surface of CNFs. When compared to Pt/AO-CNFs, the percentage of I_f decrease for Pt electrocatalysts on 1-AP-CNFs is lower (71 % *vs*. 49 %).

4.4. Summary

The preparation and characterization of Pt/CNFs by the combination of 1-AP functionalization and a polyol processing technique were studied. Pt nanoparticles with well-defined morphology and catalyst activity were obtained on functionalized CNFs. It is found that compared with the conventional AO-CNFs, the simple synthesis process of 1-AP-functionalization treatment can preserves the integrity and the electronic structure of CNFs. The diameter of Pt nanoparticles on 1-AP-CNFs is 3.2 nm in average, which is smaller than that of Pt/AO-CNFs prepared from the conventional acid-treated AO-CNFs. Moreover, Pt nanoparticles are much more evenly distributed on 1-AP-CNFs without any agglomerates. The resulting Pt/1-AP-CNFs possess the properties of higher active surface area, better performance towards the oxidation of methanol, and good long-time stability. Therefore, the chemical deposition of Pt nanoparticles on 1-AP-CNFs provides an alternative method to obtain a good catalyst toward the oxidation of methanol. However, investigations

into the catalytic ability of such composites in MEAs in direct methanol fuel cells are needed for future applications.

CHAPTER 5. ANODE: CARBON NANOFIBER-SUPPORTED PLATINUM-RUTHENIUM BY CHEMICAL DEPOSITION

Abstract

To address the carbon monoxide poison problem, PtRu/carbon composite nanofibers were prepared by depositing PtRu nanoparticles directly onto electrospun CNFs using a polyol processing technique. The morphology and size of PtRu nanoparticles were controlled by 1-aminopyrene functionalization. The noncovalent functionalization of CNFs by 1-aminopyrene is simple and can be carried out at ambient temperature without damaging the integrity and electronic structure of CNFs. The resulting PtRu/carbon composite nanofibers were characterized by running cyclic voltammogram in 0.5 M H_2SO_4 and 0.125 M CH_3OH + 0.2 M H_2SO_4 solutions, respectively. Results show that PtRu/carbon composite nanofibers with 1-aminopyrene functionalization have PtRu nanoparticles with smaller size and better distribution, compared with those pretreated with conventional acids. Moreover, PtRu/1-aminopyrene functionalized CNFs possess the properties of high active surface area and improved performance towards the electrocatalytic oxidation of methanol.

5.1. Introduction

To meet ever-increasing energy demands and tackle the daunting environmental pollution, direct methanol fuel cells (DMFCs) have recently attracted much attention, since they can provide green power for electric vehicles and electronic portable devices by direct conversion of methanol fuel.[90, 107, 129] The methanol conversion is carried in a membrane electrode assembly (MEA), which is the key component of DMFCs and is consisted of a polymer electrolyte membrane and two catalyst-loaded porous electrodes for methanol oxidation at the anode and oxygen reduction at the cathode. The methanol oxidation reaction (MOR), typically catalyzed by Pt in acidic environment, can be expressed in the following equation:[253]

$$CH_3OH + H_2O \rightarrow CO_2 + 6H^+ + 6e^- \qquad (5.1)$$

$$E^o\,(\text{MOR}) = 0.016\ \text{V}\ \textit{vs.}\ \text{SHE at 25 }^oC$$

During the reaction, one of the intermediates, CO, often poisons Pt catalyst by adsorbing deeply on the surface of the catalyst. In order to remove the adsorbed CO, a high potential is required to oxidize CO by reacting with -OH produced during water activation, which limits the use of a pure Pt catalyst in DMFCs. Therefore, to provide -OH at lower potentials for the oxidative removal of adsorbed CO, a second metal, *i.e.,* Ru, has been used to form alloy with Pt to promote the oxidation of CO to CO_2 by a bi-functional mechanism.[140, 141]

Until now, one major challenge for the commercial applications of DMFCs is the high cost of

precious Pt or Pt alloy electrocatalysts.[2, 254, 266, 267] Therefore, the development of highly active electrode catalysts coupled with a suitable electrode structure and low catalyst loading is an important subject for attaining the high efficiency in DMFCs, and subsequently lowering the cost. Carbon nanomaterials are currently being considered as the suitable material for supporting catalysts in DMFCs,[268-270] because of their unique graphite properties combined with three-dimensional flexible structures. Carbon nanofibers (CNFs), one of promising carbon nanomaterials for supporting catalysts, have been investigated by several research groups due to their unique 1-dimensional structure, high electronic and thermal conductivities, and good electrochemical stability.[256, 257] However, since CNFs are chemically inert, it is necessary to activate their graphitic surface because the deposition, distribution, and size of Pt or Pt alloy nanoparticles strongly depend on the surface properties of CNFs.[106]

In order to anchor and deposit catalyst nanoparticles well on the surface of carbon nanomaterials, many harsh oxidative methods, such as refluxing in concentrated mixtures of H_2SO_4 and HNO_3, and cycling in H_2SO_4 solution using cyclic voltammogram, have been widely utilized. However, those methods result in lots of defects on carbon nanomaterials, which are harmful to the electrochemical active surface area of Pt or Pt alloy electrocatalysts and their durability during fuel cell operation.[271] Recently, novel noncovalent functionalization methods of carbon nanomaterials, such as coating carbon nanotubes (CNTs) with 1 % sodium dodecyl sulfate [234] or functionalizing of CNTs with 1-aminopyrene [260], have attracted particular attention because they enable the surface activation of carbon

nanomaterials without destroying their intrinsic properties.[85, 232, 233]

In this paper, we prepared and characterized PtRu/carbon composite nanofibers (PtRu/CNFs) by the combination of 1-aminopyrene functionalization and a polyol processing technique, *i.e.*, functionalizing electrospun carbon nanofibers with 1-aminopyrene, followed by the deposition of PtRu using ethylene glycol as a reducing agent. The most important advantage of this approach is that the 1-aminopyrene functionalization treatment preserves the integrity and the electronic structure of CNFs, which result in the long-term stability of such composite in the application of DMFCs. Moreover, PtRu nanoparticles with small diameter and homogenous distribution can be obtained and high electrochemical surface area and good activity toward the methanol oxidation are also observed on the resultant PtRu/CNFs.

5.2. Experimental

5.2.1. Chemicals and reagents

Polyacrylonitrile (PAN), N,N-dimethylformamide (DMF), chloroplatinic acid hydrate ($H_2PtCl_6 \cdot xH_2O$), ruthenium chloride ($RuCl_3$), 1-aminopyrene (1-AP), ethylene glycol (EG), nitric acid (HNO_3, 70%) ,sulfuric acid (H_2SO_4), and methanol (CH_3OH) were purchased

from Sigma-Aldrich, and they were used without further purification. Deionized water was used throughout.

5.2.2. Synthesis of CNFs

A DMF solution of 8 wt% PAN was prepared at 60 ^{o}C, with mechanical stirring for three hours. The electrospinning was conducted using a Gamma ES40P-20W/DAM variable high voltage power supply under a voltage of 15 kV. Under high voltage, a polymer stream was ejected through a syringe and accelerated toward the nanofiber collector, during which the solvent was rapidly evaporated. Aluminum foil was placed over the collector plate of the electrospinning apparatus to collect electrospun PAN fibers. These PAN nanofibers were first stabilized in an air atmosphere at 280 ^{o}C for 2 hours at the heating rate 5 min^{-1} and then carbonized at 700 ^{o}C for 1 hour in nitrogen atmosphere at the heating rate 2 ^{o}C min^{-1}. The resultant CNFs formed free-standing nonwoven membranes and were directly used as a support in the chemical deposition of PtRu nanoparticles.

5.2.3. 1-AP-functionalization of CNFs

The procedure of the noncovalent functionalization of CNFs using 1-AP is described as

follows. CNFs (0.2 g) and 1-AP (0.2 g) were added into an ethanol solution (30 ml), which was stirred mechanically for 1 hour and stored at room temperature for 24 hours. The solution was then filtered and washed several times, and the treated CNFs were dried in a vacuum oven at 70 °C for 5 hours and collected as 1-aminopyrene functionalized CNFs (1-AP-CNFs). For comparison, CNFs were also functionalized by a conventional acid treatment, *i.e.*, CNFs (0.2 g) were refluxed in a mixed strong acid solution (50 ml H_2SO_4:HNO_3 in 3:1 v/v ratio) at 80 ^oC for 3 hours. The acid-treated CNFs are denoted as AO-CNFs.

5.2.4. Synthesis of PtRu/CNF catalysts

To deposit PtRu nanoparticles on 1-AP-CNFs, 1-AP-CNFs (0.3 g) was mixed with approximate amount of $H_2PtCl_6{\cdot}xH_2O$ + $RuCl_3$ (with metal loading 25, 50, and 75 wt%, Pt:Ru = 3:2) in 50 ml ethylene glycol solution under ultrasonication in a three-neck flask. The solution was then refluxed in 70 ^oC for almost 6.0 hr until the solution changed from light yellow to dark brown, indicating the reduction and formation of PtRu nanoparticles on CNFs. The above solution was filtered and washed several times, and the resulting PtRu/1-AP-CNFs were dried in vacuum oven at 100 °C for a day. PtRu/acid-functionalized CNFs (PtRu/AO-CNFs) with the PtRu metal loading amount of 75 wt% were also prepared using the procedure described above.

5.2.5. Structural characterization of PtRu/1-AP-CNFs

X-ray diffraction (XRD) analysis was performed with a Philips XLF ATPS XRD 100 diffractometer using CuKα radiation (λ=1.5405 Å). The operating voltage and current were 40.0 kV and 60.0 mA, respectively. Raman spectra of PtRu/CNFs were obtained using Horiba Jobin Yvon LabRam Aramis Microscope with 633 nm HeNe Laser.

The structure of CNFs, PtRu/AO-CNFs, and PtRu/1-AP-CNFs, which were deposited onto 200 mesh carbon-coated Cu grids, was evaluated using a Hitachi HF-2000 TEM at 200 kV. These nanofibers were also examined using a JEOL JSM-6360LV FESEM at 15 kV.

5.2.6. Electrochemical properties of PtRu/CNFs

The electrochemical measurements of PtRu/CNFs were performed in a three-electrode cell at 25 ^{o}C on an electrochemical workstation (AQ4 Gamry Reference 600, USA). The cell consisted of a working electrode (PtRu/CNFs), a counter electrode (Pt wire), and a reference electrode (*Ag*/*AgCl*/4.0 M KCl). Nitrogen was used to bubble the testing solutions for at least 30 minutes before the measurements, and then was used continually to protect the experiment environment. All the electrochemical potentials were measured and reported with respect to Ag/AgCl/4.0 M KCl.

The measurement of hydrogen electrosorption was conducted by cyclic voltammograms (CVs) of PtRu/CNFs in 0.5 M H_2SO_4 at 50 $mV \cdot s^{-1}$ to determine the electrochemically active surface area. CV responses of PtRu/CNFs in 1 M CH_3OH + 0.2 M H_2SO_4 at 5 $mV \cdot s^{-1}$ were also measured to study their activities on the methanol oxidation.

5.3. Results and Discussions

5.3.1. CNF treatment and PtRu deposition

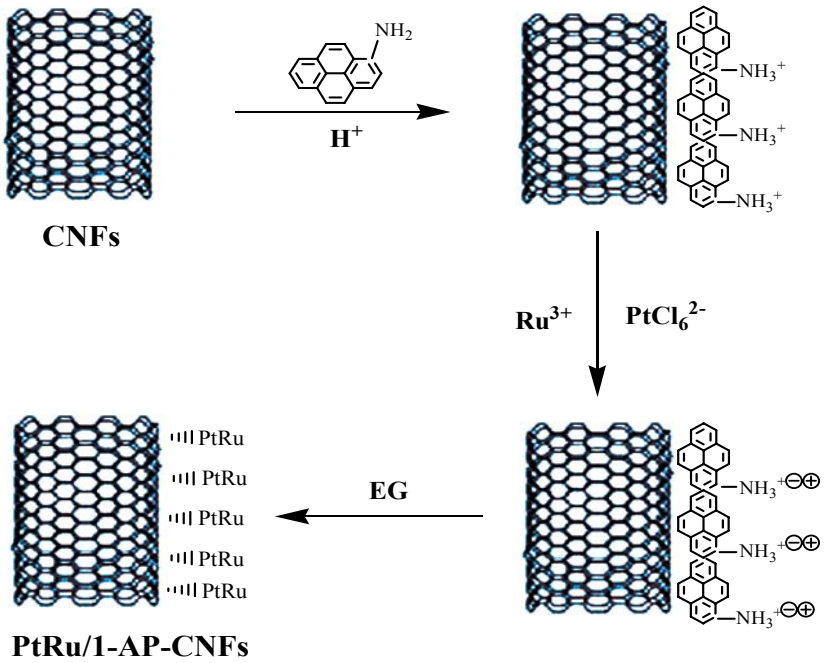

Figure 5.1. Schematic diagram of the deposition of PtRu electrocatalyst on 1-AP-CNFs.

Figure 5.1 shows the schematic diagram of the synthesis procedure of PtRu/1-AP-CNFs. Since the surface of CNFs is chemically inert and does not have functional groups, PtRu deposition on untreated CNF surface is relatively un-controlled. In order to do the surface treatment of CNFs, a noncovalent functionalization involving a reagent 1-AP was used. The reagent 1-AP, a bifunctional molecule with a pyrenyl group and an amino functional group, does not have direct chemical reaction with CNFs. Typically, the pyrenyl group of 1-AP can be attached onto the basal plane of graphite via π-stacking.[259] As a result, 1-AP can be immobilized on CNFs through the adsorption of pyrenyl groups onto the inherently hydrophobic surface of CNFs. After the immobilization of 1-AP, $H_2PtCl_6{\cdot}xH_2O$ and $RuCl_3$ can be traduced and the pH value of the solution changes to around 6.0 (*i.e.*, slightly acid). At the same time, the amino groups of immobilized 1-AP molecules become weakly positively charged, which leads to the self-assembly of negatively charged Pt precursors, $PtCl_6^{2-}$ ions, followed by the subsequent self-assembly of positively charged Ru precursors, Ru^{3+}. As a result, the uniform distribution of Pt and Ru precursors can be obtained on the surface of CNFs. After that, in the presence of ethylene glycol, self-assembled PtRu precursors are reduced to form PtRu nanoparticles on the CNF surface. Therefore, during the synthesis of 1-AP-CNFs, the $PtCl_6^{2-}$ and Ru^{3+} ions are attached onto CNF surface first, and then are reduced to PtRu nanoparticles.

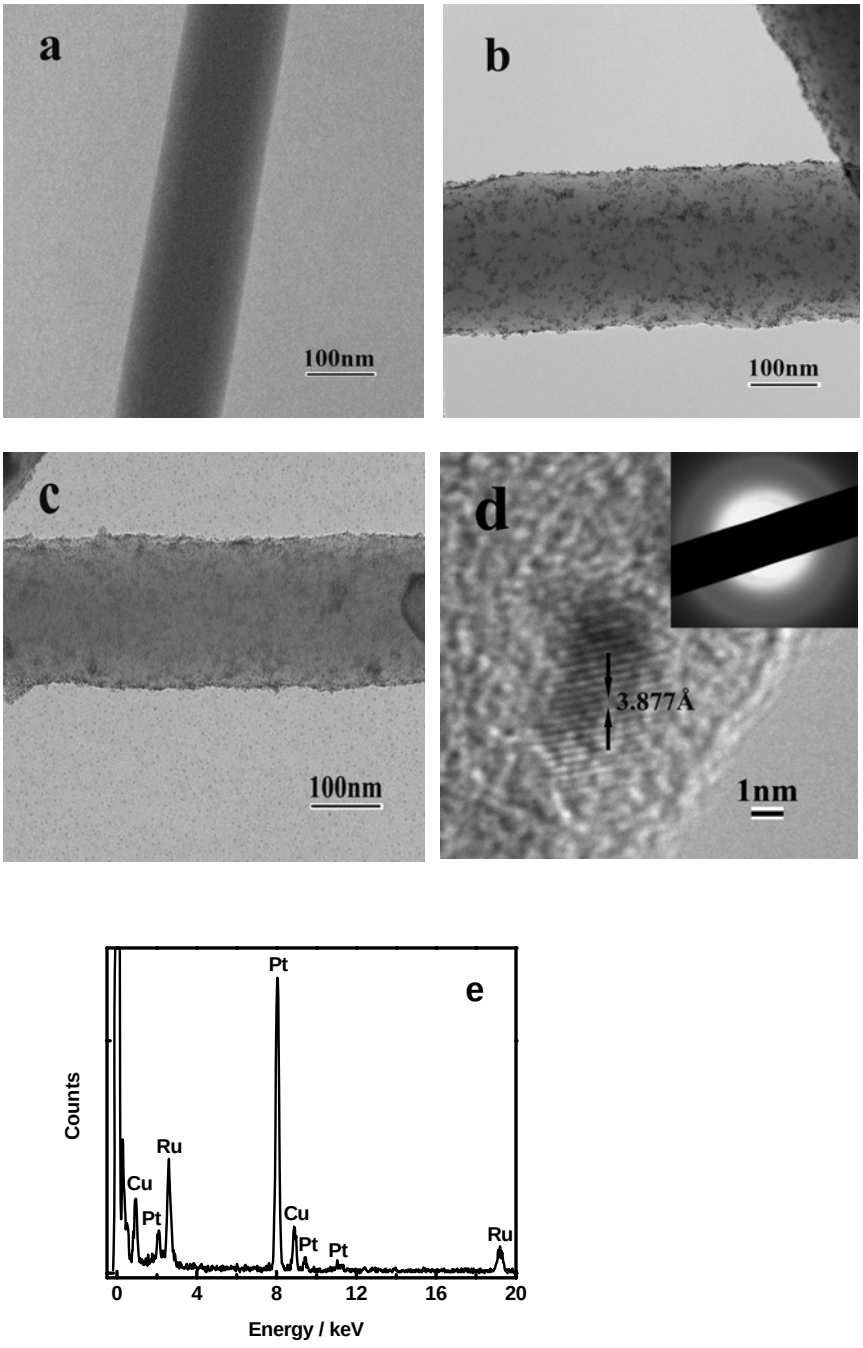

Figure 5.2. TEM images of CNFs (a), PtRu/1-AP-CNFs with metal loadings of 25 (b) and 50 (c) wt%, high resolution TEM image and inserted electron diffraction pattern (d) and EDS spectrum (e) of PtRu/1-AP-CNFs (metal loading: 25 wt%).

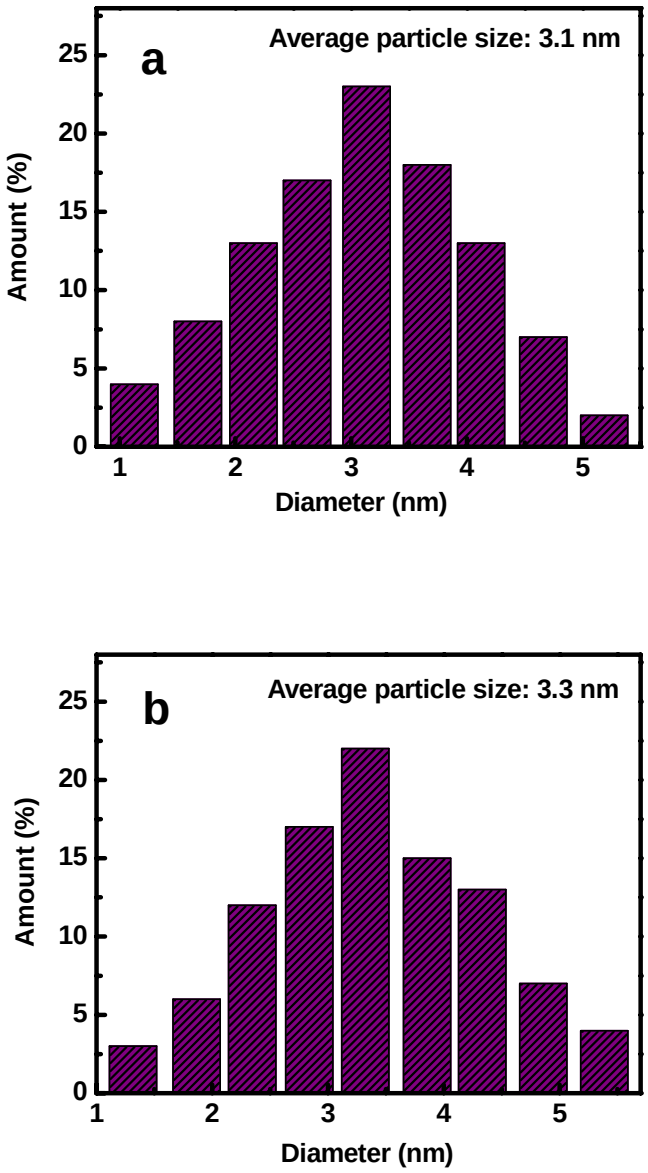

Figure 5.3. Diameter distributions of PtRu nanoparticles on PtRu/1-AP-CNFs with the metal loadings of 25 (a) and 50 (b) wt%, respectively.

5.3.2. TEM images of PtRu/1-AP-CNFs

Figure 5.2 shows TEM images of CNFs and PtRu/1-AP-CNFs. In Figure 5.2a, CNFs exhibit long and straight fibrous morphology with relatively uniform diameters between 100 and 300 nm. It is also seen that before deposition, CNF surface is smooth and there are no particles loaded. However, PtRu nanoparticles are observed on the surface of CNFs after deposition (Figures 5.2b-c). When the metal loading is 25 wt%, PtRu nanoparticles are evenly distributed on the surface of 1-AP-CNFs (Figure 5.2b) and the average diameter of PtRu nanoparticles is about 3.1 nm (Figure 5.3a). When the metal loading increases (*i.e.* 50 wt%), more PtRu nanoparticles are found on the surface of 1-AP-CNFs and they are still evenly distributed. Though there is a relatively large increase in the metal loading, the average diameter of PtRu nanoparticles increases slightly from 3.1 to 3.3 nm (Figure 5.3b), which should be due to the surface treatment of CNFs by 1-AP functionalization. A more detailed explanation is provided in Section 3.3 - Structure Comparison of PtRu/1-AP-CNFs and PtRu/AO-CNFs.

Figures 5.2d and e show the high resolution TEM image, inserted electron diffraction pattern, and energy dispersive X-ray spectroscopy (EDS) of PtRu/1-AP-CNFs (metal loading: 25 wt%), respectively. In Figure 5.2d, it shows the crystal structure of PtRu nanoparticle with crystal lattice of 3.877 Å. The EDS data in Figure 5.2e also confirm the presence of PtRu particles on the surface of 1-AP-CNFs, and the copper peaks belong to the TEM grid

background.

5.3.3. Structure comparison of PtRu/1-AP-CNFs and PtRu/AO-CNFs

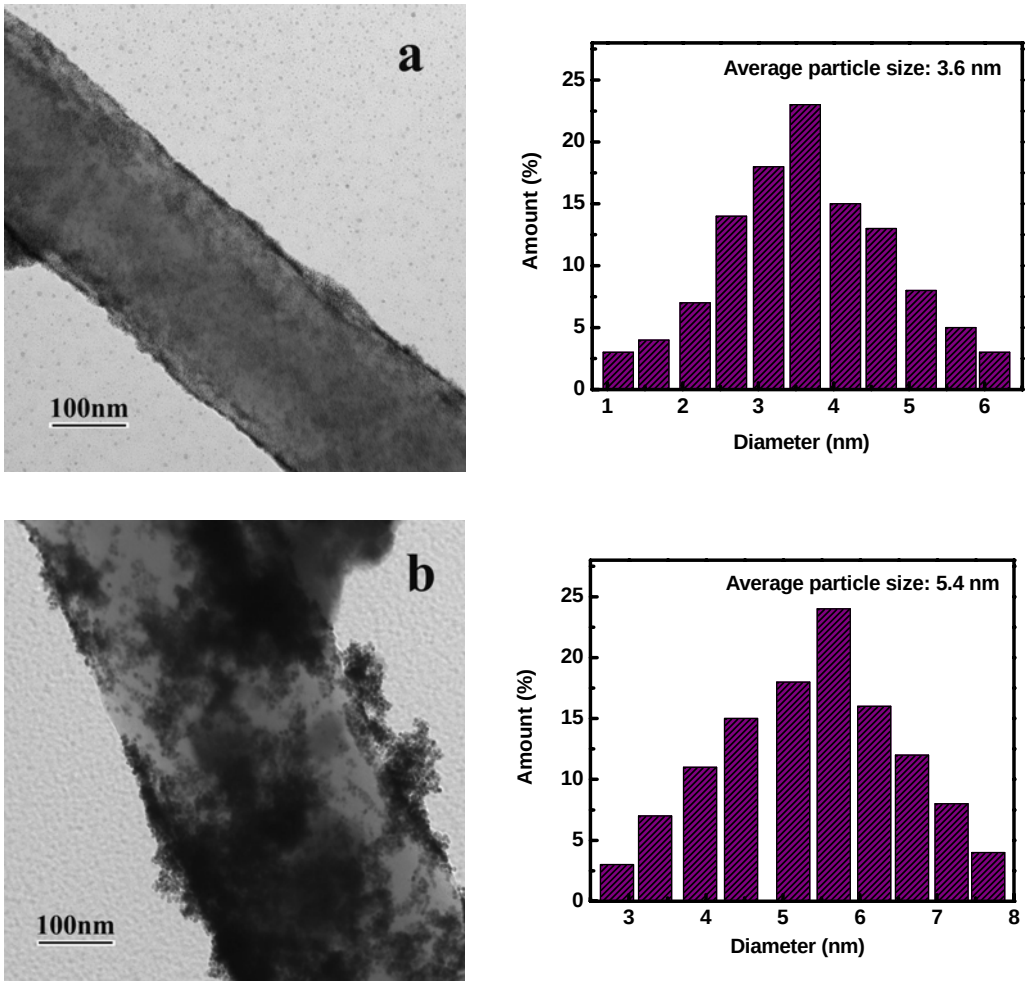

Figure 5.4. TEM images and PtRu diameter distributions of PtRu/1-AP-CNFs (a) and PtRu/AO-CNFs (b), respectively. The metal loading is 75 wt%.

Figure 5.4 shows TEM images and diameter distributions of PtRu/1-AP-CNFs and PtRu/AO-CNFs. The metal loading amount is the same, *i.e.*, 75 wt%, for both PtRu/CNFs. As shown in Figure 5.4a, the surface of 1-AP-CNFs is almost fully covered by PtRu nanoparticles, however, there are no large aggregates of PtRu particles found. Moreover, when compared with PtRu/1-AP-CNFs with metal loadings of 25 and 50 wt% (Figure 5.2b and c), more PtRu nanoparticles are evenly distributed on the surface of 1-AP-CNFs and the particle size of PtRu electrocatalysts on 1-AP-CNFs increases slightly to 3.6 nm when the metal loading increases to 75 wt%. For AO-CNFs, which were oxidized in a mixed strong acid solution (50 ml H_2SO_4:HNO_3 in 3:1 v/v ratio) at 80 ^oC, PtRu nanoparticles can also be found on the fiber surface. However, the average size of PtRu nanoparticles increases to 5.4 nm, and significant amount of PtRu particle aggregates is found. The relatively smaller size of PtRu nanoparticles on PtRu/1-AP-CNFs should be caused by the immobilization of bi-functional 1-AP molecules, which offer large and uniformly distributed active sites for anchoring $PtCl_6^{2-}$ and Ru^{3+} ions and subsequently Pt and Ru nanoparticles (Figure 5.1). Thus, compared with conventional acid-oxidized CNFs, 1-AP-functionalized CNFs are more effective for use as catalyst supporting materials.

5.3.4. XRD patterns of PtRu/CNFs

X-ray diffraction (XRD) profiles of PtRu/1-AP-CNFs and PtRu/AO-CNFs are presented in Figure 5.5. For comparison, the XRD profile of untreated CNFs is also shown. The

diffraction peak at around 25° can be assigned to the diffraction of the (002) plane of graphite layers in CNFs. The XRD profiles of PtRu/AO-CNFs and PtRu/1-AP-CNFs also confirm that the PtRu phase is formed on both CNFs and can be indexed to the reflections of crystal structure of PtRu nanoparticles at 39.9^{o} (111), 45.8^{o} (200), 68.3^{o} (220), and 82.0^{o} (222), respectively. The diffraction peaks of PtRu/1-AP-CNFs are stronger than those of PtRu/AO-CNFs due to their smaller PtRu particle size that makes the XRD measurement more sensitive.

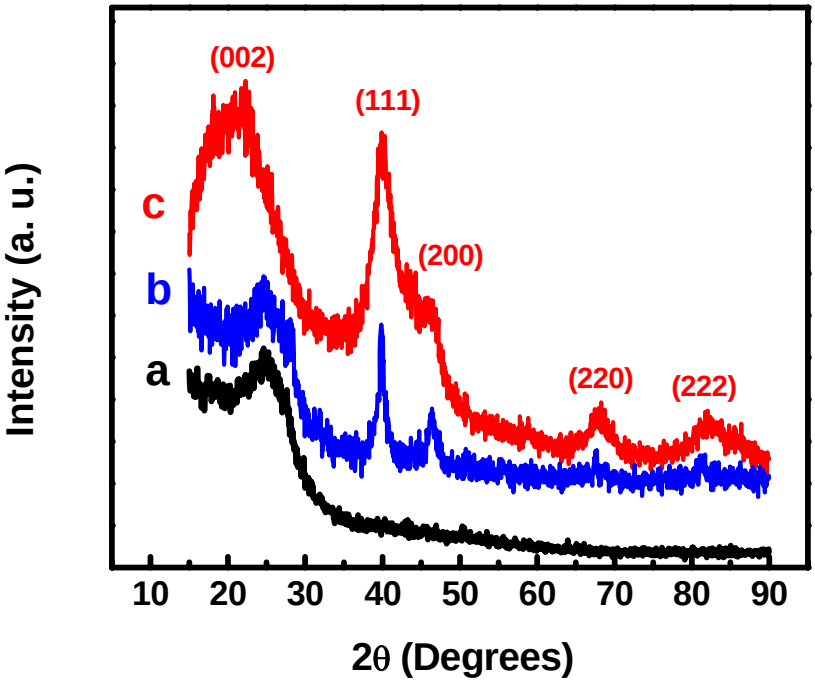

Figure 5.5. XRD profiles of CNFs (a), PtRu/AO-CNFs (b), and PtRu/1-AP-CNFs (c). The metal loading is 75 wt%.

5.3.5. XPS spectrum of PtRu/1-AP-CNFs

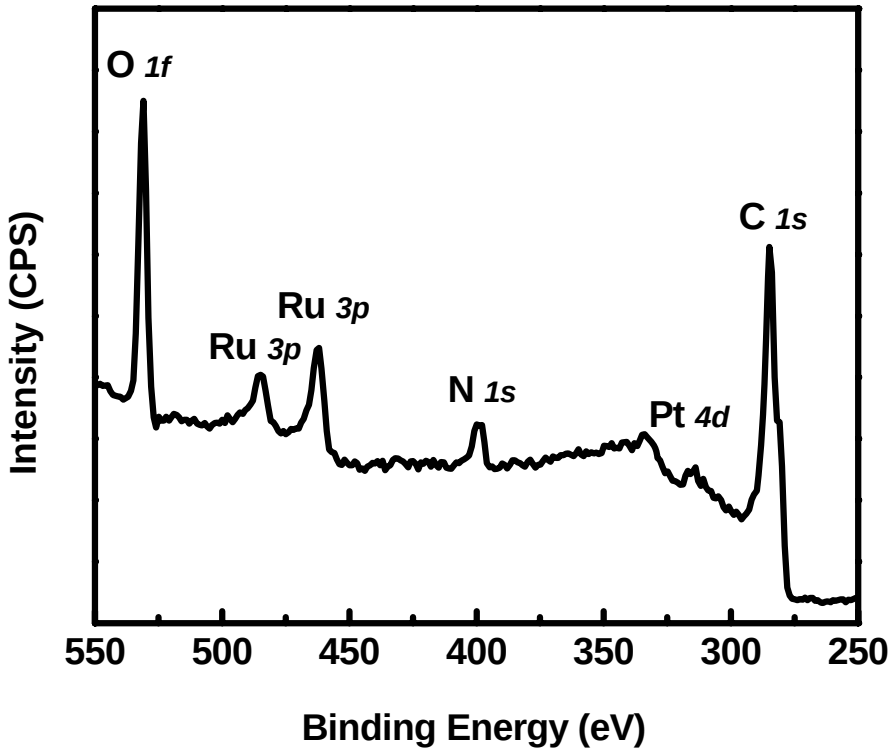

Figure 5.6. XPS spectrum of PtRu/1-AP-CNFs in the binding energy of 250-550 eV. The metal loading is 75 wt%.

X-ray photoelectron spectroscopy (XPS) spectrum obtained from PtRu/1-AP-CNFs is presented in Figure 5.6. One characteristic peak of *4d* for Pt appears at about 315 eV, two characteristic peaks of *3p* for Ru appear at around 461 and 484 eV, and one *1s* peak of carbon appears at about 285 eV, respectively.[272, 273] Moreover, based on the intensities of XPS

peaks of Pt *4d* and Ru *3p*, the elemental ratio of Pt:Ru can be calculated to be around 3:2, which is the same as the molar ratio of Pt and Ru precursors used in the preparation of PtRu/1-AP-CNFs.

5.3.6. Raman spectra of PtRu/1-AP-CNFs and PtRu/AO-CNFs

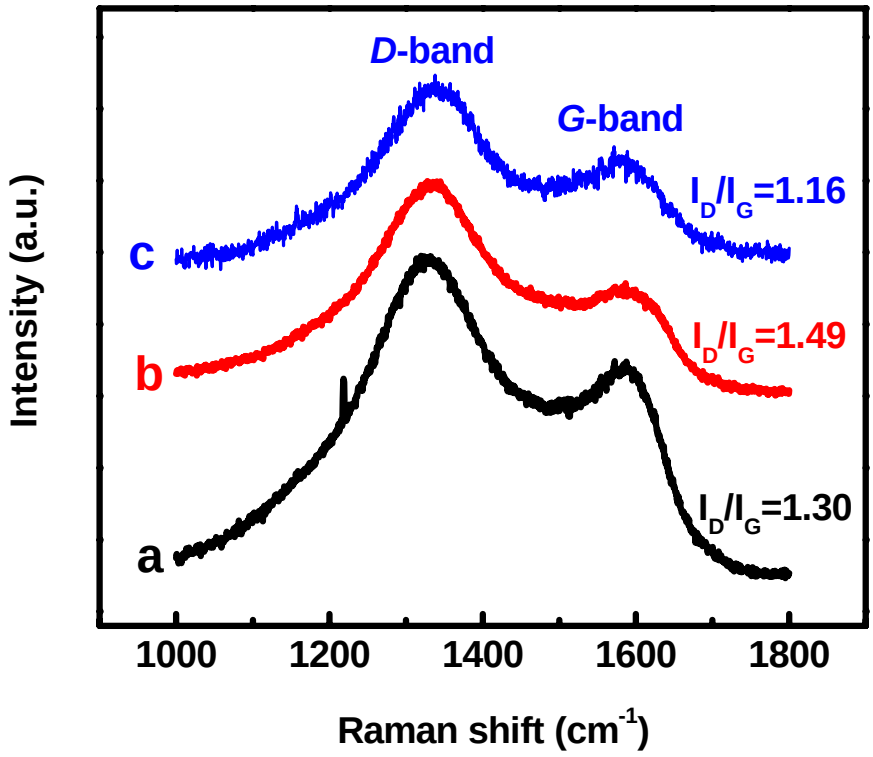

Figure 5.7. Raman spectra of CNFs (a), PtRu/AO-CNFs (b), and PtRu/1-AP-CNFs (c). The metal loading is 75 wt%.

Raman spectra of untreated CNFs, PtRu/1-AP-CNFs, and PtRu/AO-CNFs are shown in Figure 5.7. Raman spectra of carbon materials reflect the electronic structure and electron-phonon interactions and allow clear identification of graphite layers.[261] The peak at 1335 cm^{-1} is assigned to the disordered graphite structure (*D*-band), and the frequency peak at 1587 cm^{-1} (*G*-band) corresponds to a splitting of the E_{2g} stretching mode of graphite, which reflects the structural intensity of the sp^2-hybridized carbon atoms.[262] Therefore, the intensity ratio of *D*- and *G*-bands (I_D/I_G) can be used to evaluate the extent of the modification or defects on CNF surface and a higher I_D/I_G ratio typically indicates a higher degree of disorder. From Figure 5.7, it is seen that, compared to untreated CNFs, the I_D/I_G ratio of PtRu/AO-CNFs increases from 1.30 to 1.49. This indicates that the harsh acid treatment produces carboxylic acid sites on the surface, causing significant structural damage on the ordered structure of CNF surface. From Figure 5.7, it is also seen that PtRu/1-AP-CNFs have slightly lower I_D/I_G ratio (*i.e.,* 1.16) than untreated CNFs, which indicates that the immobilization or wrapping of 1-AP on the surface of CNFs via π-stacking has no detrimental effect on the ordered structure in CNFs. Rather, the slightly decreased ratio may suggest the coverage of the original defect sites by 1-AP molecules.

5.3.7. Electrochemical characterization of PtRu/CNFs

CV measurements of PtRu/AO-CNFs and PtRu/1-AP-CNFs between -0.2 and +1.0 V at 50 mV s^{-1} in 0.5 M H_2SO_4 were employed to examine whether PtRu particles on CNF surface

are electrochemically active (Figure 5.8). It is seen that redox current density peaks can be observed, which are due to the adsorption and desorption of hydrogen at the surface of PtRu nanoparticles on CNFs.

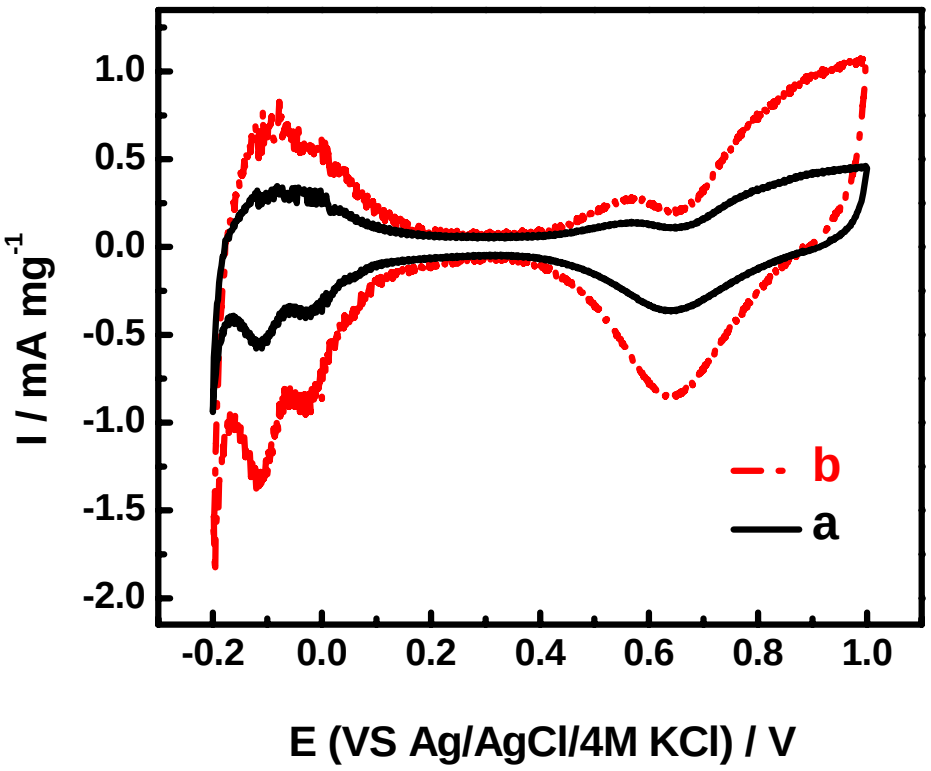

Figure 5.8. Current-potential curves of PtRu/AO-CNFs (a) and PtRu/1-AP-CNFs (b) in 0.5 M H_2SO_4 at 50 $mV \cdot s^{-1}$. The metal loading is 75 wt%.

The integration of CV curves from hydrogen desorption peaks from -0.2 to +0.2 V gives electrochemical active surface area (EASA), which can be calculated according to the

following formula:[263]

$$\text{EASA} = Q(mC\ mg^{-1})/0.22mC\ cm^{-2} \qquad (5.2)$$

where Q is the electric charge for hydrogen desorption and 0.22 mC cm^{-2} the hydrogen adsorption constant (based on Pt). Table 5.1 shows the calculated EASA values for both PtRu/AO-CNFs and PtRu/1-AP-CNFs. It is seen that the EASA for PtRu/1-AP-CNFs is 327 cm^2/mg, much higher than that of PtRu/AO-CNFs (233 cm^2/mg), which is due to the smaller PtRu particle size and less agglomerate formation on the surface of 1-AP-CNFs. This result demonstrates that PtRu nanoparticles deposited on 1-AP-CNFs are electrochemically more accessible, which is important for electrocatalyst applications in fuel cells.

5.3.8. Electro-oxidation of methanol on PtRu/CNFs

Figure 5.9 shows the current density-potential curves of PtRu/AO-CNFs and PtRu/1-AP-CNFs in 0.125 M CH_3OH + 0.2 M H_2SO_4 solution at 5 mV s^{-1}. It is seen that both PtRu/AO-CNFs and PtRu/1-AP-CNFs present the electro-oxidation of methanol, which starts at around +0.40 V and then the current density increases to a maximum at about +0.63 V; moreover, another current peak is found at about +0.43 V when scanning back. The mechanism for the methanol reaction is: first, methanol is adsorbed on the surface of PtRu nanoparticles, and then transformed to different reactive intermediates, such as $(CH_2O)_{ads}$ and $(CHO)_{ads}$, and poisoning species $(CO)_{ads}$. Both reactive and poisoning species can be further oxidized to CO_2, however, a relatively higher potential is required to oxidize the poisoning

species $(CO)_{ads}$.[170, 264, 265]

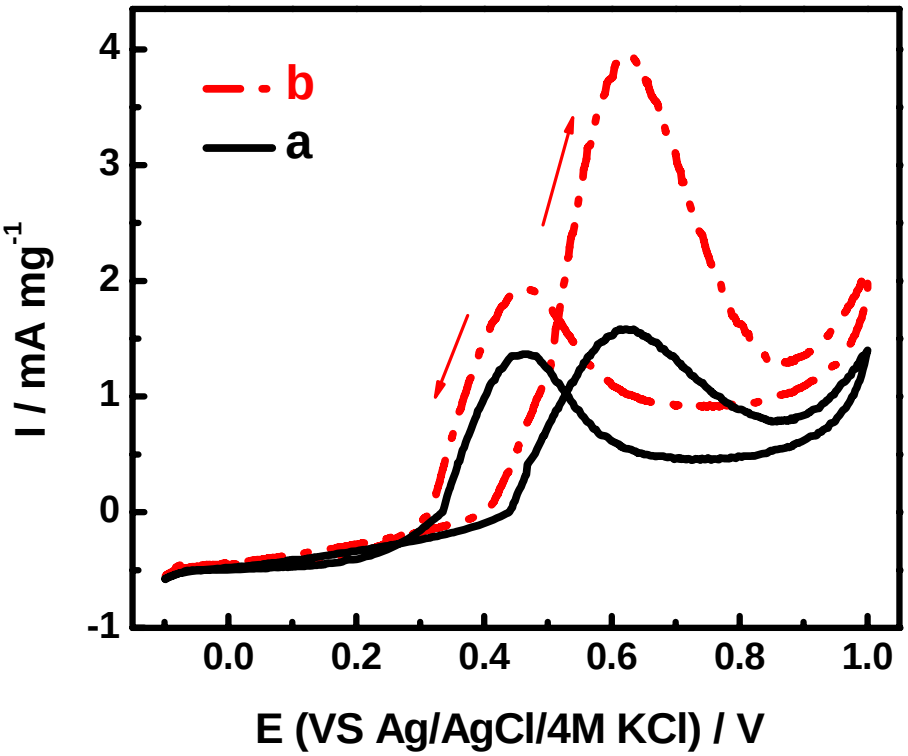

Figure 5.9. Current-potential curves of PtRu/AO-CNFs (a) and PtRu/1-AP-CNFs (b) in 0.125 M CH_3OH + 0.2 M H_2SO_4 at 5 mV s^{-1}. The metal loading is 75 wt%.

In order to study the efficiency of methanol oxidation, the electrochemical characteristic data of PtRu/AO-CNFs and PtRu/1-AP-CNFs are summarized in Table 5.1. The efficiencies of methanol oxidation were compared in items of forward onset potential, forward peak current density (I_f), backward peak current density (I_b), and the ratio of forward to backward peak

current densities (I_f/I_b). From Table 5.1, it is seen that compared with PtRu/AO-CNFs, PtRu/1-AP-CNFs have larger forward and backward peak current densities due to their reduced PtRu particle size and increased EASA. The I_f/I_b ratio of PtRu/1-AP-CNFs is also larger than that of PtRu/AO-CNFs, which may be related to the smaller PtRu particles in Pt/1-AP-CNFs. In addition, a smaller forward onset potential is obtained at PtRu/1-AP-CNFs, indicating the better catalytic activity of PtRu/1-AP-CNFs than that of PtRu/AO-CNFs.

Table 5.1. Electrochemical characteristics of PtRu/AO-CNFs and PtRu/1-AP-CNFs. Solutions: 0.5 M H_2SO_4 for EASA and 0.125 M CH_3OH + 0.2 M H_2SO_4 for other characteristics. Scanning rate: 5 mV s^{-1}. The metal loading is 75 wt%.

Catalysts	Average particle size (nm)	EASA (cm^2/mg)	Onset Potential (V *VS* Ag/AgCl/4.0 M KCl)	Backward peak current density (I_f, mA mg^{-1})	Backward peak current density (I_b, mA mg^{-1})	I_f/I_b
PtRu/AO-CNFs	5.4	233	0.42	1.58	1.46	1.08
PtRu/1-AP-CNFs	3.6	327	0.39	3.93	1.90	2.07

5.4. Summary

The preparation and characterization of PtRu/CNFs by the combination of 1-AP functionalization and a polyol processing technique were studied. PtRu nanoparticles with

well-defined morphology and good catalyst activity were obtained on functionalized CNFs. It is found that compared with the conventional acid-treated CNFs, the simple synthesis process of 1-AP-functionalization treatment can preserves the integrity and the electronic structure of CNFs. The diameter of PtRu nanoparticles on 1-AP functionalized CNFs is around 3.5 nm in average, which is smaller than that of PtRu/CNFs prepared from the conventional acid-treated CNFs. Moreover, PtRu nanoparticles are much more evenly distributed on 1-AP functionalized CNFs without forming agglomerates. The resulting PtRu/1-AP-CNFs possess the properties of higher active surface area and better performance towards the oxidation of methanol. Therefore, the chemical deposition of PtRu nanoparticles on 1-AP-CNFs provides an alternative method to obtain a good catalyst toward the oxidation of methanol. However, investigations into the catalytic ability of such composites in membrane electrode assembly in direct methanol fuel cells are needed for future applications.

CHAPTER 6. ANODE: CARBON NANOFIBER-SUPPORTED PLATINUM BY ELECTRODEPOSITION-(I)

Abstract

Pt/carbon composite nanofibers were prepared by electrodepositing Pt nanoparticles onto electrospun carbon nanofibers and were used as catalysts towards the oxidation of methanol. The morphology and size of Pt nanoparticles were controlled by selectively adjusting the electrodeposition potential and time. SEM and TEM results show that the composite nanofibers were successfully obtained and Pt particle diameters were between 10 and 55 nm. The electrocatalytic activity of the composite nanofibers expressed by current density per Pt particle mass was found to depend on the particle size, showing an increasing activity when the catalyst diameter decreased.

6.1. Introduction

Novel synthesis and processing technologies present the opportunity to design next-generation, high-efficiency energy storage and conversion systems. Among various energy systems, fuel cells are considered leading candidates for generating power in a clean manner for our future because they provide electricity without combustion and the pollutants associated with burning fossil fuels.[254] In conventional fuel cells, electrodes are typically constructed by binding catalyst-loaded carbon particles (*e.g.,* Vulcan XC-72 carbon black-supported Pt) with Nafion®, in which carbon particles facilitate electron transport. A high catalyst loading in these electrodes is typically required because they cannot ensure a simultaneous access of the catalyst to the fuel, electron-conducting diffusion layer and proton-conducting electrolyte.[274] As a result, the cost of precious metallic or alloyed catalysts will be a significant barrier to widespread commercial use of fuel cells.

Replacing carbon particles with one-dimensional carbon nanomaterials, such as carbon nanotubes (CNTs) and carbon nanofibers (CNFs), can provide effective long-range electron transfer in electrodes, thereby resulting in improved catalyst utilization and lower catalyst loading. Research has been conducted on the deposition of noble metal such as Pt nanoparticles onto CNTs,[234, 266, 275] but little has been done on CNFs. Due to the fascinating structure and thermal/electrical/mechanical properties, CNFs are of special interest recently because they can be synthesized in different graphene sheets by cheap and readily available methods.[276] Li et al. used the cyclic voltammogram method to deposit Pt

particles onto CNFs, but the diameters of deposited Pt nanoclusters are too large (50-200 nm) for practical fuel cell applications.[277] It is important to obtain catalysts with smaller particle sizes evenly distributed on CNF surface, which can exhibit increased catalytic activities concomitant with a lower necessary loading. Here, we report on the preparation and characterization of Pt/carbon composite nanofibers (Pt/CNFs) by the electrodeposition of smaller Pt nanoparticles ($\leq$ 55 nm) onto electrospun CNFs under different potentials.

6.2. Experimental

6.2.1. Preparation of CNFs

CNFs were synthesized using the electrospinning method. First, 8.0 wt% polyacrylonitrile (PAN, Sigma-Aldrich) solution in N,N-dimethylformamide (DMF, Sigma-Aldrich) was prepared at 60^{o}C. The electrospinning was conducted by a variable high voltage power supply (Gamma ES40P-20W/DAM) at a voltage of 15 kV. Under high voltage, a polymer jet was ejected and accelerated toward the counter electrode, during which the solvent was rapidly evaporated. The electrospun fibers were collected on an aluminum foil. The collected nanofibers were stabilized in an air atmosphere at 280 ^{o}C for 2 hrs at the heating rate of 5 ^{o}C min^{-1}, and then carbonized at 700 ^{o}C for 1 hr in nitrogen atmosphere at the heating rate of 2

^{o}C min^{-1}. The resultant CNFs formed free-standing nonwoven membranes and were directly used as the working electrode in the electrodeposition of Pt nanoparticles.

6.2.2. Electrodeposition of Pt nanoparticles

Figure 6.1 illustrates the procedure of electrodepositing Pt nanoparticles onto CNFs. CNFs were cycled in 1.0 M H_2SO_4 solution between -0.70 and +1.20 V for 100 cycles at 50.0 mV s^{-1} to oxidize the surface. During that process, various surface functional groups such as quinoid (=O), hydroxy (-OH) and carboxyl (-COOH) were produced, which can supply defect sites for the Pt nanoparticle deposition.[258] The presence of these functional groups on oxidized CNFs was confirmed by using Nicolet Nexus 470 Fourier Transform Infra Red spectrophotometer. The surface-treated CNFs were then immersed in 5.0 mM $H_2PtCl_6{\cdot}xH_2O$ + 1.0 M H_2SO_4 solution for 1 hr under the potentials of -0.2 V, 0.0 V and +0.2 V, respectively, to carry out the electrodeposition of Pt nanoparticles.

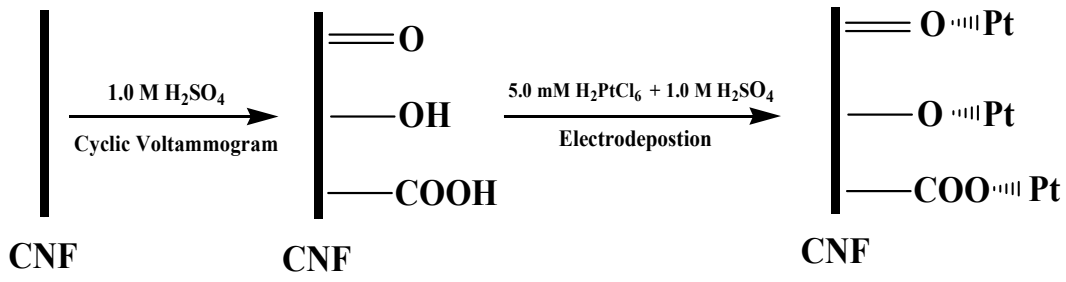

Figure 6.1. Schematic diagram illustrating the procedure of electrodepositing Pt nanoparticles onto CNFs.

6.3. Results and Discussions

6.3.1. FTIR spectra

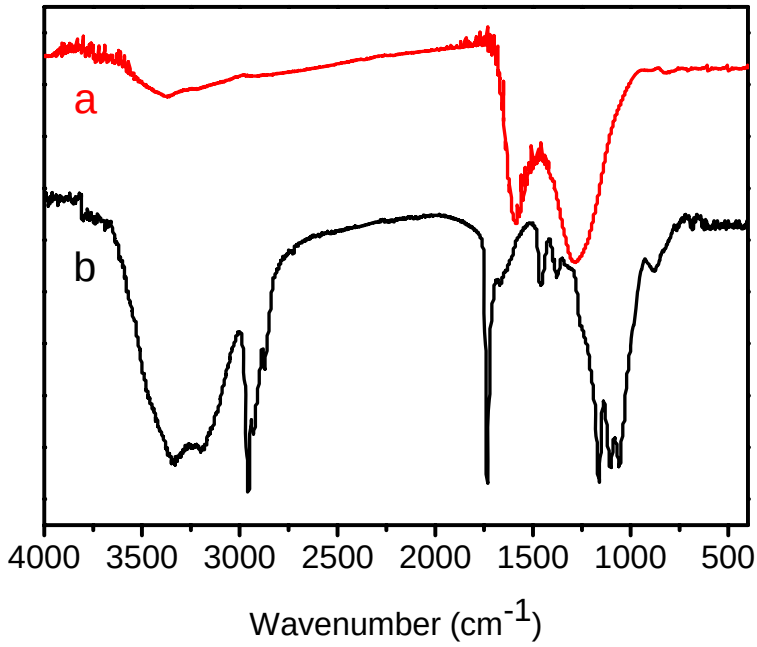

Figure 6.2. FTIR spectra of CNFs (a) and oxidized CNFs (b).

FTIR spectra of CNFs and oxidized CNFs are shown in Figure 6.2. For un-oxidized CNFs, two major characteristic IR bands are found at 1280 cm^{-1} and 1590 cm^{-1}, respectively, which are related to the C-C and C=C stretch bonds. However, oxidized CNFs present peaks with

relatively high intensities at around 3333 and 2957 cm^{-1}, the -OH vibration peaks of -COOH , and at 1162 cm^{-1}, the -C-O stretch peak of -C-OH. Oxidized CNFs also show two characteristic bending mode peaks at 1733 cm^{-1} and 1690 cm^{-1}, which are the -C=O stretch bond in esters and benzophenones, respectively. As a result, FTIR spectra suggest that the CNF surface has been oxidized, which can form defects and are suitable for the deposition of Pt nanoparticles.

6.3.2. TEM images

Figure 6.3 shows TEM images of CNFs and Pt/CNFs, in which Pt was electrodeposited at -0.2 V. It is seen that before electrodeposition, the CNF surface is smooth and there are no particles. However, Pt nanoparticles are evenly distributed on the surface of CNFs after the electrodeposition, and the particle size ranges from 10 to 35 nm. The energy dispersive X-ray spectroscopy (EDS) of Pt/CNFs is also showed in Figure 6.3, and confirms the presence of Pt on CNF surface. The peak of Cu comes from the TEM grid used in the experiment.

6.3.3. SEM images

Figure 6.4 shows SEM images of Pt/CNFs, in which Pt nanoparticles were deposited in three different potentials: -0.2, 0.0, and +0.2 V. In SEM images, the well-dispersed Pt nanoparticles

can be observed on the surface of CNFs after electrodeposition. The amount (m_{Pt}) of Pt loading was calculated by the following equation:

$$m_{Pt} = \frac{Q_{Pt} \cdot M}{4F \cdot S} \qquad (6.1)$$

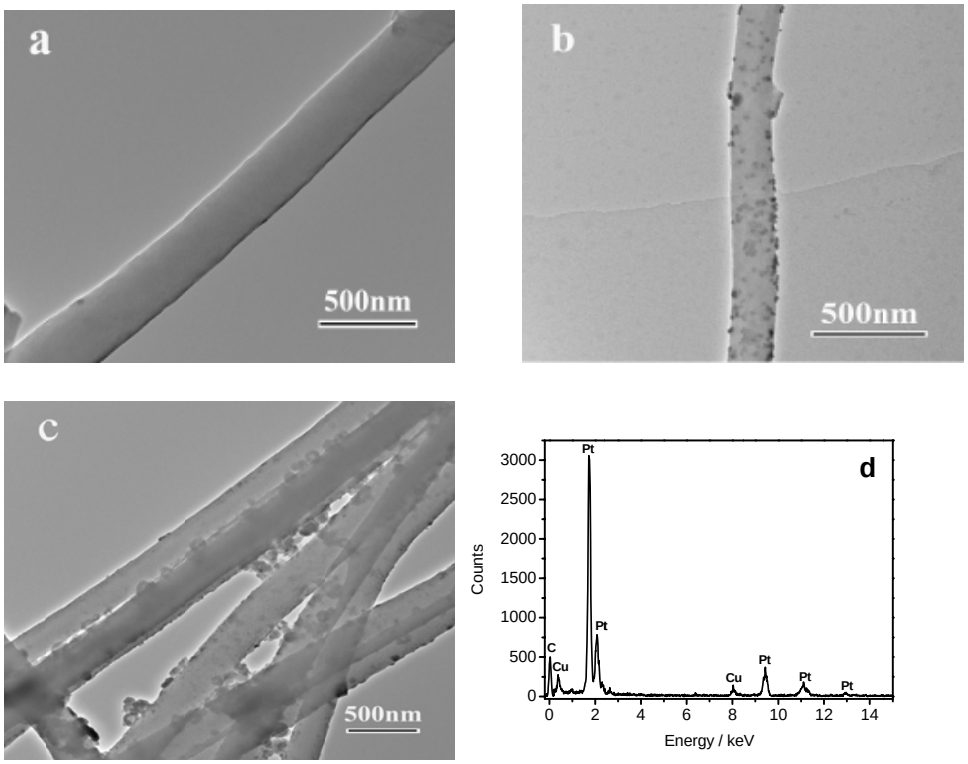

Figure 6.3. TEM images of CNFs (a), Pt/CNFs (b, c), and EDS spectrum of Pt/CNFs (d). Electrodeposition potential: -0.2 V.

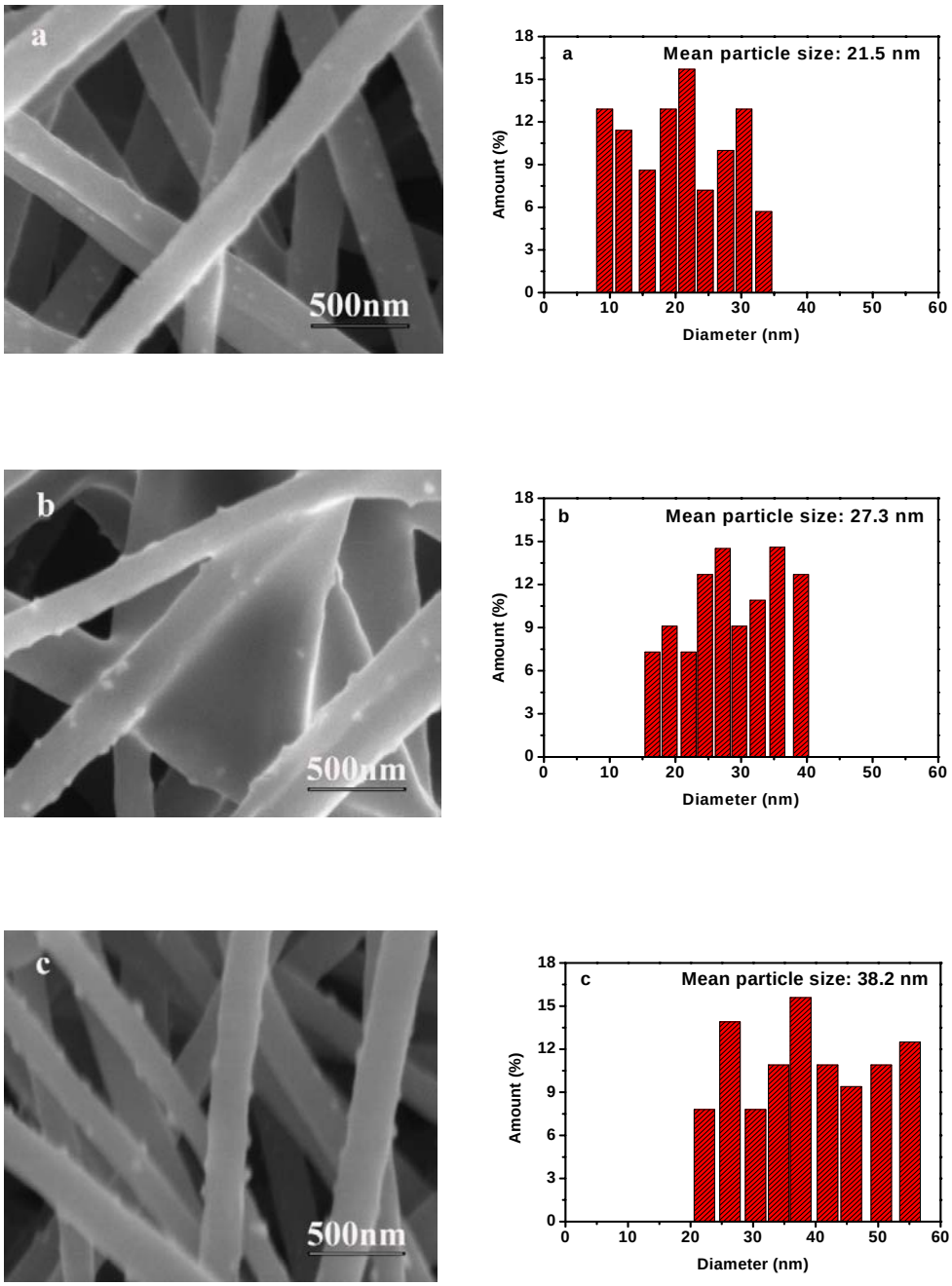

Figure 6.4. SEM images and diameter distributions of Pt/CNFs prepared with different electrodeposition potentials: (a) -0.2, (b) 0.0, and (c) +0.2 V.

where M is the atomic weight of Pt (195.09 g mol^{-1}), Q_{Pt} the electrons transferred (C), S the geometric area of CNF electrode (cm^{-2}), and F the Faraday constant (96,485 C mol^{-1}). The deposition amount is 0.17, 0.26, and 0.57 mg cm^{-2} when the potential used is -0.2, 0.0, and +0.2 V, respectively. The Pt particle diameter distribution is also shown in Figure 6.3. From the histogram analysis, the diameter of Pt nanoparticles decreases with decrease in electrodeposition potential. This is because the application of more negative potential favors the formation of a greater quantity of nuclei, resulting in smaller Pt particle size [278]. Moreover, the less deposition amount at lower potentials should also be responsible for the smaller particle size.

6.3.4. Electrochemical performance of Pt/CNF nanocomposites

Figure 6.5 shows the current density-potential curves of CNF and Pt/CNF electrodes (electrodeposition potential: -0.2 V) in 0.125 M CH_3OH + 0.20 M H_2SO_4 solution at 5.0 mV s^{-1}. There is almost no methanol oxidation peak found for the CNF electrode. In comparison, the Pt/CNF electrode presents the electro-oxidation of methanol, which starts at +0.40 V with a maximum peak at +0.62 V. After reaching the maximum, a decrease in current density is observed due to the formation of oxides on the Pt surface, which decreases the number of active sites. Moreover, another current density peak is found at +0.55 V while reducing the potential, which signifies the desorption of CO generated through the methanol oxidation.[274]

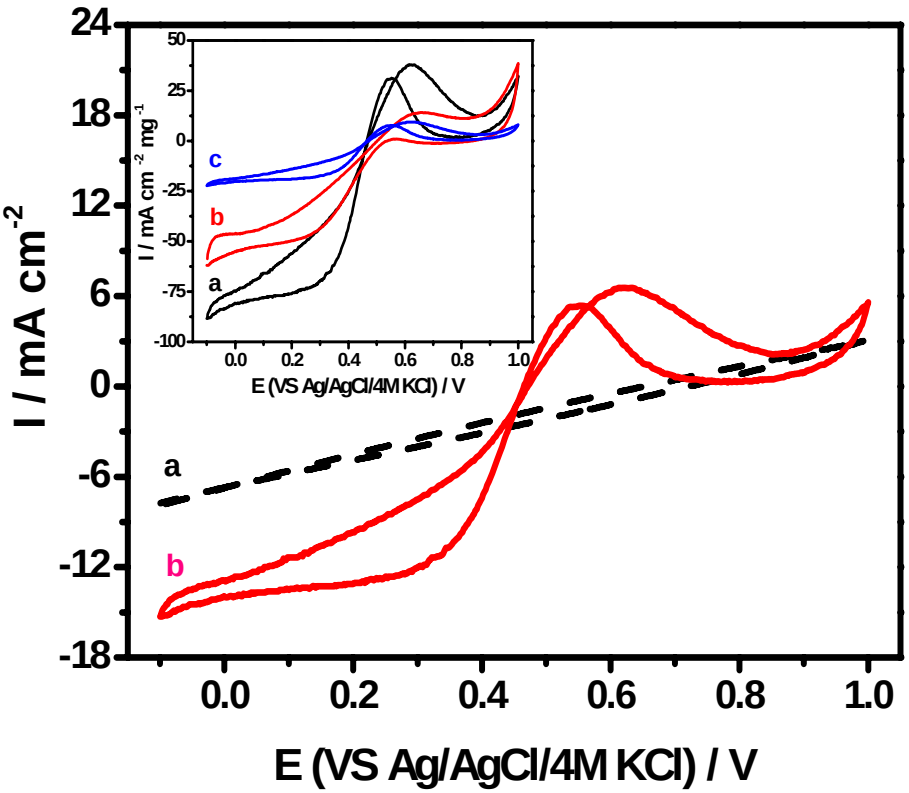

Figure 6.5. Current density-potential curves of CNF (a) and Pt/CNF (b) electrodes in the 0.125 M methanol + 0.20 M sulfuric acid solution at 5.0 mV s^{-1}. The inset shows the normalized curves of three Pt/CNF electrodes prepared with different electrodeposition potentials: (a) -0.2, (b) 0.0, and (c) +0.2 V.

To compare the catalytic activity of Pt/CNF electrodes prepared under different potentials, the current density-potential curves of these electrodes are shown in the inset of Figure 6.5 with the current density expressed by per mg of Pt nanoparticles. The maximum methanol

oxidation current density is found in the Pt/CNF electrode prepared under -0.2 V, and the minimum is in the electrode deposited under +0.2 V. The better performance of the Pt/CNF electrode under -0.2 V can be associated to the smaller Pt nanoparticle diameter since the electrochemical reaction depends on the electrocatalyst surface area. Among the three electrodes, Pt nanoparticles in the Pt/CNF electrode under -0.2 V are the smallest in diameter, which make them more accessible to the reactants.

6.4. Summary

Pt/CNF nanocomposites with well-defined morphology and particle size were prepared by electrodepositing Pt nanoparticles onto electrospun carbon nanofibers under different potentials. TEM and SEM results show that the Pt particle diameters are between 10 - 55 nm. The Pt/CNF electrodes were characterized by their good electrocatalytic properties towards the oxidation of methanol and it is demonstrated that the Pt/CNF electrode prepared under the potential -0.2 V has the best activity due to the lowest catalyst diameter.

CHAPTER 7. ANODE: CARBON NANOFIBER-SUPPORTED PLATINUM BY ELECTRODEPOSITION-(II)

Abstract

Pt/carbon composite nanofibers were prepared by electrodepositing Pt nanoparticles directly onto electrospun carbon nanofibers. The morphology and size of Pt nanoparticles were controlled by the electrodeposition time. The resulting Pt/carbon composite nanofibers were characterized by running cyclic voltammograms in 0.20 M H_2SO_4 and 5.0 mM $K_4[Fe(CN)_6]$ + 0.10 M KCl solutions, respectively. The electrocatalytic activities of Pt/carbon composite nanofibers were measured by the oxidation of methanol. Results show that Pt/carbon composite nanofibers possess the properties of high active surface area and fast electron transfer rate, which lead to a good performance towards the electrocatalytic oxidation of methanol. It is also found that the Pt/carbon nanofiber electrode with a Pt loading of 0.170 mg cm^{-2} has the highest activity.

7.1. Introduction

Nanomaterials have received growing interest due to their unique chemical and physical properties according to their sizes and shapes.[2] Nanostructured carbons with different forms, such as fullerenes, nanotubes, and nanofibers, have fascinating structures and thermal/electric/mechanical properties, and hence they gained much attention due to their potential applications in diverse areas, ranging from fuel cells, supercapacitor, hydrogen storage, field emission devices, to chemical/biological sensors.[279-282] In many of these applications, the deposition of precious metallic or alloyed catalysts onto the carbon substrate is necessary to provide such desired functionalities as the electrocatalytic activity. In these cases, the structure and properties of the supporting carbon materials are crucial because they have significant impact on the size, distribution, and activity of the supported catalysts. For example, in direct methanol fuel cells, the methanol oxidation reaction (MOR) in acidic solution, typically catalyzed by Pt or its alloy, can be expressed in the following equation:[253]

$$CH_3OH + H_2O \rightarrow CO_2 + 6H^+ + 6e^- \qquad (7.1)$$

E^o (MOR) = 0.016V *vs.* SHE at 25 ^oC

For the reaction to happen, the catalyst particles must have simultaneous exposure to the reactants, protons, and electrons. Therefore, the development of highly active electrode

catalysts coupled with a suitable electrode structure for the oxidation of methanol is an important subject to attaining the high efficiency in direct methanol fuel cells.

Carbon nanomaterials are currently being considered as the catalysts supports in direct methanol fuel cells, because of their unique graphite properties combined with three-dimensional flexible structures. Among various carbon nanomaterials, 1-dimentional nano-carbons, such as carbon nanotubes and carbon nanofibers, are considered as promising support materials for catalysts in direct methanol fuel cells, thanks to their unique structures, high electronic and thermal conductivities, and good electrochemical stability.[256, 257] Compared with carbon nanotubes, carbon nanofibers are inexpensive and can be produced with various controlled structures at relatively high speeds. However, most current research focused on the deposition of noble metal such as Pt nanoparticles onto carbon nanotubes[283-286] and there are only few literature reports on utilizing carbon nanofibers as the catalyst support . For example, Li et. al., recently utilized the pulsed electrodeposition method to prepare Pt-deposited carbon nanofibers, but the resultant Pt particle sizes are relatively large (~ 150 nm).[277] Here, we report the preparation and characterization of Pt/carbon composite nanofibers by electrodepositing Pt nanoparticles with smaller diameters onto carbon nanofibers.

7.2. Experimental

7.2.1. Chemicals and reagents

Polyacrylonitrile (PAN), N,N-dimethylformamide (DMF), chloroplatinic acid hydrate ($H_2PtCl_6 \cdot xH_2O$), potassium hexacyanoferrate (II) ($K_4[Fe(CN)_6]$), sulfuric acid (H_2SO_4) and methanol (CH_3OH) were purchased from Sigma-Aldrich, and they were used without further purification. Deionized water was used throughout.

7.2.2. Synthesis of carbon nanofibers

A/DMF solution 8 wt% PAN was prepared at 60 ^oC, with mechanical stirring for three hours. The electrospinning was conducted using a Gamma ES40P-20W/DAM variable high voltage power supply under a voltage of 15 kV. Under high voltage, a polymer jet was ejected and accelerated toward the nanofiber collector, during which the solvent was rapidly evaporated. The electrospun PAN fibers were collected on an aluminum foil placed on the collector. These PAN nanofibers were first stabilized in an air atmosphere at 280 ^oC for 2.0 hrs at the heating rate 5.0 $^oC\ min^{-1}$, and then carbonized at 700 ^oC for 1.0 hr in nitrogen atmosphere at the heating rate 2.0 $^oC\ min^{-1}$. The resulting carbon nanofibers were used as the working

electrode in the electrodeposition of Pt nanoparticles.

7.2.3. Electrodeposition of Pt onto carbon nanofibers

First, carbon nanofibers were directly used as the working electrode and were cycled in 1.0 M H_2SO_4 solution between -0.70 and 1.20 V for 100 cycles at 50.0 mV s^{-1} to form oxidized carbon nanofibers. The electrodepostion of Pt particles was carried out by applying a potential of -0.2 V with different deposition durations on the oxidized carbon nanofibers in a 5.0 mM $H_2PtCl_6 \cdot xH_2O$ + 1.0 M H_2SO_4 solution.

The structure of carbon and Pt/carbon nanofibers, which were deposited onto 200 mesh carbon-coated Cu grids, was evaluated using a Hitachi HF-2000 TEM at 200 kV. These carbon and Pt/carbon nanofibers were also examined using a JEOL JSM-6360LV FESEM at 15 kV.

7.2.4. Electrochemical properties of Pt/carbon nanofibers

The electrochemical measurements of Pt/carbon nanofibers were performed in a three-electrode cell at 25.0 ^{o}C on an AQ4 Gamry Reference 600 electrochemical workstation. The cell consisted of a working electrode (Pt/carbon nanofibers), a counter electrode (Pt

wire), and a reference electrode (*Ag*/*AgCl*/4.0 M KCl). Nitrogen was used to bubble the testing solutions for at least 30 mins before the measurements, and then was used continually to protect the experiment environment. All the electrochemical potentials were measured and reported with respect to Ag/AgCl/4.0 M KCl.

The measurement of hydrogen electrosorption was conducted by cyclic voltammograms (CVs) of Pt/carbon nanofiber electrodes in 0.50 M H_2SO_4 at 50.0 $mV \cdot s^{-1}$ to determine the electrochemically active surface area (Ar/cm^2). The electron transfer properties were determined by CVs of Pt/carbon nanofibers in 5.0 mM $K_4[Fe(CN)]_6$ + 0.50 M KCl at 50.0 $mV \cdot s^{-1}$. CVs of Pt/carbon nanofibers in 0.125 M CH_3OH + 0.20 M H_2SO_4 at 5.0 $mV \cdot s^{-1}$ were also carried out to study their activities on the methanol oxidation.

7.3. Results and Discussions

7.3.1. Surface oxidation of carbon nanofibers in 1.0 M H_2SO_4

Figure 7.1 shows the SEM image of carbon nanofibers before surface oxidation. It is shown that carbon nanofibers from PAN precursor have relatively smooth and regular surface morphology, with fiber diameters ranging from 200 nm to 300 nm. The fiber diameters can

be further reduced by manipulating spinning voltage, solution concentration, solvent type, and other processing parameters. Typically, smaller fiber diameter benefits the electrodeposition of Pt nanoparticles due to increased accessible surface area.

In order to carry out the surface oxidation, carbon nanofibers were used as the working electrode and were cycled in 1.0 M H_2SO_4 at different scan rates using CVs, and the results are shown in Figure 7.2. It is seen that two current peaks are found at ± 0.48 V, respectively, and they can be attributable to the redox reactions of surface functional groups as quinoid. Moreover, the current density increases with increase in scan rate. The response of the anodic current density peak (I_{pa}) was measured as a function of scan rate and is shown in the inset of Figure 7.2. I_{pa} depends almost linearly upon the scan rate, which is due to the Faradic process occurring on the surface of carbon nanofibers.

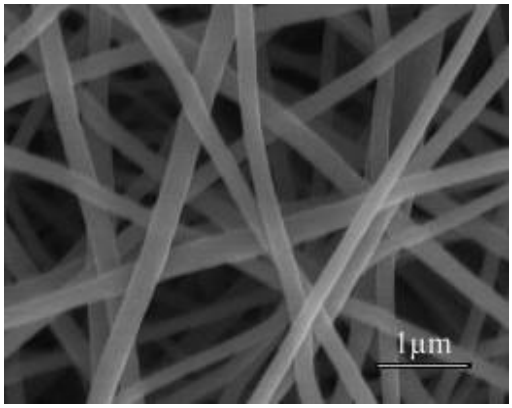

Figure 7.1. SEM image of carbon nanofibers before surface oxidation.

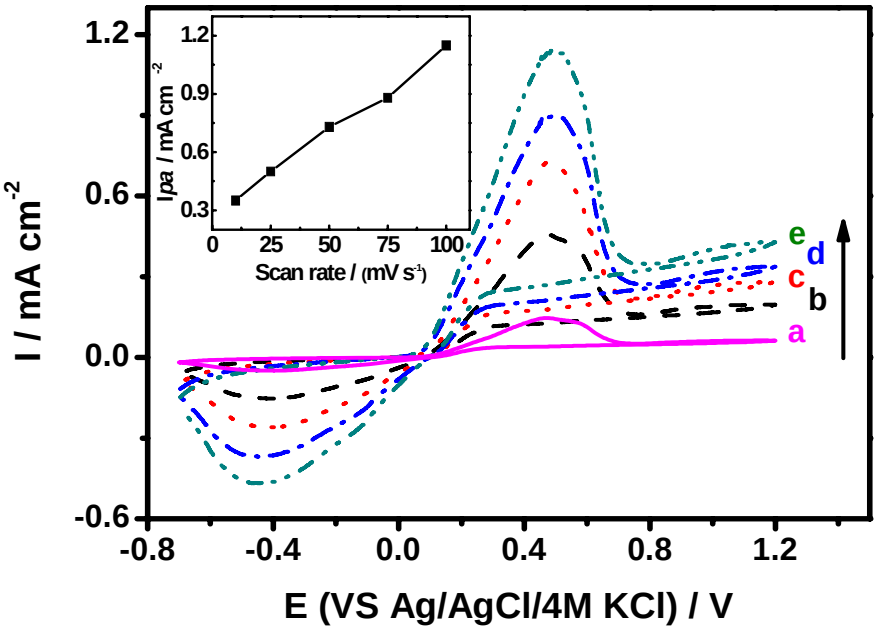

Figure 7.2. Surface oxidation of carbon nanofibers in 1.0 M H_2SO_4 at the scan rate of (a) 10.0, (b) 25.0, (c) 50.0, (d) 75.0, (e) 100.0 $mV \cdot S^{-1}$, respectively. The relationship between anodic peak current (*Ipa*) and scan rate is shown in the inset.

7.3.2. TEM images of carbon and Pt/carbon nanofibers

After the surface oxidation, Pt particles were electrodeposited onto the carbon nanofiber surface. Figure 7.3 shows TEM images of carbon nanofibers and Pt/carbon composite nanofibers with 1.0 hr deposition time. It is seen that before electrodeposition, the carbon

nanofiber surface is smooth and there are no particles loaded. However, Pt nanoparticles are evenly distributed on the surface of carbon nanofibers after the electrodeposition. The typical particle diameters are around 20 nm and they are smaller than those reported by some literature, in which a pulsed electrodeposition method was used . Figure 7.3d shows the energy dispersive X-ray spectroscopy (EDS) of Pt/carbon nanofibers. The EDS curve also confirms the presence of Pt particles on the surface of carbon nanofibers. The Cu peak in Figure 7.3d belongs to the TEM grid background.

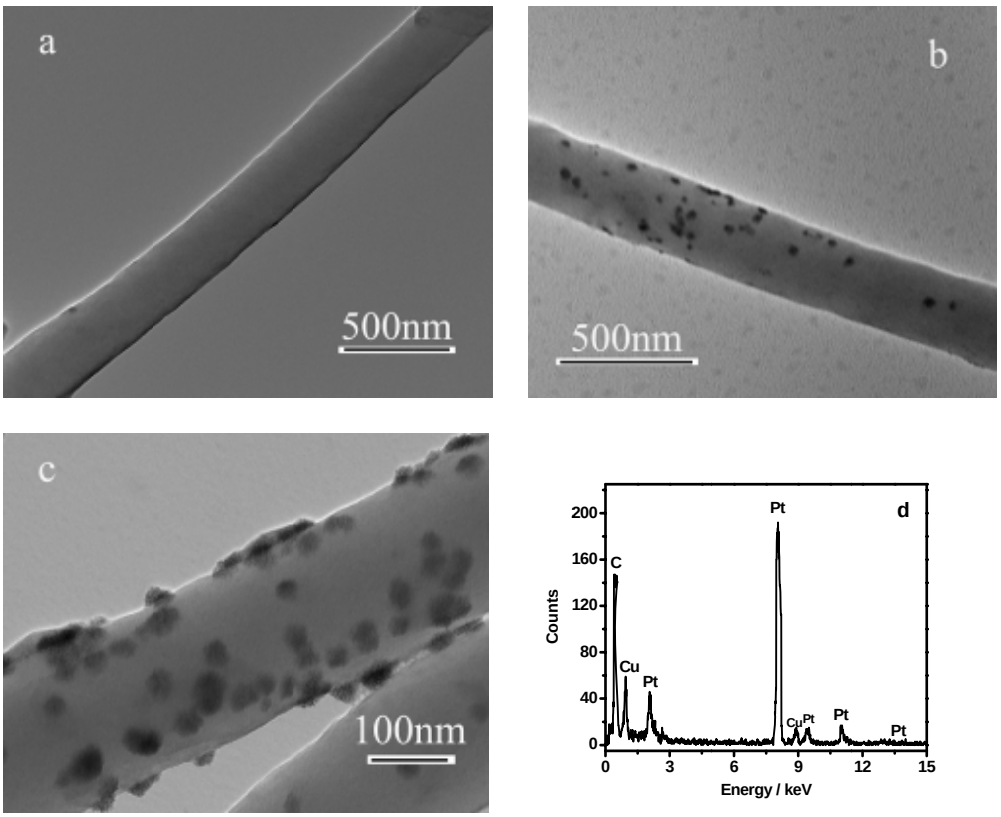

Figure 7.3. TEM images of carbon (a) Pt/carbon (b, c) nanofibers, and EDS spectrum of Pt/carbon nanofibers (d). Deposition time: 1.0 hr.

7.3.3. SEM images of Pt/carbon nanofibers

The amount (m_{Pt}) of Pt loading can be calculated by the following equation:

$$m_{Pt} = \frac{Q_{Pt} \cdot M}{4F \cdot S} \qquad (7.2)$$

where M is the atomic weight of Pt (195.09 g mol^{-1}), Q_{Pt} the electrons transferred (C), S the geometric area of carbon nanofiber electrode (cm^{-2}), and F the Faraday constant (96485 C mol^{-1}). In this work, four different deposition durations of 0.5, 1.0, 2.0, and 3.0 hr were used, and the Pt loadings of the resultant Pt/carbon nanofibers are 0.085, 0.170, 0.335, and 0.545 mg cm^{-2}, respectively. Figure 7.4 shows SEM images of these Pt/carbon composite nanofibers. When the deposition time is 0.5 hr, the resultant Pt loading of 0.085 mg cm^{-2} is relatively low, and hence Pt nanoparticles cannot be visually seen on the surface of carbon nanofibers. However, the electrochemical measurements discussed in the following sections show the presence of Pt nanoparticles on carbon nanofibers at this low loading. When the deposition time is beyond 0.5 hr, well-distributed Pt nanoparticles can be observed on the surface of carbon nanofibers. Moreover, with increase in deposition time, the surface morphology of carbon nanofibers becomes rougher and the diameter of Pt nanoparticles increases. That is because the application of a longer deposition time results in higher Pt nanoparticle loading without increasing the quantity of nuclei. As a result, with increase in deposition time (*i.e.,* Pt loading), the Pt nanoparticle size increases.

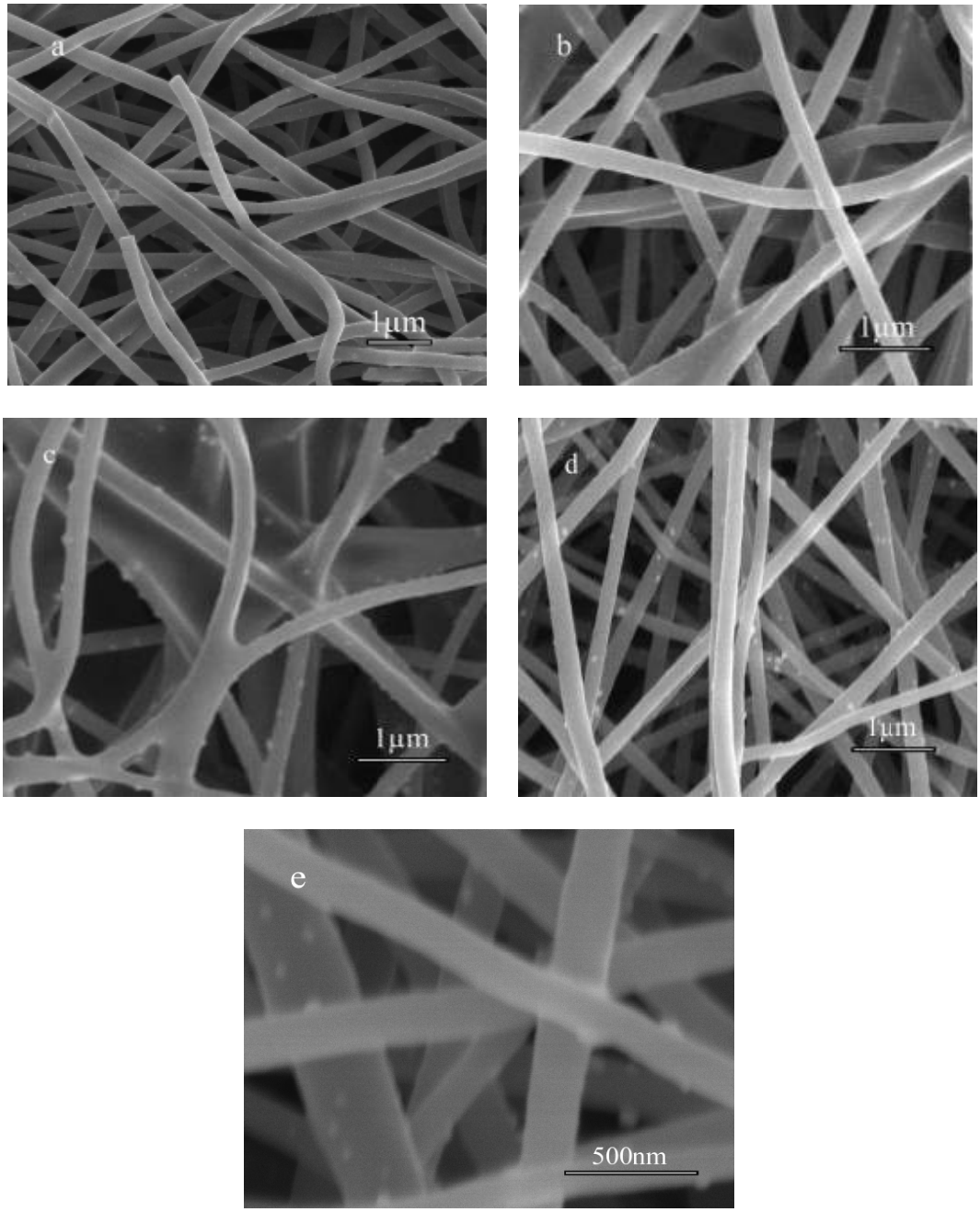

Figure 7.4. SEM images of Pt/carbon nanofibers prepared using different deposition durations (a. 0.5, b. 1.0, c. 2.0, d. and e. 3.0 hr).

Figures 7.4a, b, c, and d only show Pt nanoparticles deposited on the outer nanofiber layers. In order to ensure that nanoparticles have been deposited onto the surface of deeper layers, a SEM image was taken after mechanically peeling off three layers of Pr/carbon composite nanofibers (Figure 7.4e). It is seen that Pt nanoparticles are distributed on the nanofiber surface, indicating that Pt ions can penetrate deep into carbon nanofiber layers during electrodeposition and be reduced to Pt nanoparticles.

7.3.4. Electrochemical characterization of Pt/carbon nanofibers

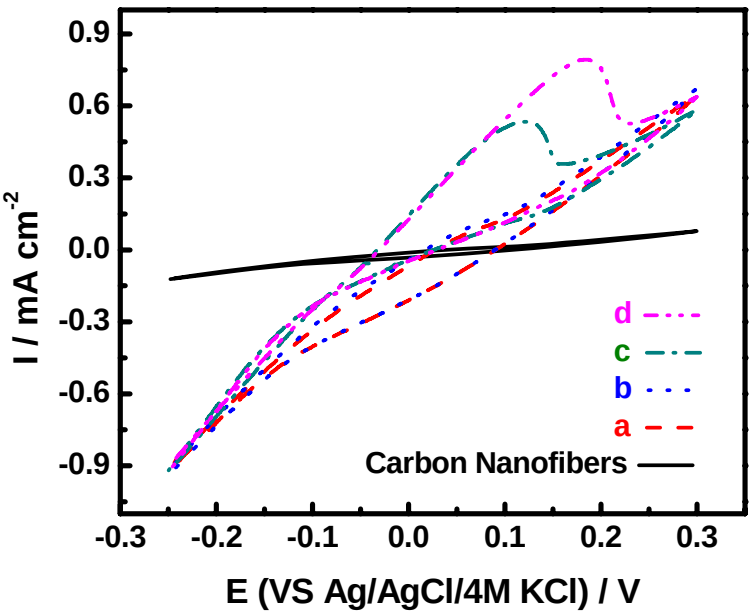

Figure 7.5. CV responses in 0.2 M H_2SO_4 for carbon and Pt/carbon nanofibers prepared using different deposition durations (a: 0.5, b: 1.0, c: 2.0, and d: 3.0 hr). Scanning rate: 50.0 $mV \cdot s^{-1}$.

CV measurements of carbon and Pt/carbon nanofibers between -0.25 and +0.30 V at 50.0 $mV \cdot s^{-1}$ in 0.20 M H_2SO_4 were employed to examine whether Pt particles on carbon nanofiber surface are electrochemically active (Figure 7.5). It is seen that there is no redox peak found in carbon nanofibers, indicating no electrochemical activity. However, after the electrochemical deposition of Pt particles, redox current density peaks were observed. These redox peaks are due to the adsorption and desorption of hydrogen at the surface of Pt particles on carbon nanofibers. Moreover, the integration of CV curves after correcting for the double layer charging gives the quantities of charge, Q_H (μC), which are showed in Table 7.1. According to the theoretical value of electricity Q_H^0 = 210 μC per real cm^2 of Pt [267], the electrochemically active surface areas of Pt/carbon nanofibers can be estimated from $Ar = Q_H / Q_H^0$, which are also shown in Table 7.1. From Table 1, it is found that with increase in deposition time, the Pt electroactive surface area increases.

Table 7.1. Charge quantities and electrochemically active surface areas of Pt/carbon nanofibers with different deposition durations. Solution: 0.20 M H_2SO_4. Scanning rate: 50.0 $mV \cdot s^{-1}$.

Deposition duration (hr)	0.5	1.0	2.0	3.0
Q_H / μC	77.3	92.7	122.8	187.0
Ar / cm^2	0.37	0.44	0.58	0.89

In order to study the electron transfer properties of carbon nanofibers before and after Pt particle deposition, steady-stated CV experiments were carried out at 50.0 $mV \cdot s^{-1}$ in 5.0 mM $K_4[Fe(CN)_6]$ + 1.0 M KCl, in which $K_4[Fe(CN)_6]$ served as a probe for the fast electron transfer (Figure 7.6). A pair of well-defined redox peaks for $Fe(CN)_6^{3-}/Fe(CN)_6^{4-}$ are found in Pt/carbon nanofibers at E = -0.12 and 0.04 V, respectively, indicating that Pt/carbon nanofibers have fast electron transfer kinetics, which may be due to the high electric conductivity and fascinating 3-dimensional structures of these nanofibers .

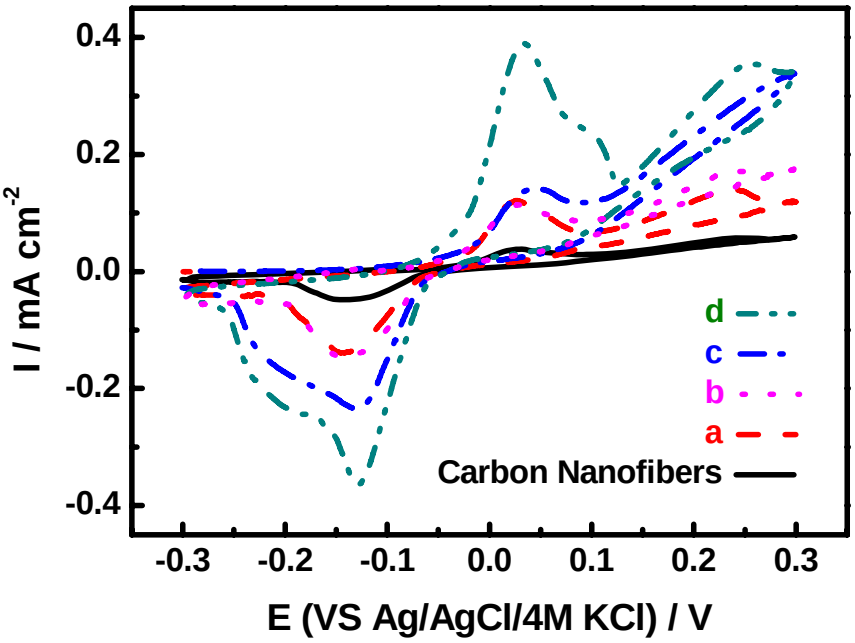

Figure 7.6. CV responses in 5.0 mM $K_4[Fe(CN)_6]$ + 0.1 M KCl for carbon and Pt/carbon nanofibers prepared using different deposition durations (a: 0.5, b: 1.0, c: 2.0, and d:. 3.0 hr). Scanning rate: 50.0 $mV \cdot s^{-1}$.

7.3.5. Electro-oxidation of methanol on Pt/carbon nanofibers

Figure 7.7 shows the current density-potential curves of carbon and Pt/carbon nanofibers in 0.125 M CH_3OH + 0.20 M H_2SO_4 solution at 5.0 $mV \cdot s^{-1}$. There is no methanol oxidation peak found for carbon nanofibers. In comparison, Pt/carbon nanofibers present a relatively large methanol electro-oxidation peak, which starts at +0.40 V with a maximum current peak +0.62 V. After the maximum, a decrease in current is observed due to the formation of oxides on the Pt surface, which decreases the number of active sites. Moreover, another current density peak is found at +0.55 V, which signifies the desorption of CO generated during the methanol oxidation .

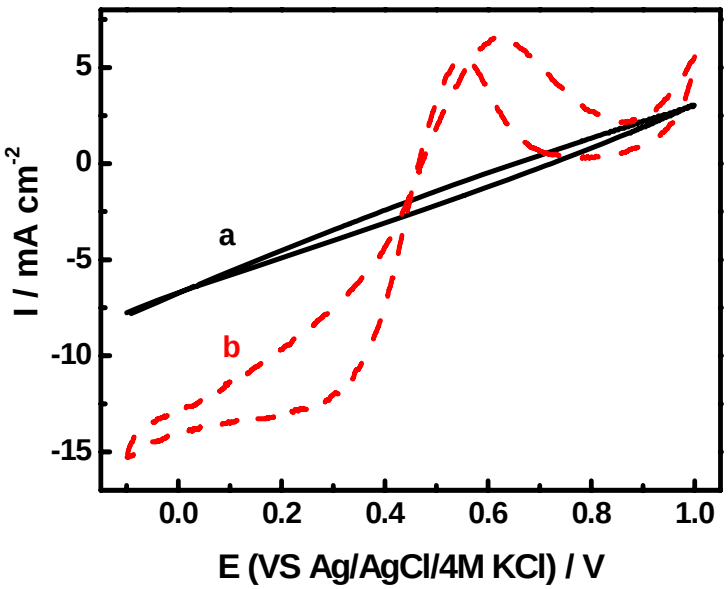

Figure 7.7. Current-potential curves of carbon (a) and Pt/carbon (b) in 0.125 M CH_3OH + 0.20 M H_2SO_4 at 5.0 $mV \cdot s^{-1}$. Deposition time: 1.0 hr.

Table 7.2. Electrochemical characteristics of Pt/carbon nanofibers with different deposition durations. Solution: 0.125 M CH_3OH + 0.20 M H_2SO_4. Scanning rate: 5.0 $mV \cdot s^{-1}$.

Deposition duration (hr)	Catalyst loading (mg cm^{-2})	Forward peak potential ($V_{VS\ Ag/AgCl/4.0\ M\ KCl}$)	Forward peak current density (*Ipa*, mA cm^{-2})	Mass activity (A g^{-1})
0.5	0.085	+ 0.63	2.33	27.41
1.0	0.170	+ 0.62	6.55	38.53
2.0	0.335	+ 0.63	10.43	31.13
3.0	0.545	+ 0.65	12.67	23.24

In order to study the efficiency of methanol oxidation, the electrochemical characteristic data of Pt/carbon nanofibers with different deposition durations are summarized in Table 7.2. The efficiencies of methanol oxidation were compared in items of forward peak potential, forward peak current density (*Ipa*), and the mass activity (peak current density of methanol oxidation per unit of Pt loading [287]). From Table 7.2, it is seen that with increase in Pt loading, the forward peak current density increases due to increased amount of available Pt catalyst. With increase in Pt loading, the mass activity increases first and then reach a maximum when the loading is 0.170 mg cm^{-2}, *i.e.,* deposition time = 1.0 hr. The existence of a maximum mass activity may be related to the size effect of Pt particles. When the Pt loading is higher than 0.170 mg cm^{-2}, the size of Pt particles become larger, which may play

a role in reducing the mass activity of Pt/carbon nanofibers. In addition to the maximum mass activity, a minimum forward peak potential is obtained at the loading of 0.170 mg cm^{-2}, indicating that superior catalytic activity at that loading.

Figure 7.8 shows the effect of methanol concentration on the anodic current density of Pt/carbon nanofibers during methanol oxidation. It is seen that, with increase in methanol concentration, the anodic current density increases first, but keeps relatively constant when the methanol concentration is greater than 0.50 M due to the saturation of Pt active sites at high methanol concentrations.

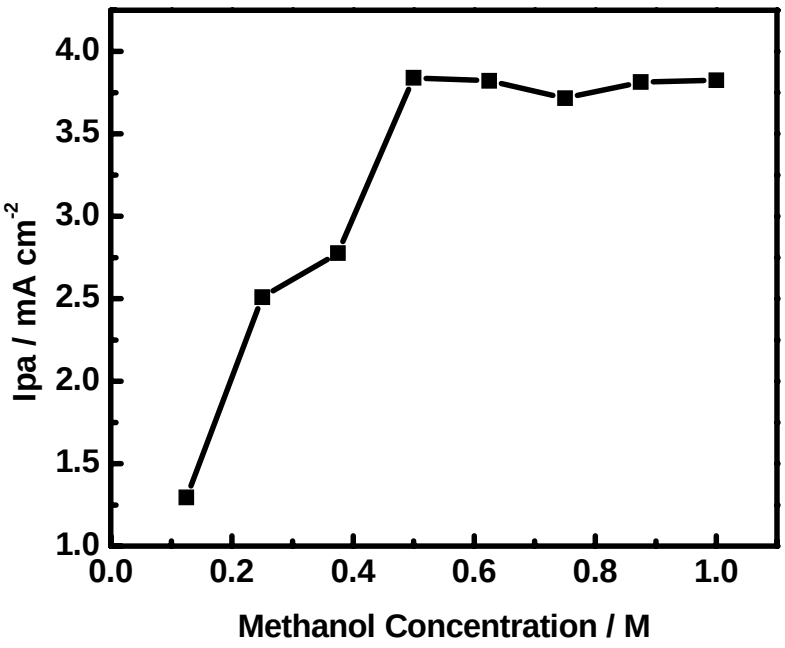

Figure 7.8. Anodic peak current as a functional of methanol concentration for Pt/carbon nanofibers in 0.50 M CH_3OH + 0.20 M H_2SO_4 at 5.0 $mV \cdot s^{-1}$. Deposition time: 1.0 hr.

The effect of solution temperature on the anodic peak current density of Pt/carbon nanofibers during methanol oxidation is shown in Figure 7.9. With increasing temperature, a linear increase in the anodic peak current is observed from 25.0 to 70.0 ^{o}C. After reaching 70.0 ^{o}C, the anodic peak current starts to decrease. The increase in the peak current density can be attributed to the acceleration of the electrode reaction kinetics. At temperatures beyond 70 ^{o}C, the decrease in anodic peak is caused by the evaporation of methanol, which has a boiling point of 64.7 ^{o}C.

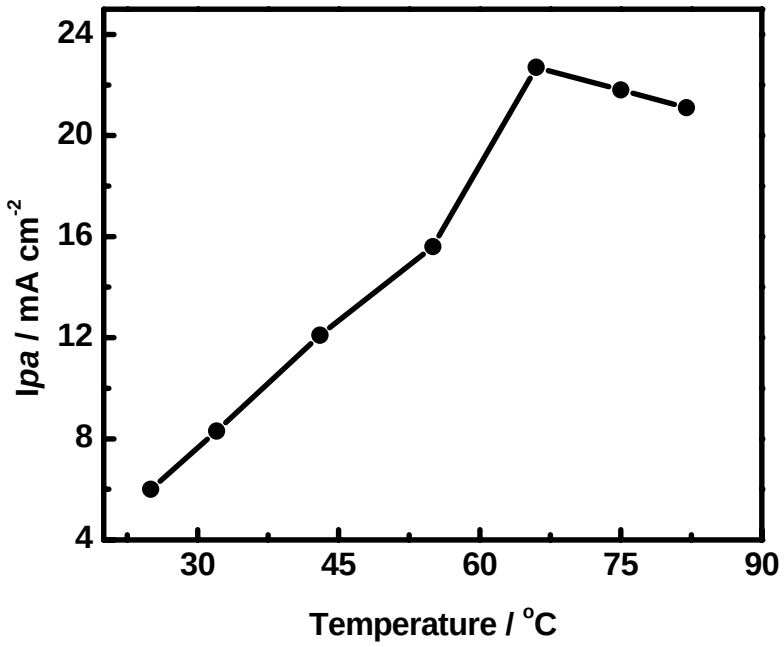

Figure 7.9. Anodic peak current density as a function of solution temperature for Pt/carbon nanofibers in 0.50 M CH_3OH + 0.20 M H_2SO_4 at 5.0 mV·s^{-1}. Deposition time: 1.0 hr.

7.4. Summary

Pt/carbon nanofibers have been prepared by electrodepositing Pt nanoparticles onto electrospun carbon nanofibers under the potential -0.2 V. Particles with well-defined morphology and size were obtained by controlling the electrodeposition time. The deposition time can also be used to control the Pt loading and the catalyst activity. The resulting Pt/carbon nanofibers possess the properties of high active surface area and fast electron transfer rate, which leads to a good performance towards the electrocatalytic oxidation of methanol. The electrocatalytical activities of Pt/carbon nanofibers with different deposition times have been evaluated. The results show that the Pt/carbon electrode with suitable deposition time (1.0 hr here) has the highest electrocatalytic activity. Therefore, the electrochemical deposition of Pt nanoparticles on carbon nanofibers provides an alternative method to obtain a good catalyst toward the oxidation of methanol. However, investigations into the catalytic ability of such composites in Membrane Electrode Assembly in direct methanol fuel cells are needed for future applications.

CHAPTER 8. CATHODE: CARBON NANOFIBER-SUPPORTED PLATINUM-PALLADIUM BY ELECTRODEPOSITION

Abstract

Carbon nanofiber-supported Pt-Pd alloy composites were prepared by co-electrodepositing Pt-Pd alloy nanoparticles directly onto electrospun carbon nanofibers. The morphology and size of Pt-Pd alloy nanoparticles were controlled by the surface treatment of carbon nanofibers and electrodeposition duration time. SEM/EDS and XPS were used to study the composition of Pt-Pd alloy on the composites, and the co-electrodeposition mechanism of Pt-Pd alloy was investigated. The resultant Pt-Pd/carbon nanofiber composites were characterized by running cyclic voltammograms in oxygen-saturated 0.1 M $HClO_4$ at 25 ^{o}C to study their electrocatalytic ability toward oxygen reduction. Results show that Pt-Pd/carbon nanofiber composites possess good performance towards the electrocatalytic reduction of oxygen. Among all Pt-Pd/carbon nanofibers prepared, the composite with a Pt-Pd loading of 0.90 mg cm^{-2} has the highest electrocatalytic activity by catalyst mass.

8.1. Introduction

Due to high-energy demands, fossil fuel depletions, and environmental pollution throughout the world, considerable efforts have been dedicated to developing fuel cells with good performance.[219, 288-291] However, the commercialization of fuel cells is still hindered by certain problems, including poor kinetics of both the anodic and cathodic reactions and high cost of Pt-based electrocatalysts.[84, 89, 292-295] At the cathode, the oxygen reduction reaction is kinetically-limited due to endothermic and irreversible reactions and "mixed potential effect", which are caused by the competitive reactions between the adsorption of oxygen molecules on the catalyst surface and the formation of oxide and hydroxide intermediates. For instance, the overpotential losses of oxygen reduction on Pt, a commonly used fuel cell electrocatalyst, amount to 0.3-0.4 V.[147, 295] In order to improve the performance of the catalytic ability toward oxygen reduction, a second element or third is often alloyed into Pt. Fundamentally, the second (or third) element can alter the inter-atomic spacing of Pt and increase the Pt 5d orbital vacancies, thereby enhancing the efficiency of the oxygen reduction.[148-151] So far, many second or third elements (such as Pd) have been alloyed into Pt-based catalysts for the oxygen reduction, and most of them used carbon particles as the catalyst support.[296-301] However, the optimized efficiency of carbon particle-supported catalysts is relatively hard to attain due to the specific physical and chemical properties of carbon particles, and their high ohmic resistance and mass transport limitation during fuel cell operation.[162]

Nanostructured carbons with different forms, such as fullene, graphene, nanotubes, and nanofibers, have fascinating structures and thermal/electric/mechanical properties, and hence they are gaining much attention due to their potential applications in diverse areas, ranging from fuel cells, supercapacitor, hydrogen storage, field emission devices, to chemical/biological sensors.[229, 255, 274, 302] Among various carbon nanomaterials, carbon nanofibers (CNFs) are considered as a promising support candidate for fuel cell catalysts due to their high electronic and thermal conductivities, 1-dimentional structure, and good electrochemical stability.[25, 72, 303] Moreover, they are inexpensive and can be produced with various controlled structures at relatively high speeds. However, until now there are few research reports on utilizing CNFs as the catalyst support in fuel cells.[282, 304-306] In this paper, we report the preparation and characterization of Pt-Pd/CNF composites by co-electrodepositing Pt-Pd alloy nanoparticles onto CNFs.

8.2. Experimental

8.2.1. Chemicals and reagents

Polyacrylonitrile (PAN), N,N-dimethylformamide (DMF), chloroplatinic acid hydrate

($H_2PtCl_6 \cdot xH_2O$), ammonium hexachloropalladate [$(NH_4)_2PdCl_6$], sulfuric acid (H_2SO_4), and perchloric acid ($HClO_4$) were purchased from Sigma-Aldrich, and they were used without further purification. Deionized water was used throughout.

8.2.2. Synthesis of CNFs

A DMF solution of 8 wt% PAN was prepared at 60 ^oC, with mechanical stirring for three hours. The electrospinning was conducted using a Gamma ES40P-20W/DAM variable high voltage power supply under a voltage of 15 kV. Under high voltage, a polymer jet was ejected and accelerated toward the nanofiber collector, during which the solvent was rapidly evaporated. The electrospun PAN fibers were collected on an aluminum foil placed on the collector. These PAN nanofibers were first stabilized in air at 280 ^oC for 2.0 hours with a heating rate of 5.0 $^oC\ min^{-1}$, and then carbonized in nitrogen atmosphere at 700 ^oC for 1.0 hour with a heating rate of 2.0 $^oC\ min^{-1}$. The resultant CNFs were used as the working electrode during the electrodeposition of Pt-Pd alloy nanoparticles.

8.2.3. Electrodeposition of Pt-Pd alloy particles onto CNFs

Before electrodeposition, CNFs were oxidized by cycling in a 1.0 M H_2SO_4 solution between -0.70 and 1.20 V at a rate of 50 mV s^{-1} for 100 cycles. The electrodepostion of Pt-Pd alloy

particles was carried out by applying a potential of -0.2 V (*vs.* Ag/AgCl/4.0 M KCl) with different deposition durations on the oxidized CNFs in a 2.5 mM $H_2PtCl_6 \cdot xH_2O$ + 2.5 mM $(NH_4)_2PdCl_6$ + 1.0 M H_2SO_4 solution.

8.2.4. Characterization of Pt-Pd/CNFs

X-ray diffraction (XRD) analysis was performed with a Philips XLF ATPS XRD 100 diffractometer using CuKα radiation (λ=1.5405 Å). The operating voltage and current were 45 kV and 40 mA, respectively. X-ray photoelectron spectrometer (XPS) was used to analyze the composition of Pt-Pd alloy particles using a Kratos Analytical Axis Ultra spectrometer.

The structure of CNFs and Pt-Pd/CNFs, which were deposited onto 200 mesh carbon-coated Cu grids, was evaluated using a Hitachi HF-2000 TEM at 200 kV. These CNFs and Pt-Pd/CNFs were also examined using a JEOL JSM-6360LV FESEM at 15 kV. The diameters of Pt-Pd alloy nanoparticles were determined by measuring 75 randomly selected particles for each sample using an ImageJ software package.

8.2.5. Electrochemical properties of Pt-Pd/CNFs

Cyclic voltammograms (CVs) were used to measure the catalytic ability of Pt-Pd/CNFs

toward oxygen reduction in oxygen-saturated 0.1 M $HClO_4$ with the scan rate of 5.0 $mV \cdot s^{-1}$. The electrochemical measurements of Pt-Pd/CNFs were performed in a three-electrode cell at 25 ^{o}C on an AQ4 Gamry Reference 600 electrochemical workstation. The cell consisted of a working electrode (Pt-Pd/CNFs), a counter electrode (Pt wire), and a reference electrode (*Ag*/*AgCl*/4.0 M KCl). Oxygen was used to bubble the testing solution for at least 30 minutes before the measurements, and then was used continually throughout the experiment. All the electrochemical potentials were measured and reported with respect to Ag/AgCl/4.0 M KCl.

8.3. Results and Discussion

8.3.1. TEM images of CNFs and Pt-Pd/CNFs

Before the electrodeposition, CNFs were used as the working electrode and were cycled in 1.0 M H_2SO_4 to carry out the surface oxidation. During that process, various surface functional groups such as quinoid (=O), hydroxy (-OH) and carboxyl (-COOH) were produced, and they can supply defect sites for the Pt-Pd alloy deposition.[228] After the surface oxidation, Pt-Pd alloy nanoparticles were electrodeposited onto the CNF surface. Figure 8.1 shows TEM images of CNFs and Pt-Pd/CNFs with different deposition durations. It is seen that before electrodeposition, the CNF surface is smooth and there are no particles

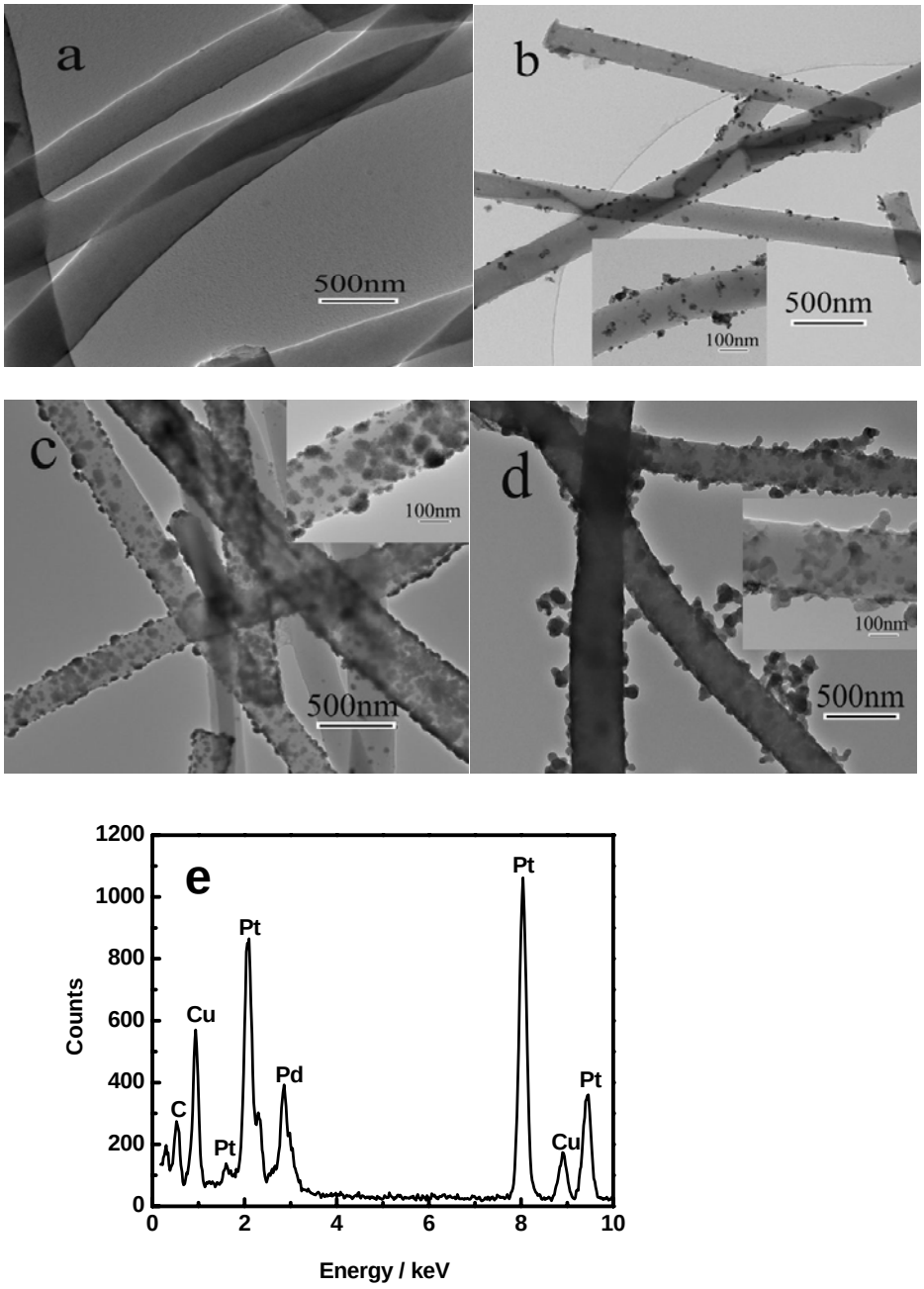

Figure 8.1. TEM images of CNFs (a) and Pt-Pd/CNFs with different deposition durations of 1.0 (b), 2.0 (c), and 4.0 (d) hours, respectively; and EDS spectrum (e) of Pt-Pd/CNFs with 1.0 hour deposition. Insets in (b), (c), and (d) show the composites with larger magnification.

loaded. However, Pt-Pd alloy nanoparticles are found on the surface of CNFs after 1.0 hour electrodeposition. When the deposition time increases from 1.0 to 2.0 hours, more Pt-Pd alloy nanoparticles are distributed on the surface of CNFs. However, when the deposition time is 4.0 hours, a large number of aggregates appear. Figure 8.1e shows the energy dispersive X-ray spectroscopy (EDS) of Pt-Pd/CNFs with 1.0 hour deposition. The EDS curve confirms the presence of Pt-Pd alloy particles on the surface of CNFs. The Cu peak in Figure 8.1e belongs to the TEM grid background.

Table 8.1. Quantitative data of Pt-Pd alloy particles in Pt-Pd/CNF nanocomposites from EDS and XPS analysis.

Deposition duration (hour)	Pt/Pd ratio obtained by EDS	Pt/Pd ratio obtained by XPS	Pt-Pd/CNFs
1.0	39.5/60.5	37.9/62.1	$Pt_{40}Pd_{60}$/CNFs
2.0	52.2/47.8	52.3/47.7	$Pt_{50}Pd_{50}$/CNFs
4.0	54.0/46.0	57.5/42.5	$Pt_{55}Pd_{45}$/CNFs

The amount ($m_{Pt\text{-}Pd}$) of Pt-Pd alloy loading can be calculated by the following equation:

$$m_{Pt-Pd} = \frac{Q(M_{Pt}W_{Pt}+M_{Pd}W_{Pd})}{4F \cdot S} \quad (8.1)$$

where M_{Pt} and M_{Pd} are the atomic weights of Pt (195.09 g mol^{-1}) and Pd (106.42 g mol^{-1}), W_{Pt} and W_{Pd} the weight percentages of Pt and Pd, respectively, Q the electrons transferred (C), S the electrode geometric area (cm^{-2}), and F the Faraday constant (96485 C mol^{-1}). In this work, the compositions of Pt-Pd alloy nanoparticles deposited with different deposition durations were analyzed by EDS, and the results are showed in Table 8.1. The Pt-Pd alloy loadings of the resultant composites of Pt-Pd/CNFs are 0.42, 0.90, and 1.85 mg cm^{-2}, respectively, when the deposition durations are 1.0, 2.0, and 4.0 hours.

8.3.2. SEM images of Pt-Pd/CNFs

Figures 8.2a, b, and c show SEM images of Pt-Pd/CNFs with different deposition durations. When the deposition time is 1.0 hour, the resultant Pt-Pd alloy loading is relatively low (0.42 mg cm^{-2}), and hence there are just a few Pt-Pd alloy nanoparticles found on the surface of CNFs, and the average alloy particle size is around 29 nm (Figure 8.3a). When the deposition time is longer than 1.0 hour, well-distributed Pt-Pd alloy nanoparticles can be observed on the surface of CNFs and the diameter of Pt-Pd alloy nanoparticles increases from 29, 41 to 64 nm when the deposition time increases from 1.0, 2.0 to 4.0 hours (Figure 8.3). That is because the application of a longer deposition time results in higher Pt-Pd nanoparticle

loading without increasing the quantity of nuclei. As a result, with increase in deposition time (*i.e.,* Pt-Pd alloy loading), the Pt-Pd alloy nanoparticle size increases.

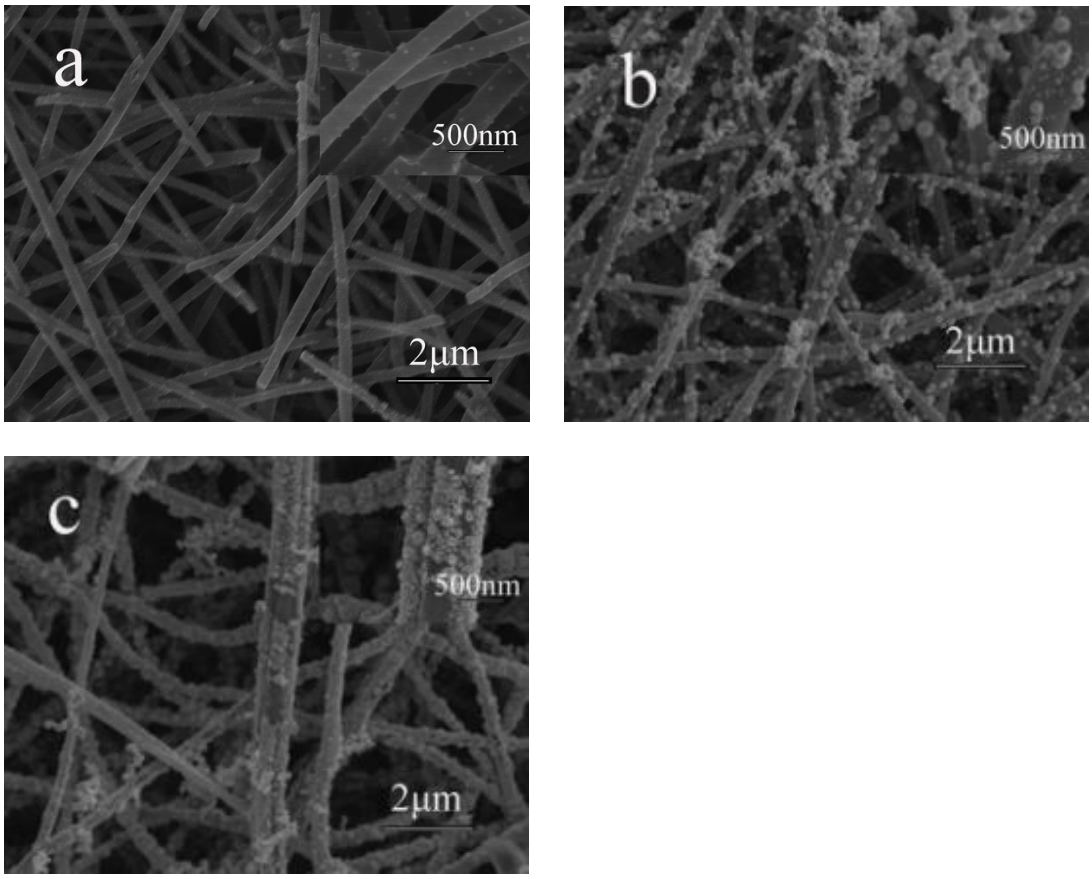

Figure 8.2. SEM images of Pt-Pd/CNFs prepared with different deposition durations of 1.0 (a), 2.0 (b), and 4.0 (c) hours. The insets in (a), (b), and (c) show the composites with larger magnification.

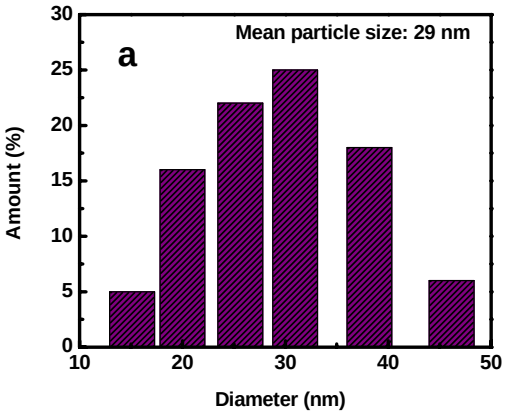

c

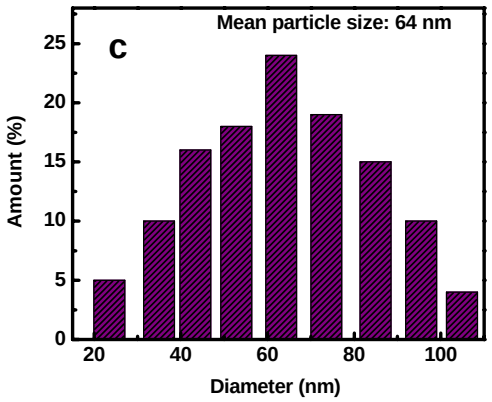

Figure 8.3. Diameter distributions of Pt-Pd alloy particles in Pt-Pd/CNFs prepared with different deposition durations: 1.0 (a), 2.0 (b), and 4.0 (c) hours. Deposition potential: -0.2 V.

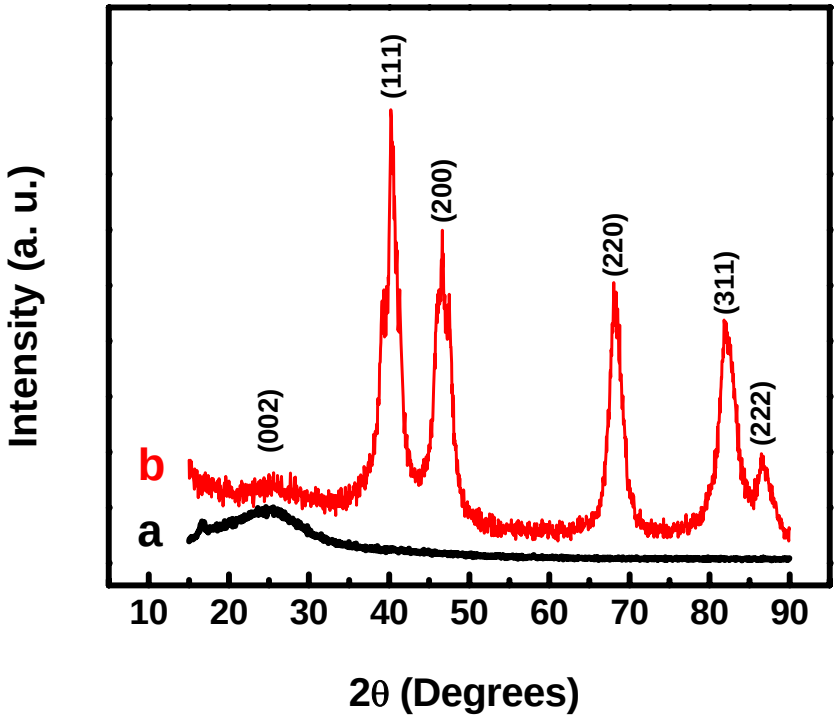

Figure 8.4. XRD patterns of CNFs (a) and Pt-Pd/CNFs (b). Deposition potential: -0.2 V. Deposition time: 1.0 hour.

8.3.3. XRD Patterns and XPS analysis of Pt-Pd/CNFs

X-ray diffraction (XRD) patterns obtained from electrospun CNFs and Pt-Pd/CNF composites are presented in Figure 8.4. The diffraction peak at 25.5° can be assigned to the diffraction of the (002) plane of graphite layers. The XRD pattern of Pt-Pd/CNFs presents

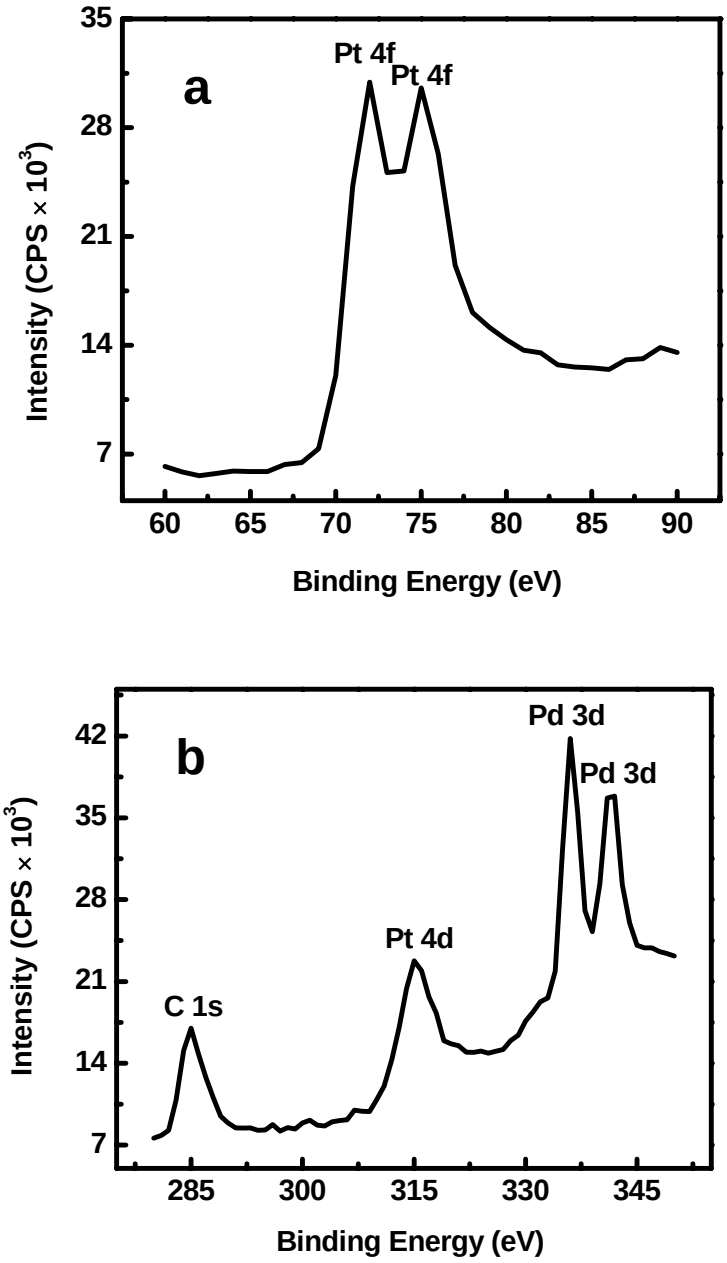

Figure 8.5. XPS spectra of Pt-Pd/CNFs in the binding energy of 60-90 (a) and 280-350 (b) eV, respectively. Deposition potential: -0.2 V. Deposition time: 1.0 hour.

typical diffraction peaks at 40.2^{o} (111), 46.6^{o} (200), 68.5^{o} (220), 82.0^{o} (311), and 86.5^{o} (222), respectively, which belong to Pt-Pd alloy crystals formed on CNFs.

X-ray photoelectron spectroscopy (XPS) spectra obtained from the Pt-Pd/CNF composite with 1.0 hour deposition are presented in Figure 8.5. Three characteristic peaks of *4f* and *4d* for Pt appear at about 73, 75, and 315 eV, and two characteristic peaks of *3d* for Pd appear at around 336 and 342 eV, and the *1s* peak of carbon appears at about 285 eV, respectively.[272, 307] Moreover, from the intensities of XPS peaks Pt 4f and Pd 3d, the elemental ratio of Pt/Pd can be obtained and the results are shown in Table 8.1.

The Pt/Pd ratios calculated from XPS data are comparable to those obtained from EDS results. Based on the Pt/Pd ratios obtained by EDS and XPS, the Pt-Pd/CNFs can be denoted as $Pt_{40}Pd_{60}$/CNFs, $Pt_{50}Pd_{50}$/CNFs, and $Pt_{55}Pd_{45}$/CNFs for the composites obtained with deposition durations of 1.0, 2.0, and 4.0 hours, respectively.

8.3.4. Electrodeposition mechanism of Pt-Pd/CNFs

During the electrodeposition, Pt and Pd components from their corresponding precursors are involved in a series of electrochemical and accompanying chemical reactions. The deposition processes of Pt from $PtCl_6^{2-}$ salt can be described as:

$$PtCl_6^{2-} + 2e \leftrightarrow PtCl_4^{2-} + 2Cl^- \qquad E^o = 0.726\ V \qquad (8.2)$$

$$PtCl_4^{2-} + 2e \leftrightarrow Pt + 4Cl^- \qquad E^o = 0.758\ V \qquad (8.3)$$

Similarly, the reactions involved in the electrodeposition of Pd from $PdCl_6^{2-}$ salt can be shown as:

$$PdCl_6^{2-} + 2e \leftrightarrow PdCl_4^{2-} + 2Cl^- \qquad E^o = 1.467\ V \qquad (8.4)$$

$$PdCl_4^{2-} + 2e \leftrightarrow Pd + 4Cl^- \qquad E^o = 0.62\ V \qquad (8.5)$$

The classical model of metal nucleation and growth includes a surface term and a bulk term for each metal,[308] which can be used to illustrate the reduction procedure of Pt and Pd on the surface of CNFs. Equations 8.2 and 8.4 show the first step of deposition for Pt and Pd, respectively, and it is seen that the reduction potential of $PdCl_6^{2-}$ is much lower than that of $PtCl_6^{2-}$, which favors the formation of $PdCl_4^{2-}$ ions and subsequently higher $PdCl_4^{2-}$ concentration in the electrodeposition solution. This should be responsible for the higher Pd composition in $Pt_{40}Pd_{60}$/CNFs when the deposition duration is 1.0 hour since the reduction potentials of $PtCl_4^{2-}$ and $PdCl_4^{2-}$ are comparable to each other according to Equations 8.3 and 8.5. However, with the increase in the deposition time, more $PtCl_4^{2-}$ ions are formed and less $PdCl_4^{2-}$ ions are produced due to the reduced concentration of $PdCl_6^{2-}$ ions. As a result, the relatively higher $PtCl_4^{2-}$ ion concentration in the electrodeposition solution results in increased Pt composition in Pt-Pd/CNFs, from $Pt_{40}Pd_{60}$/CNFs, $Pt_{50}Pd_{50}$/CNFs, to $Pt_{55}Pd_{45}$/CNFs when the deposition duration increases from 1.0, 2.0, to 4.0 hours.

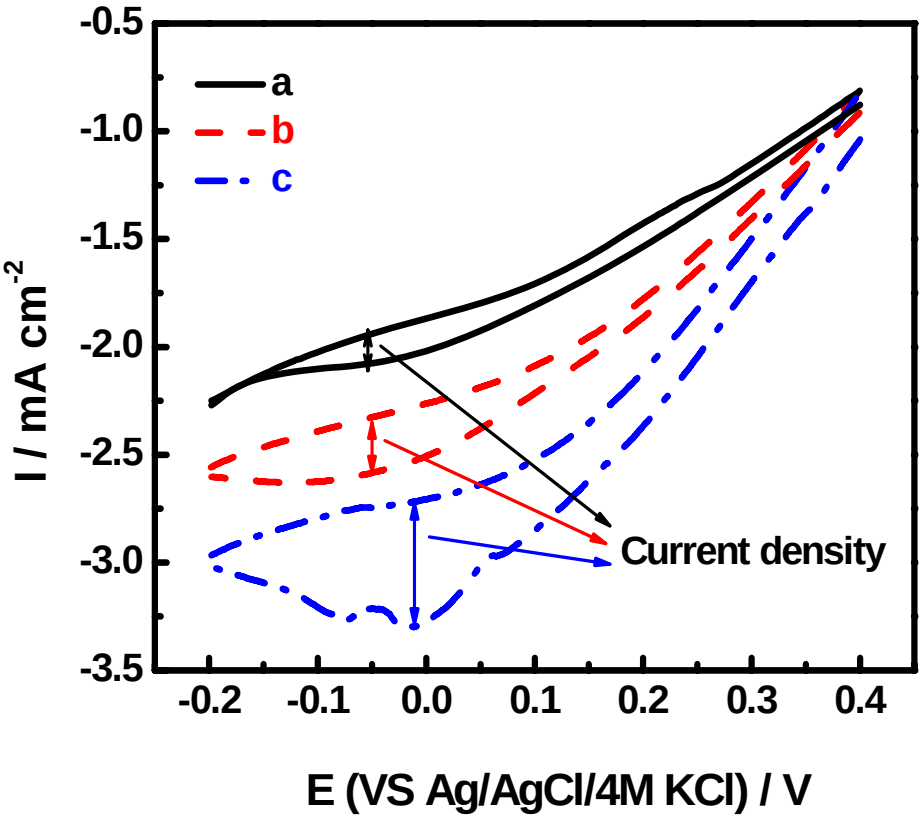

Figure 8.6. CV responses in oxygen-saturated 0.1 M $HClO_4$ at 25 ^oC on $Pt_{40}Pt_{60}$/CNFs (a), $Pt_{50}Pt_{50}$/CNFs (b), and $Pt_{55}Pt_{45}$/CNFs (c). Scanning rate: 5.0 $mV \cdot s^{-1}$.

8.3.5. Oxygen reduction performance of Pt-Pd/CNFs

CV measurements of Pt-Pd/CNFs between -0.2 and +0.40 V at 5.0 $mV \cdot s^{-1}$ in oxygen-saturated 0.1 M $HClO_4$ at 25 ^oC were employed to examine the catalytic ability of the

composites toward the oxygen reduction, and the results are shown in Figure 8.6. It is seen that there are reduction peaks around -0.05 V, indicating that Pt-Pd/CNFs are electrochemically active toward the oxygen reduction.

In order to study the efficiency of oxygen reduction, the electrochemical characteristic data of those Pt-Pd/CNF composites with different deposition durations are summarized in Table 8.2. The oxygen reduction efficiencies are compared in items of O_2 reduction peak potential, O_2 reduction current density (current density difference at reduction peak potential shown in Figure 8.6), and mass activity (reduction current density of oxygen reduction per unit of Pt-Pd alloy loading). From Table 8.2, it is seen that with increase in Pt-Pd alloy loading, the O_2 reduction current density increases due to increased amount of available Pt-Pd alloy catalyst. In addition to the current density, a maximum peak potential on Pt-Pd/CNFs is also obtained at the loading of 1.85 mg cm^{-2} (*i.e.*, $Pt_{55}Pd_{45}$/CNFs), indicating that the highest catalytic activity is achieved at this loading.

Moreover, it is also seen from Table 8.2 that a maximum mass activity of 0.24 A g^{-1} can be obtained when the loading is 0.90 mg cm^{-2}, *i.e.,* deposition time = 2.0 hours. The existence of a maximum mass activity may be related to the size effect of Pt-Pd alloy nanoparticles. When the Pt-Pd alloy loading is higher than 0.90 mg cm^{-2}, the size of Pt-Pd alloy particles become larger and some particles even form aggregates, which may play a role in reducing the mass activity of Pt-Pd/CNF composites at higher loading of 1.85 mg cm^{-2}.

Table 8.2. Electrochemical characteristics of Pt-Pd/CNF composites with different deposition durations. Solution: oxygen-saturated 0.1 M $HClO_4$ at 25 ^oC. Scanning rate: 5.0 $mV \cdot s^{-1}$.

Pt-Pd/CNFs	Catalyst loading ($mg\ cm^{-2}$)	O_2 reduction peak potential ($V_{VS\ Ag/AgCl/4.0\ M\ KCl}$)	O_2 reduction current density ($mA\ cm^{-2}$)	Mass activity ($A\ g^{-1}$)
$Pt_{40}Pd_{60}$/CNFs	0.42	-0.06	0.08	0.20
$Pt_{50}Pd_{50}$/CNFs	0.90	-0.05	0.22	0.24
$Pt_{55}Pd_{45}$/CNFs	1.85	-0.02	0.41	0.22

8.4. Summary

Pt-Pd/CNF composites have been prepared by co-electrodepositing Pt-Pd alloy nanoparticles onto electrospun CNFs under the potential -0.2 V. Particles with well-defined morphology and size were obtained by controlling the electrodeposition time. The deposition time can also be used to control the Pt-Pd alloy loading and the catalyst activity. The resultant Pt-Pd/CNF composites possess good performance towards the electrocatalytic reduction of oxygen. The results show that Pt-Pd/CNF composites with a suitable deposition time (2.0 hours) and composition ($Pt_{50}Pd_{50}$/CNFs) has the best electrocatalytic activity by mass toward the oxygen reduction. The electrochemical deposition of Pt nanoparticles on CNFs provides

an alternative method to obtain a good catalyst toward the reduction of oxygen. However, the assembling of such composites into membrane electrode assemblies (MEAs) and the investigation of their catalytic ability in MEAs are needed for future fuel cell applications.

CHAPTER 9. CONCLUSIONS

To tackle worldwide critical energy issue and environmental pollution problems, the development of sustainable, clean, and renewable energy technologies, such as energy storage and conversion systems, has been recognized as an economically and environmentally friendly alternative to solve those urgent global problems facing our society. Among various energy storage and conversion systems, direct methanol fuel cells (DMFCs) have recently attracted much attention since they can provide green power for electric vehicles and electronic portable devices by methanol conversion.

Recently, particular attention has been given to the design and synthesis of high-performance nanostructured electrodes because innovative and nano-scale materials have proven to be critical to improve the electrochemical performance of DMFCs. The wide-spread use of DMFCs is currently hindered by their unsatisfactory properties, such as low activity, limited reliability and poor durability. Nanostructured carbon materials with varieties of forms, such as carbon nanotubes (CNTs), carbon nanofibers (CNFs), and graphene, have been utilized to construct the electrodes of DMFCs through various syntheses and fabrication methods. CNFs, one of the promising nanostructured carbon materials produced by the combination of electrospinning and carbonization, have been potentially considered as an efficient, simple, and inexpensive material to fabricate the electrodes in DMFCs.

Electrospinning, which produces continuous polymer nanofibers through the action of an external electric field imposed on a polymer solution or melt, has been considered as a simple and effective method to produce one-dimensional (1D) polymer fibers at the nano- and meso-scale levels. The resultant polymer nanofibers are promising material candidates for numerous practical applications (including DMFCs) because of their large surface area, nano-scale fiber diameter, and unique functionalities. Based on the carbonizaition of polymer nanofibers, electrospun CNFs can be fabricated to support for catalysts in the electrodes of DMFCs due to their high surface area, large pore volume, and good chemical resistance.

In our study, we focused on the prepararion of electrospun CNFs through electrospinning and carbonization processes and exploring them as support materials for catalysts in the anodes and cathodes in DMFCs. In order to develop highly active electrode catalysts coupled with a suitable electrode structure for the oxidation of methanol at the anode and the reduction of oxygen at the cathode, two approaches, *i.e.,* chemical deposition and electrodeposition, were used to prepare catalyst-loaded CNF electrodes. The research in this dissertation can be divided into the following three parts:

(I) Synthesis and electrocatalysis of CNF-supported Pt and Pt-Ru nanoparticles by chemical deposition for use as anode electrodes in DMFCs.

In this part, Pt and Pt-Ru/CNF composite anodes (Pt/CNFs and PtRu/CNFs) were prepared by depositing Pt and PtRu nanoparticles onto electrospun CNFs by a chemical deposition

technique and were used as anode electrodes in DMFCs.

Pt/CNFs were first prepared by depositing Pt nanoparticles directly onto CNFs, and the morphology and size of Pt nanoparticles were controlled by 1-aminopyrene functionalization and $HNO_3 + H_2SO_4$ acid oxidation, respectively. The noncovalent functionalization of CNFs by 1-aminopyrene is simple and can be carried out at ambient temperature without damaging the integrity and electronic structure of CNFs. The resulting Pt/CNFs were characterized by running cyclic voltammogram in 0.5 M H_2SO_4 and 0.125 M CH_3OH + 0.2 M H_2SO_4 solutions, respectively. Results show that Pt/CNFs with 1-aminopyrene functionalization have Pt nanoparticles with smaller size and better distribution, compared with those treated with $HNO_3 + H_2SO_4$ acid. Moreover, Pt/1-aminopyrene-functionalized CNFs possess the properties of higher active surface area and improved electrocatalytic performance towards the oxidation of methanol.

PtRu/CNFs were also prepared by alloying Ru into Pt using the procedure described above, and their electrocatalytic ability toward the methanol oxidation was also studied. The results show that PtRu/CNFs with 1-aminopyrene functionalization have better electrocatalytic ability toward the methanol oxidation than that of Pt/1-aminopyrene-functionalized CNFs, since the introduction of Ru into Pt promotes the oxidation of CO to CO_2, thereby reducing the CO poisoning toward Pt electrocatalyst.

In summary, Pt and PtRu nanoparticles deposited on CNFs by 1-aminopyrene

functionalization and the polyol processing technique exhibit good electrocatalytic activity toward the methanol oxidation, and can be used as anodes in DMFCs.

(II) Synthesis and electrocatalysis of CNF-supported Pt nanoparticles by electrodeposition for use as anodes in DMFCs.

In this part, Pt/CNF composite anodes (Pt/CNFs) were prepared by depositing Pt nanoparticles onto electrospun CNFs using electrodeposition technique.

Pt/CNF nanocomposites were first prepared by electrodepositing Pt nanoparticles onto electrospun CNFs under different potentials of -0.2, 0.0, and 0.2 V, respectively. TEM and SEM results show that Pt/CNF nanocomposites have well-defined morphology and the Pt particle diameters are between 10 - 55 nm. The Pt/CNF electrodes were characterized by their good electrocatalytic properties towards the oxidation of methanol and it is demonstrated that the Pt/CNF electrode prepared under the potential -0.2 V has the best activity due to the lowest catalyst diameter.

In addition to the deposition voltage, the deposition time can also be used to control the Pt loading and the catalyst activity. Pt/CNFs were futhere prepared by electrodepositing Pt nanoparticles onto electrospun CNFs under the potential -0.2 V by controlling the electrodeposition time. The electrocatalytical activities of Pt/CNFs with different deposition times have been evaluated. The results show that the Pt/carbon anode with suitable

deposition time (*i.e.* 2.0 hours) has the highest electrocatalytic activity. Therefore, the electrochemical deposition of Pt nanoparticles on CNFs provides an alternative method to obtain a good catalyst toward the oxidation of methanol, and can be used as anodes in DMFCs.

(III) Synthesis and electrocatalysis of CNF-supported Pt-Pd nanoparticles by electrodeposition for use as cathodes in DMFCs.

In this part, Pt-Pd/CNF composite cathodes (PtPd/CNFs) were prepared by depositing Pt-Pd nanoparticles onto electrospun CNFs using co-electrodeposition technique.

Pt-Pd/CNF composites were prepared by co-electrodepositing Pt-Pd alloy nanoparticles onto electrospun CNFs under the potential -0.2 V. Particles with well-defined morphology and size were obtained by controlling the electrodeposition time. The deposition time can also be used to control the Pt-Pd alloy loading and the catalyst activity. The resultant Pt-Pd/CNF composites possess good performance towards the electrocatalytic reduction of oxygen. The results show that Pt-Pd/CNF composites with a suitable deposition time (*i.e.* 2.0 hours) and composition ($Pt_{50}Pd_{50}$/CNFs) have the best electrocatalytic activity by mass toward the oxygen reduction. The co-electrodeposition of Pt and Pd nanoparticles on CNFs provides an alternative method to obtain a good catalyst toward the reduction of oxygen used as cathode electrodes in DMFCs.

CHAPTER 10. FUTURE WORK

In order to further the research, the recommended future work is included in the following but not limited to:

(I) Incorporate CNF-supported electrocatalysts into membrane electrode assemblies (MEAs) to study their electrochemical performance in practical DMFCs.

MEA, which is consisted of a polymer electrolyte membrane and catalyst loaded porous electrodes for methanol oxidation at the anode and oxygen reduction at the cathode, is the key component of DMFCs. In order to study the electrochemical properties of CNF-supported electrocatalysts in the electrodes of pratical DMFCs, those electrocatalysts need to be incorported into MEAs to investigate full cell performance, such as voltage *vs.* current density or power density *vs.* current density. From the information of the full cell performance, we can compare the properties of CNF-supported electrocatalysts to those of commercial available carbon black-supported electrocatalysts. Results obtained from the detailed exploration of comparisons can be used to improve the structure and properties of CNF-supported electrocatalysts and the overall electrochemical performance of fuel cells.

(II) Prepare CNF-supported Pt-Pd particles by chemical deposition as cathodes in DMFCs.

As mentioned in Chapter 7, CNF-supported Pt-Pd alloy composites were prepared by

co-electrodepositing Pt-Pd alloy nanoparticles directly onto electrospun CNFs. The morphology and size of Pt-Pd alloy nanoparticles were controlled by the surface treatment of CNFs and electrodeposition duration time. However, the average size of Pt-Pd nanoparticles by co-electrodeposition is relatively large (*i.e.* 29 nm when the deposition time is 1 hour), which should be reduced by chemical deposition consisting of 1-aminopyrene functionalization and polyol processing techque. Moreover, 1-aminopyrene functionalization can also help to preserve the integrities of the CNF-based cathode electrodes, which would improve the overall electrochemical performance of DMFCs, especially the long-term stability.

(III) Prepare CNF-supported non-noble metal nanoparticles for use as electrodes in DMFCs.

Noble metals, such as Pt, Ru, and Pd, have been widely used as the catalysts in the electrodes of DMFCs, however, the high cost of those metals have greatly hindered the commercial applications of DMFCs. In order to synthesize high-performance, non-noble metals, such as chromium-decorated nickel and silver, have been utilized as catalysts for anodes and cathodes in fuel cells recently. However, most of electrocatalysts were loaded on carbon black. In order to improve their electrochemical performance, CNFs can be used as support materials for non-noble catalysts, which may benefit the future development of DMFCs.

REFERENCES

[1] J. T. Hu, T. W. Odom, C. M. Lieber. Chemistry and physics in one dimension: Synthesis and properties of nanowires and nanotubes. Acc. Chem. Res. 32 (1999) 435-445.

[2] Y. N. Xia, P. D. Yang, Y. G. Sun, Y. Y. Wu, B. Mayers, B. Gates, Y. D. Yin, F. Kim, Y. Q. Yan. One-dimensional nanostructures: Synthesis, characterization, and applications. Adv. Mater. 15 (2003) 353-389.

[3] D. Li, Y. N. Xia. Electrospinning of nanofibers: Reinventing the wheel? Adv. Mater. 16 (2004) 1151-1170.

[4] M. M. Bergshoef, G. J. Vancso. Transparent nanocomposites with ultrathin, electrospun nylon-4,6 fiber reinforcement. Adv. Mater. 11 (1999) 1362-1365.

[5] P. Gibson, D. Rivin, C. Kendrick, H. Schreuder-Gibson. Humidity-dependent air permeability of textile materials. Text. Res. J. 69 (1999) 311-317.

[6] L. Huang, R. A. McMillan, R. P. Apkarian, B. Pourdeyhimi, V. P. Conticello, E. L. Chaikof. Generation of synthetic elastin-mimetic small diameter fibers and fiber networks. Macromolecules 33 (2000) 2989-2997.

[7] J. S. Kim, D. H. Reneker. Mechanical properties of composites using ultrafine electrospun fibers. Polym. Compos. 20 (1999) 124-131.

[8] M. Ikegame, K. Tajima, T. Aida. Template synthesis of polypyrrole nanofibers insulated within one-dimensional silicate channels: Hexagonal versus lamellar for recombination of polarons into bipolarons. Angew. Chem. Int. Ed. 42 (2003) 2154-2157.

[9] H. Y. Li, Y. C. Ke, Y. L. Hu. Polymer nanofibers prepared by template melt extrusion. J. Appl. Polym. Sci. 99 (2006) 1018-1023.

[10]X. M. Feng, G. Yang, Q. Xu, W. H. Hou, J. P. Zhu. Self-assembly of polyaniline/Au composites: From nanotubes to nanofibers. Macromol. Rapid Commun. 27 (2006) 31-36.

[11]Z. Yang, B. Xu. Supramolecular hydrogels based on biofunctional nanofibers of self-assembled small molecules. J. Mater. Chem. 17 (2007) 2385-2393.

[12]P. X. Ma, R. Y. Zhang. Synthetic nano-scale fibrous extracellular matrix. J. Biomed. Mater. Res. 46 (1999) 60-72.

[13]B. K. Gu, M. K. Shin, K. W. Sohn, S. I. Kim, S. J. Kim, S. K. Kim, H. Lee, J. S. Park.

Direct fabrication of twisted nanofibers by electrospinning. Appl. Phys. Lett. 90 (2007).

[14]G. Kim, W. Kim. Formation of oriented nanofibers using electrospinning. Appl. Phys. Lett. 88 (2006).

[15]P. K. Panda, S. Ramakrishna. Electrospinning of alumina nanofibers using different precursors. J. Mater. Sci. 42 (2007) 2189-2193.

[16]W. E. Teo, S. Ramakrishna. A review on electrospinning design and nanofibre assemblies. Nanotechnology 17 (2006) R89-R106.

[17]A. Frenot, I. S. Chronakis. Polymer nanofibers assembled by electrospinning. Curr. Opin. Colloid Interface Sci. 8 (2003) 64-75.

[18]R. Kessick, J. Fenn, G. Tepper. The use of AC potentials in electrospraying and electrospinning processes. Polymer 45 (2004) 2981-2984.

[19]D. H. Reneker, I. Chun. Nanometre diameter fibres of polymer, produced by electrospinning. Nanotechnology 7 (1996) 216-223.

[20]A. Formhals. US Patent 1975504. (1934).

[21]T. Subbiah, G. S. Bhat, R. W. Tock, S. Pararneswaran, S. S. Ramkumar. Electrospinning of nanofibers. J. Appl. Polym. Sci. 96 (2005) 557-569.

[22]G. I. Taylor. Proc. Roy. Soc. London A313 (1969) 453.

[23]Baumgart.Pk. Electrostatic Spinning of Acrylic Microfibers. J. Colloid Interface Sci. 36 (1971) 71.

[24]A. Greiner, J. H. Wendorff. Electrospinning: A fascinating method for the preparation of ultrathin fibres. Angew. Chem. Int. Ed. 46 (2007) 5670-5703.

[25]Z. M. Huang, Y. Z. Zhang, M. Kotaki, S. Ramakrishna. A review on polymer nanofibers by electrospinning and their applications in nanocomposites. Compos. Sci. Technol. 63 (2003) 2223-2253.

[26]R. Jaeger, M. M. Bergshoef, C. M. I. Batlle, H. Schonherr, G. J. Vancso. Electrospinning of ultra-thin polymer fibers. Macromol. Symp. 127 (1998) 141-150.

[27]I. D. Norris, M. M. Shaker, F. K. Ko, A. G. MacDiarmid. Electrostatic fabrication of ultrafine conducting fibers: polyaniline/polyethylene oxide blends. Synth. Met. 114 (2000) 109-114.

[28]A. G. MacDiarmid, W. E. Jones, I. D. Norris, J. Gao, A. T. Johnson, N. J. Pinto, J. Hone,

B. Han, F. K. Ko, H. Okuzaki, M. Llaguno. Electrostatically-generated nanofibers of electronic polymers. Synth. Met. 119 (2001) 27-30.

[29]J. S. Kim, D. H. Reneker. Polybenzimidazole nanofiber produced by electrospinning. Polym. Eng. Sci. 39 (1999) 849-854.

[30]H. Fong, W. D. Liu, C. S. Wang, R. A. Vaia. Generation of electrospun fibers of nylon 6 and nylon 6-montmorillonite nanocomposite. Polymer 43 (2002) 775-780.

[31]K. H. Lee, H. Y. Kim, Y. M. La, D. R. Lee, N. H. Sung. Influence of a mixing solvent with tetrahydrofuran and N,N-dimethylformamide on electrospun poly(vinyl chloride) nonwoven mats. J. Appl. Polym. Sci.B 40 (2002) 2259-2268.

[32]M. M. Demir, I. Yilgor, E. Yilgor, B. Erman. Electrospinning of polyurethane fibers. Polymer 43 (2002) 3303-3309.

[33]D. H. Reneker, W. Kataphinan, A. Theron, E. Zussman, A. L. Yarin. Nanofiber garlands of polycaprolactone by electrospinning. Polymer 43 (2002) 6785-6794.

[34]H. Fong, D. H. Reneker. Elastomeric nanofibers of styrene-butadiene-styrene triblock copolymer. J. Appl. Polym. Sci.B 37 (1999) 3488-3493.

[35]Z. Jun, H. Q. Hou, A. Schaper, J. H. Wendorff, A. Greiner. Poly-L-lactide nanofibers by electrospinning - Influence of solution viscosity and electrical conductivity on fiber diameter and fiber morphology. E-Polymers (2003).

[36]J. Fang, H. T. Niu, T. Lin, X. G. Wang. Applications of electrospun nanofibers. Chin. Sci. Bull. 53 (2008) 2265-2286.

[37]T. C. Lim, M. Kotaki, T. K. J. Yang, K. Fujihara, S. Ramakrishna. Recent advances in tissue engineering applications of electrospun nanofibers. Mater. Res. 19 (2004) 20-27.

[38]K. M. Sawicka, P. Gouma. Electrospun composite nanofibers for functional applications. J. Nanopart. Res. 8 (2006) 769-781.

[39]V. Thavasi, G. Singh, S. Ramakrishna. Electrospun nanofibers in energy and environmental applications. Energy Environ. Sci. 1 (2008) 205-221.

[40]K. Fujihara, M. Kotaki, S. Ramakrishna. Guided bone regeneration membrane made of polycaprolactone/calcium carbonate composite nano-fibers. Biomaterials 26 (2005) 4139-4147.

[41]Y. K. Luu, K. Kim, B. S. Hsiao, B. Chu, M. Hadjiargyrou. Development of a nanostructured DNA delivery scaffold via electrospinning of PLGA and PLA-PEG block copolymers. J. Controlled Release 89 (2003) 341-353.

[42]H. Q. Dai, J. Gong, H. Kim, D. Lee. A novel method for preparing ultra-fine alumina-borate oxide fibres via an electrospinning technique. Nanotechnology 13 (2002) 674-677.

[43]D. Li, Y. N. Xia. Fabrication of titania nanofibers by electrospinning. Nano Lett. 3 (2003) 555-560.

[44]K. Sawicka, P. Gouma, S. Simon. Electrospun biocomposite nanofibers for urea biosensing. Sens. Actuators, B 108 (2005) 585-588.

[45]H. Y. Guan, C. L. Shao, S. B. Wen, B. Chen, J. Gong, X. H. Yang. A novel method for preparing Co3O4 nanofibers by using electrospun PVA/cobalt acetate composite fibers as precursor. Mater. Chem. Phys. 82 (2003) 1002-1006.

[46]L. W. Ji, C. Saquing, S. A. Khan, X. W. Zhang. Preparation and characterization of silica nanoparticulate-polyacrylonitrile composite and porous nanofibers. Nanotechnology 19 (2008) 085605-085613.

[47]C. M. Hsu, S. Shivkumar. Nano-sized beads and porous fiber constructs of poly(epsilon-caprolactone) produced by electrospinning. J. Mater. Sci. 39 (2004) 3003-3013.

[48]J. Ayutsede, M. Gandhi, S. Sukigara, H. H. Ye, C. M. Hsu, Y. Gogotsi, F. Ko. Carbon nanotube reinforced Bombyx mori silk nanofibers by the electrospinning process. Biomacromolecules 7 (2006) 208-214.

[49]J. J. Ge, H. Q. Hou, Q. Li, M. J. Graham, A. Greiner, D. H. Reneker, F. W. Harris, S. Z. D. Cheng. Assembly of well-aligned multiwalled carbon nanotubes in confined polyacrylonitrile environments: Electrospun composite nanofiber sheets. J. Am. Chem. Soc. 126 (2004) 15754-15761.

[50]P. W. Gibson, H. L. Schreuder-Gibson, D. Rivin. Electrospun fiber mats: Transport properties. AlChE J. 45 (1999) 190-195.

[51]S. F. Fennessey, R. J. Farris. Fabrication of aligned and molecularly oriented electrospun polyacrylonitrile nanofibers and the mechanical behavior of their twisted yams. Polymer 45 (2004) 4217-4225.

[52]I. C. Kim, H. G. Yun, K. H. Lee. Preparation of asymmetric polyacrylonitrile membrane with small pore size by phase inversion and post-treatment process. J. Membr. Sci. 199 (2002) 75-84.

[53]S. Gupta, R. Q. Ou, R. A. Gerhardt. Effect of the fabrication method on the electrical properties of poly(acrylonitrile-co-butadiene-co-styrene)/carbon black composites. J. Electron. Mater. 35 (2006) 224-229.

[54]M. S. A. Rahaman, A. F. Ismail, A. Mustafa. A review of heat treatment on polyacrylonitrile fiber. Polym. Degrad. Stab. 92 (2007) 1421-1432.

[55]K. S. Perera, M. A. K. L. Dissanayake, S. Skaarup, K. West. Application of polyacrylonitrile-based polymer electrolytes in rechargeable lithium batteries. J. Solid State Electrochem. 12 (2008) 873-877.

[56]D. Shan, S. X. Wang, Y. Y. He, H. G. Xue. Amperometric glucose biosensor based on in situ electropolymerized polyaniline/poly(acrylonitrile-co-acrylic acid) composite film. Mater. Sci. Eng. C 28 (2008) 213-217.

[57]X. P. Gao, J. L. Bao, G. L. Pan, H. Y. Zhu, P. X. Huang, F. Wu, D. Y. Song. Preparation and electrochemical performance of polycrystalline and single crystalline CuO nanorods as anode materials for Li ion battery. J. Phys. Chem. B 108 (2004) 5547-5551.

[58]J. S. Guo, G. Q. Sun, Q. Wang, G. X. Wang, Z. H. Zhou, S. H. Tang, L. H. Jiang, B. Zhou, Q. Xin. Carbon nanofibers supported Pt-Ru electrocatalysts for direct methanol fuel cells. Carbon 44 (2006) 152-157.

[59]T. H. Cho, T. Sakai, S. Tanase, K. Kimura, Y. Kondo, T. Tarao, M. Tanaka. Electrochemical performances of polyacrylonitrile nanofiber-based nonwoven separator for lithium-ion battery. Electrochem. Solid-State Lett. 10 (2007) A159-A162.

[60]J. Jang, J. Bae. Carbon nanofiber/polypyrrole nanocable as toxic gas sensor. Sens. Actuators, B 122 (2007) 7-13.

[61]J. Mittal, O. P. Bahl, R. B. Mathur. Single step carbonization and graphitization of highly stabilized PAN fibers. Carbon 35 (1997) 1196-1197.

[62]D. Zhu, C. Y. Xu, N. Nakura, M. Matsuo. Study of carbon films from PAN/VGCF composites by gelation/crystallization from solution. Carbon 40 (2002) 363-373.

[63]H. Pierson. Handbook of carbon, graphite, diamond, and fullerenes: properties, processing and applications. Noyes publications (1993).

[64]G. P. Tandon, Y. Ran. Influence of Vapor-Grown Carbon Nanofibers on Thermomechanical properties of Graphite-Epoxy Composites. Proceedings for the 17th Annual Technical Conference ASC (2002).

[65]I. C. Finegan, G. G. Tibbetts, D. G. Glasgow, J. M. Ting, M. L. Lake. Surface treatments for improving the mechanical properties of carbon nanofiber/thermoplastic composites. J. Mater. Sci. 38 (2003) 3485-3490.

[66]S. G. Prolongo, M. Campo, M. R. Gude, R. Chaos-Moran, A. Urena. Thermo-physical characterisation of epoxy resin reinforced by amino-functionalized carbon nanofibers.

Compos. Sci. Technol. 69 (2009) 349-357.

[67]L. Wu, X. J. Zhang, H. X. Ju. Amperometric glucose sensor based on catalytic reduction of dissolved oxygen at soluble carbon nanofiber. Biosens. Bioelectron. 23 (2007) 479-484.

[68]Z. Z. Li, X. L. Cui, J. S. Zheng, Q. F. Wang, Y. H. Lin. Effects of microstructure of carbon nanofibers for amperometric detection of hydrogen peroxide. Anal. Chim. Acta 597 (2007) 238-244.

[69]G. X. Wang, X. P. Shen, J. Yao, J. Park. Graphene nanosheets for enhanced lithium storage in lithium ion batteries. Carbon 47 (2009) 2049-2053.

[70]J. Y. Yan, H. H. Song, S. B. Yang, J. D. Yan, X. H. Chen. Preparation and electrochemical properties of composites of carbon nanotubes loaded with Ag and TiO2 nanoparticle for use as anode material in lithium-ion batteries. Electrochim. Acta 53 (2008) 6351-6355.

[71]J. T. Yin, M. Wada, Y. Kitano, S. Tanase, O. Kajita, T. Sakai. Nanostructured Ag-Fe-Sn/carbon nanotubes composites as anode materials for advanced lithium-ion batteries. J. Electrochem. Soc. 152 (2005) A1341-A1346.

[72]C. Kim, K. S. Yang, M. Kojima, K. Yoshida, Y. J. Kim, Y. A. Kim, M. Endo. Fabrication of electrospinning-derived carbon nanofiber webs for the anode material of lithium-ion secondary batteries. Adv. Funct. Mater. 16 (2006) 2393-2397.

[73]J. Fan, T. Wang, C. Z. Yu, B. Tu, Z. Y. Jiang, D. Y. Zhao. Ordered, nanostructured tin-based oxides/carbon composite as the negative-electrode material for lithium-ion batteries. Adv. Mater. 16 (2004) 1432.

[74]M. S. Wu, P. C. J. Chiang. Electrochemically deposited nanowires of manganese oxide as an anode material for lithium-ion batteries. Electrochem. Commun. 8 (2006) 383-388.

[75]M. S. Wu, P. C. J. Chiang, J. T. Lee, J. C. Lin. Synthesis of manganese oxide electrodes with interconnected nanowire structure as an anode material for rechargeable lithium ion batteries. J. Phys. Chem. B 109 (2005) 23279-23284.

[76]H. J. Kim, Y. S. Kim, M. H. Seo, S. M. Choi, W. B. Kim. Pt and PtRh nanowire electrocatalysts for cyclohexane-fueled polymer electrolyte membrane fuel cell. Electrochem. Commun. 11 (2009) 446-449.

[77]J. W. Liu, Y. T. Kuo, K. J. Klabunde, C. Rochford, J. Wu, J. Li. Novel Dye-Sensitized Solar Cell Architecture Using TiO2-Coated Vertically Aligned Carbon Nanofiber Arrays. ACS Appl. Mater. Interfaces 1 (2009) 1645-1649.

[78]W. R. Grove. Fuel cells. Philosophical Magazine 14 (1838) 127.

[79]L. Mond, C. Langer. Proceedings of the Royal Society of London 46 (1889) 296 - 304.

[80]F. T. Bacon. The High Pressure Hydrogen-Oxygen Fuel Cell. Ind. Eng. Chem. 52 (1960) 301-303.

[81]F. T. Bacon. Fuel-Cell - Some Thoughts and Recollections. J. Electrochem. Soc. 126 (1979) C7-C16.

[82]S. Banerjee. Nafion (R) perfluorinated membranes in fuel cells. Abstracts of Papers of the American Chemical Society 226 (2003) U524-U524.

[83]S. Banerjee, D. E. Curtin. Nafion (R) perfluorinated membranes in fuel cells. J. Fluorine Chem. 125 (2004) 1211-1216.

[84]L. Carrette, K. A. Friedrich, U. Stimming. Fuel Cells-Fundamentals and Applications. Fuel Cells 1 (2001) 5-39.

[85]D. Q. Yang, J. F. Rochette, E. Sacher. Spectroscopic evidence for pi-pi interaction between poly(diallyl dimethylammonium) chloride and multiwalled carbon nanotubes. J. Phys. Chem. B 109 (2005) 4481-4484.

[86]G. Hoogers. Fuel cell technology handbook. CRC PRESS, Boca Raton London New York Washington, D.C. (2003).

[87]R. O'Hayre, S.-W. Cha, W. Colella, F. B. Prinz. Ryan O'Hayre (Author), Suk-Won Cha (Author), Whitney Colella (Author), Fritz B. Prinz (Author) John Wiley & Sons, Inc., Hoboken, New Jersey. (2006).

[88]D. K. Ross. Hydrogen storage: The major technological barrier to the development of hydrogen fuel cell cars. Vacuum 80 (2006) 1084-1089.

[89]S. Wasmus, A. Kuver. Methanol oxidation and direct methanol fuel cells: a selective review. J. Electroanal. Chem. 461 (1999) 14-31.

[90]C. Yang, S. Srinivasan, A. S. Arico, P. Creti, V. Baglio, V. Antonucci. Composition Nafion/zirconium phosphate membranes for direct methanol fuel cell operation at high temperature. Electrochem. Solid-State Lett. 4 (2001) A31-A34.

[91](http://en.wikipedia.org/wiki/Methanol).

[92]A. J. Appleby, F. R. Foulkes. Fuel Cell Handbook. Van Nostrand Reinhold Company January (1989).

[93]S. Gottesfeld, J. Pafford. A New Approach to the Problem of Carbon-Monoxide Poisoning in Fuel-Cells Operating at Low-Temperatures. J. Electrochem. Soc. 135 (1988)

2651-2652.

[94]K. Kolbrecka, J. Przyluski. Sub-Stoichiometric Titanium-Oxides as Ceramic Electrodes for Oxygen Evolution - Structural Aspects of the Voltammetric Behavior of Tino2n-1. Electrochim. Acta 39 (1994) 1591-1595.

[95]I. Gatto, A. Sacca, A. Carbone, R. Pedicini, F. Urbani, E. Passalacqua. CO-tolerant electrodes developed with PhosphoMolybdic acid for polymer electrolyte fuel cell (PEFCs) application. J. Power Sources 171 (2007) 540-545.

[96]A. T. Haug, R. E. White, J. W. Weidner, W. Huang. Development of a novel CO tolerant proton exchange membrane fuel cell anode. J. Electrochem. Soc. 149 (2002) A862-A867.

[97]D. H. Lim, D. H. Choi, W. D. Lee, H. I. Lee. A new synthesis of a highly dispersed and CO tolerant PtSn/C electrocatalyst for low-temperature fuel cell; its electrocatalytic activity and long-term durability. Appl. Catal. B Environ. 89 (2009) 484-493.

[98]K. Tanaka, M. Shou, H. He, C. B. Zhang, D. L. Lu. A CO-Tolerant Hydrogen Fuel Cell System Designed by Combining with an Extremely Active Pt/CNT Catalyst. Catal. Lett. 127 (2009) 148-151.

[99]M. Watanabe, H. Igarashi, T. Fujino. Design of CO tolerant anode catalysts for polymer electrolyte fuel cell. Electrochemistry 67 (1999) 1194-1196.

[100] M. C. Denis, P. Gouerec, D. Guay, J. P. Dodelet, G. Lalande, R. Schulz. Improvement of the high energy ball-milling preparation procedure of CO tolerant Pt and Ru containing catalysts for polymer electrolyte fuel cells. J. Appl. Electrochem. 30 (2000) 1243-1253.

[101] M. T. M. Koper, T. E. Shubina, R. A. van Santen. Periodic density functional study of CO and OH adsorption on Pt-Ru alloy surfaces: Implications for CO tolerant fuel cell catalysts. J. Phys. Chem. B 106 (2002) 686-692.

[102] L. Li, H. X. Wang, B. Q. Xu, J. L. Li, T. H. Lu, Z. Q. Mao. Study of PEMFC electro-catalysts: Characteristics of a homemade CO-tolerant Pt-Ru/C catalyst. Acta Chim. Sinica 61 (2003) 818-823.

[103] H. Uchida, K. Izumi, M. Watanabe. Temperature dependence of CO-tolerant hydrogen oxidation reaction activity at Pt, Pt-Co, and Pt-Ru electrodes. J. Phys. Chem. B 110 (2006) 21924-21930.

[104] M. Wakisaka, S. Mitsui, Y. Hirose, K. Kawashima, H. Uchida, M. Watanabe. Electronic structures of Pt-Co and Pt-Ru alloys for Co-tolerant anode catalysts in polymer electrolyte fuel cells studied by EC-XPS. J. Phys. Chem. B 110 (2006) 23489-23496.

[105] H. Yano, C. Ono, H. Shiroishi, T. Okada. New CO tolerant electro-catalysts exceeding Pt-Ru for the anode of fuel cells. Chem. Commun. (2005) 1212-1214.

[106] Z. Q. Tian, S. P. Jiang, Y. M. Liang, P. K. Shen. Synthesis and characterization of platinum catalysts on muldwalled carbon nanotubes by intermittent microwave irradiation for fuel cell applications. J. Phys. Chem. B 110 (2006) 5343-5350.

[107] K. Y. Chan, J. Ding, J. W. Ren, S. A. Cheng, K. Y. Tsang. Supported mixed metal nanoparticles as electrocatalysts in low temperature fuel cells. J. Mater. Chem. 14 (2004) 505-516.

[108] A. R. Kucernak, E. Toyoda. Studying the oxygen reduction and hydrogen oxidation reactions under realistic fuel cell conditions. Electrochem. Commun. 10 (2008) 1728-1731.

[109] J. G. Oh, H. Kim. Synthesis and characterization of PtNx/C as methanol-tolerant oxygen reduction electrocatalysts for a direct methanol fuel cell. J. Power Sources 181 (2008) 74-78.

[110] S. Walch, A. Dhanda, M. Aryanpour, H. Pitsch. Mechanism of molecular oxygen reduction at the cathode of a PEM fuel cell: Non-electrochemical reactions on catalytic Pt particles. J. Phys. Chem. C 112 (2008) 8464-8475.

[111] B. Z. Fang, J. H. Kim, J. S. Yu. Colloid-imprinted carbon with superb nanostructure as an efficient cathode electrocatalyst support in proton exchange membrane fuel cell. Electrochem. Commun. 10 (2008) 659-662.

[112] E. Kjeang, J. Goldak, M. R. Golriz, J. Gu, D. James, K. Kordesch. A parametric study of methanol crossover in a flowing electrolyte-direct methanol fuel cell. J. Power Sources 153 (2006) 89-99.

[113] Q. Z. Lai, G. P. Yin, Z. B. Wang, C. Y. Du, P. J. Zuo, X. Q. Cheng. Influence of Methanol Crossover on the Fuel Utilization of Passive Direct Methanol Fuel Cell. Fuel Cells 8 (2008) 399-403.

[114] W. W. Yang, T. S. Zhao. Numerical investigations of effect of membrane electrode assembly structure on water crossover in a liquid-feed direct methanol fuel cell. J. Power Sources 188 (2009) 433-446.

[115] W. E. Billups. Fullerenes: Principles and Applications. J. Am. Chem. Soc. (2008).

[116] D. Arunbabu, A. Sannigrahi, T. Jana. Blends of polybenzimidazole and poly(vinylidene fluoride) for use in a fuel cell. J. Phys. Chem. B 112 (2008) 5305-5310.

[117] P. P. Kundu, B. T. Kim, J. E. Ahn, H. S. Han, Y. G. Shul. Formation and evaluation of semi-IPN of nafion 117 membrane for direct methanol fuel cell - 1. Crosslinked sulfonated

polystyrene in the pores of nafion 117. J. Power Sources 171 (2007) 86-91.

[118] J. K. Lee, W. Li, A. Manthiram. Sulfonated poly(ether ether ketone) as an ionomer for direct methanol fuel cell electrodes. J. Power Sources 180 (2008) 56-62.

[119] W. Lee, H. Kim, H. Lee. Proton exchange membrane using partially sulfonated polystyrene-b-poly (dimethylsiloxane) for direct methanol fuel cell. J. Membr. Sci. 320 (2008) 78-85.

[120] A. Kuver, K. Potje-Kamloth. Comparative study of methanol crossover across electropolymerized and commercial proton exchange membrane electrolytes for the acid direct methanol fuel cell. Electrochim. Acta 43 (1998) 2527-2535.

[121] R. Thangamuthu, C. W. Lin. Preparation of gas diffusion electrodes using PEG/SiO2 hybrid materials and the effect of their composition on microstructure of the catalyst layer and on fuel cell performance. J. Power Sources 161 (2006) 160-167.

[122] H. Grune. Model Analysis of Gas-Electrolyte Balance of Supported Gas-Diffusion Electrodes for Fuel-Cells. Siemens Forschungs-Und Entwicklungsberichte-Siemens Research and Development Reports 6 (1977) 364-370.

[123] B. Markicevic, A. Bazylak, N. Djilali. Determination of transport parameters for multiphase flow in porous gas diffusion electrodes using a capillary network model. J. Power Sources 171 (2007) 706-717.

[124] I. D. Raistrick, T. E. Springer. A Dynamical Model of Porous Gas-Diffusion Electrodes. J. Electrochem. Soc. 135 (1988) C345-C345.

[125] D. M. Bernardi, M. W. Verbrugge. Mathematical-Model of a Gas-Diffusion Electrode Bonded to a Polymer Electrolyte. AlChE J. 37 (1991) 1151-1163.

[126] J. Giner, C. Hunter. Mechanism of Operation of Teflon-Bonded Gas Diffusion Electrode - a Mathematical Model. J. Electrochem. Soc. 116 (1969) 1124-&.

[127] X. C. Yu, B. Zhou, A. Sobiesiak. Water and thermal management for Ballard PEM fuel cell stack. J. Power Sources 147 (2005) 184-195.

[128] J. S. Yi, T. V. Nguyen. An along-the-channel model for proton exchange membrane fuel cells. J. Electrochem. Soc. 145 (1998) 1149-1159.

[129] V. Mehta, J. S. Cooper. Review and analysis of PEM fuel cell design and manufacturing. J. Power Sources 114 (2003) 32-53.

[130] E. Anderson, E. J. Taylor, N. R. K. Vilambi, A. Gelb. Preliminary-Analysis of Fuel-Cell Derived Technologies Applied to Energy-Conservation in the Chloralkali Industry.

Sep. Sci. Technol. 25 (1990) 1537-1554.

[131] D. Bevers, N. Wagner, M. von Bradke. Innovative production procedure for low cost PEFC electrodes and electrode/membrane structures. Int. J. Hydrogen Energy 23 (1998) 57-63.

[132] E. J. Taylor, E. B. Anderson, N. R. K. Vilambi. Preparation of High-Platinum-Utilization Gas-Diffusion Electrodes for Proton-Exchange-Membrane Fuel-Cells. J. Electrochem. Soc. 139 (1992) L45-L46.

[133] S. Srinivasan, A. Ferreira, R. Mosdale, S. Mukerjee, J. Kim, S. Hirano, S. Lee, F. Buchi, A. Appleby. Proceeding of the Fuel Cell-Program and Abstracts on the Proton Exchange Membrane Fuel Cells For Space and Electric Vehicle Application. 2 (1994) 424-427.

[134] E. Gulzow, M. Schulze, N. Wagner, T. Kaz, R. Reissner, G. Steinhilber, A. Schneider. Dry layer preparation and characterisation of polymer electrolyte fuel cell components. J. Power Sources 86 (2000) 352-362.

[135] M. S. Wilson, S. Gottesfeld. High-Performance Catalyzed Membranes of Ultra-Low Pt Loadings for Polymer Electrolyte Fuel-Cells. J. Electrochem. Soc. 139 (1992) L28-L30.

[136] M. S. Wilson, S. Gottesfeld. Thin-Film Catalyst Layers for Polymer Electrolyte Fuel-Cell Electrodes. J. Appl. Electrochem. 22 (1992) 1-7.

[137] P. S. Fedkiw, W. H. Her. An Impregnation-Reduction Method to Prepare Electrodes on Nafion Spe. J. Electrochem. Soc. 136 (1989) 899-900.

[138] J. Kua, W. A. Goddard. Oxidation of methanol on 2nd and 3rd row Group VIII transition metals (Pt, Ir, Os, Pd, Rh, and Ru): Application to direct methanol fuel cells. J. Am. Chem. Soc. 121 (1999) 10928-10941.

[139] A. Hamnett. Mechanism and electrocatalysis in the direct methanol fuel cell. Catal. Today 38 (1997) 445-457.

[140] P. S. Kauranen, E. Skou, J. Munk. Kinetics of methanol oxidation on carbon-supported Pt and Pt+Ru catalysts. J. Electroanal. Chem. 404 (1996) 1-13.

[141] M. Watanabe, S. Motoo. Electrocatalysis by Ad-Atoms .2. Enhancement of Oxidation of Methanol on Platinum by Ruthenium Ad-Atoms. J. Electroanal. Chem. 60 (1975) 267-273.

[142] W. Vielstich, A. Lamm, H. A. Gasteiger. Handbook of Fuel Cells: Fundamentals, Technology, Applications. Wiley. (2003) 443-464.

[143] O. Antoine, Y. Bultel, R. Durand. Oxygen reduction reaction kinetics and mechanism on platinum nanoparticles inside Nafion (R). J. Electroanal. Chem. 499 (2001) 85-94.

[144] V. S. Murthi, R. C. Urian, S. Mukerjee. Oxygen reduction kinetics in low and medium temperature acid environment: Correlation of water activation and surface properties in supported Pt and Pt alloy electrocatalysts. J. Phys. Chem. B 108 (2004) 11011-11023.

[145] U. A. Paulus, T. J. Schmidt, H. A. Gasteiger, R. J. Behm. Oxygen reduction on a high-surface area Pt/Vulcan carbon catalyst: a thin-film rotating ring-disk electrode study. J. Electroanal. Chem. 495 (2001) 134-145.

[146] V. R. Stamenkovic, B. Fowler, B. S. Mun, G. F. Wang, P. N. Ross, C. A. Lucas, N. M. Markovic. Improved oxygen reduction activity on Pt3Ni(111) via increased surface site availability. Science 315 (2007) 493-497.

[147] J. K. Norskov, J. Rossmeisl, A. Logadottir, L. Lindqvist, J. R. Kitchin, T. Bligaard, H. Jonsson. Origin of the overpotential for oxygen reduction at a fuel-cell cathode. J. Phys. Chem. B 108 (2004) 17886-17892.

[148] M. K. Min, J. H. Cho, K. W. Cho, H. Kim. Particle size and alloying effects of Pt-based alloy catalysts for fuel cell applications. Electrochim. Acta 45 (2000) 4211-4217.

[149] S. Mukerjee, S. Srinivasan, M. P. Soriaga, J. Mcbreen. Role of Structural and Electronic-Properties of Pt and Pt Alloys on Electrocatalysis of Oxygen Reduction - an in-Situ Xanes and Exafs Investigation. J. Electrochem. Soc. 142 (1995) 1409-1422.

[150] S. Mukerjee, S. Srinivasan, M. P. Soriaga, J. Mcbreen. Effect of Preparation Conditions of Pt Alloys on Their Electronic, Structural, and Electrocatalytic Activities for Oxygen Reduction-Xrd, Xas, and Electrochemical Studies. J. Phys. Chem. 99 (1995) 4577-4589.

[151] Y. Xu, A. V. Ruban, M. Mavrikakis. Adsorption and dissociation of O-2 on Pt-Co and Pt-Fe alloys. J. Am. Chem. Soc. 126 (2004) 4717-4725.

[152] F. T. B. J. Vandenbrink, E. Barendrecht, W. H. M. Visscher. Determination of the Rate of Chemical Decomposition of H2o2 by Electrocatalysts for O2 Reduction. J. Electrochem. Soc. 126 (1979) C111-C111.

[153] J. F. Drillet, A. Ee, J. Friedemann, R. Kotz, B. Schnyder, V. M. Schmidt. Oxygen reduction at Pt and Pt70Ni30 in H2SO4/CH3OH solution. Electrochim. Acta 47 (2002) 1983-1988.

[154] Y. Mo, R. R. Adzic. PT monolayer electrocatalysts for O2 reduction. Abstracts of Papers of the American Chemical Society 225 (2003) U682-U682.

[155] W. Chen, J. M. Kim, S. H. Sun, S. W. Chen. Electrocatalytic reduction of oxygen by FePt alloy nanoparticles. J. Phys. Chem. C 112 (2008) 3891-3898.

[156] F. Lufrano, G. Squadrito, A. Patti, E. Passalacqua. Sulfonated polysulfone as promising membranes for polymer electrolyte fuel cells. J. Appl. Polym. Sci. 77 (2000) 1250-1256.

[157] G. Alberti, M. Casciola, L. Massinelli, B. Bauer. Polymeric proton conducting membranes for medium temperature fuel cells (110-160 degrees C). J. Membr. Sci. 185 (2001) 73-81.

[158] D. J. Jones, J. Roziere. Recent advances in the functionalisation of polybenzimidazole and polyetherketone for fuel cell applications. J. Membr. Sci. 185 (2001) 41-58.

[159] K. D. Kreuer. On the development of proton conducting polymer membranes for hydrogen and methanol fuel cells. J. Membr. Sci. 185 (2001) 29-39.

[160] Y. S. Kim, M. J. Sumner, W. L. Harrison, J. S. Riffle, J. E. McGrath, B. S. Pivovar. Direct methanol fuel cell performance of disulfonated poly-arylene ether benzonitrile) copolymers. J. Electrochem. Soc. 151 (2004) A2150-A2156.

[161] V. Saarinen, I. Kallio, M. Paronen, P. Tikkanen, E. Rauhala, K. Kontturi. New ETFE-based membrane for direct methanol fuel cell. Electrochim. Acta 50 (2005) 3453-3460.

[162] H. S. Liu, C. J. Song, L. Zhang, J. J. Zhang, H. J. Wang, D. P. Wilkinson. A review of anode catalysis in the direct methanol fuel cell. J. Power Sources 155 (2006) 95-110.

[163] M. Watanabe, S. Motoo. Electrocatalysis by Ad-Atoms .1. Enhancement of Oxidation of Methanol on Platinum and Palladium by Gold Ad-Atoms. J. Electroanal. Chem. 60 (1975) 259-266.

[164] M. Watanabe, S. Motoo. Electrocatalysis by Ad-Atoms .3. Enhancement of Oxidation of Carbon-Monoxide on Platinum by Ruthenium Ad-Atoms. J. Electroanal. Chem. 60 (1975) 275-283.

[165] T. Frelink, W. Visscher, J. A. R. Vanveen. On the Role of Ru and Sn as Promoters of Methanol Electrooxidation over Pt. Surf. Sci. 335 (1995) 353-360.

[166] R. Dillon, S. Srinivasan, A. S. Arico, V. Antonucci. International activities in DMFC R&D: status of technologies and potential applications. J. Power Sources 127 (2004) 112-126.

[167] H. A. Gasteiger, N. Markovic, P. N. Ross, E. J. Cairns. Methanol Electrooxidation

on Well-Characterized Pt-Rn Alloys. J. Phys. Chem. 97 (1993) 12020-12029.

[168] H. A. Gasteiger, N. Markovic, P. N. Ross, E. J. Cairns. Electrooxidation of Small Organic-Molecules on Well-Characterized Pt-Ru Alloys. Electrochim. Acta 39 (1994) 1825-1832.

[169] H. A. Gasteiger, N. Markovic, P. N. Ross, E. J. Cairns. Temperature-Dependent Methanol Electrooxidation on Well-Characterized Pt-Ru Alloys. J. Electrochem. Soc. 141 (1994) 1795-1803.

[170] A. Kabbabi, R. Faure, R. Durand, B. Beden, F. Hahn, J. M. Leger, C. Lamy. In situ FTIRS study of the electrocatalytic oxidation of carbon monoxide and methanol at platinum-ruthenium bulk alloy electrodes. J. Electroanal. Chem. 444 (1998) 41-53.

[171] K. Jambunathan, S. Jayaraman, A. C. Hillier. A multielectrode electrochemical and scanning differential electrochemical mass spectrometry study of methanol oxidation on electrodeposited PtxRuy. Langmuir 20 (2004) 1856-1863.

[172] N. Benker, C. Roth, M. Mazurek, H. Fuess. Synthesis and characterisation of ternary Pt/Ru/Mo catalysts for the anode of the PEM fuel cell. J. New Mater. Electrochem. Syst. 9 (2006) 121-126.

[173] T. Kawaguchi, Y. Rachi, W. Sugimoto, Y. Murakami, Y. Takasu. Performance of ternary PtRuRh/C electrocatalyst with varying Pt : Ru : Rh ratio for methanol electro-oxidation. J. Appl. Electrochem. 36 (2006) 1117-1125.

[174] T. Y. Kim, K. Kobayashi, M. Takahashi, M. Nagai. Effect of Sn in Pt-Ru-Sn ternary catalysts for CO/H-2 and methanol electrooxidation. Chem. Lett. 34 (2005) 798-799.

[175] K. L. Ley, R. X. Liu, C. Pu, Q. B. Fan, N. Leyarovska, C. Segre, E. S. Smotkin. Methanol oxidation on single-phase Pt-Ru-Os ternary alloys. J. Electrochem. Soc. 144 (1997) 1543-1548.

[176] B. Lim, M. J. Jiang, P. H. C. Camargo, E. C. Cho, J. Tao, X. M. Lu, Y. M. Zhu, Y. A. Xia. Pd-Pt Bimetallic Nanodendrites with High Activity for Oxygen Reduction. Science 324 (2009) 1302-1305.

[177] H. Q. Li, Q. Xin, W. Z. Li, Z. H. Zhou, L. H. Jiang, S. H. Yang, G. Q. Sun. An improved palladium-based DMFCs cathode catalyst. Chem. Commun. (2004) 2776-2777.

[178] X. Zhang, K. Y. Chan. Microemulsion synthesis and electrocatalytic properties of platinum-cobalt nanoparticles. J. Mater. Chem. 12 (2002) 1203-1206.

[179] J. H. Zeng, J. Y. Lee. Effects of preparation conditions on performance of carbon-supported nanosize Pt-Co catalysts for methanol electro-oxidation under acidic

conditions. J. Power Sources 140 (2005) 268-273.

[180] T. Okada, Y. Suzuki, T. Hirose, T. Ozawa. Novel system of electro-catalysts for methanol oxidation based on platinum and organic metal complexes. Electrochim. Acta 49 (2004) 385-395.

[181] S. Mukerjee, S. Srinivasan. Enhanced Electrocatalysis of Oxygen Reduction on Platinum Alloys in Proton-Exchange Membrane Fuel-Cells. J. Electroanal. Chem. 357 (1993) 201-224.

[182] S. Mukerjee, S. Srinivasan, A. J. Appleby. Effect of Sputtered Film of Platinum on Low Platinum Loading Electrodes on Electrode-Kinetics of Oxygen Reduction in Proton-Exchange Membrane Fuel-Cells. Electrochim. Acta 38 (1993) 1661-1669.

[183] X. Zhang, F. Zhang, K. Y. Chan. Preparation of Pt-Ru-Co trimetallic nanoparticles and their electrocatalytic properties. Catal. Commun. 5 (2004) 749-753.

[184] V. A. Bogdanovskaya, M. R. Tarasevich, L. N. Kuznetsova, M. V. Radina. The structure and characteristics of a PtCoCr nanosized polymetallic cathode catalyst on a carbon carrier. Russ. J. Phys. Chem. A 83 (2009) 2045-2049.

[185] T. Page, R. Johnson, J. Hormes, S. Noding, B. Rambabu. A study of methanol electro-oxidation reactions in carbon membrane electrodes and structural properties of Pt alloy electro-catalysts by EXAFS. J. Electroanal. Chem. 485 (2000) 34-41.

[186] A. K. Shukla, R. K. Raman. Methanol-rusistant oxygen-reduction catalysts for direct methanol fuel celms. Annu. Rev. Mater. Res. 33 (2003) 155-168.

[187] T. Toda, H. Igarashi, H. Uchida, M. Watanabe. Enhancement of the electroreduction of oxygen on Pt alloys with Fe, Ni, and Co. J. Electrochem. Soc. 146 (1999) 3750-3756.

[188] T. Toda, H. Igarashi, M. Watanabe. Enhancement of the electrocatalytic O-2 reduction on Pt-Fe alloys. J. Electroanal. Chem. 460 (1999) 258-262.

[189] W. Roh, J. Cho, H. Kim. Characterization of Pt-Cu-Fe ternary electrocatalysts supported on carbon black. J. Appl. Electrochem. 26 (1996) 623-630.

[190] K. R. Lee, M. K. Jeon, S. I. Woo. Composition optimization of PtRuM/C (M = Fe and Mo) catalysts for methanol electro-oxidation via combinatorial method. Appl. Catal. B Environ. 91 (2009) 428-433.

[191] L. Xiong, A. M. Kannan, A. Manthiram. Pt-M (M = Fe, Co, Ni and Cu) electrocatalysts synthesized by an aqueous route for proton exchange membrane fuel cells. Electrochem. Commun. 4 (2002) 898-903.

[192] B. Moreno, E. Chinarro, J. L. G. Fierro, J. R. Jurado. Synthesis of the ceramic-metal catalysts (PtRuNi-TiO2) by the combustion method. J. Power Sources 169 (2007) 98-102.

[193] X. Zhang, F. Zhang, R. F. Guan, K. Y. Chan. Preparation of Pt-Ru-Ni ternary nanoparticles by microemulsion and electrocatalytic activity for methanol oxidation. Mater. Res. Bull. 42 (2007) 327-333.

[194] X. S. Zhao, W. Z. Li, L. H. Jiang, W. J. Zhou, Q. Xin, B. L. Yi, G. Q. Sun. Multi-wall carbon nanotube supported Pt-Sn nanoparticles as an anode catalyst for the direct ethanol fuel cell. Carbon 42 (2004) 3263-3265.

[195] F. Colmati, E. Antolini, E. R. Gonzalez. Pt-Sn/C electrocatalysts for methanol oxidation synthesized by reduction with formic acid. Electrochim. Acta 50 (2005) 5496-5503.

[196] W. J. Zhou, S. Q. Song, W. Z. Li, Z. H. Zhou, G. Q. Sun, Q. Xin, S. Douvartzides, P. Tsiakaras. Direct ethanol fuel cells based on PtSn anodes: the effect of Sn content on the fuel cell performance. J. Power Sources 140 (2005) 50-58.

[197] C. J. Tseng, S. T. Lo, S. C. Lo, P. P. Chu. Characterization of Pt-Cu binary catalysts for oxygen reduction for fuel cell applications. Mater. Chem. Phys. 100 (2006) 385-390.

[198] K. Endo, Y. Katayama, T. Miura. Pt-Ir and Pt-Cu binary alloys as the electrocatalyst for ammonia oxidation. Electrochim. Acta 49 (2004) 1635-1638.

[199] L. Liu, G. Pu, R. Viswanathan, Q. B. Fan, R. X. Liu, E. S. Smotkin. Carbon supported and unsupported Pt-Ru anodes for liquid feed direct methanol fuel cells. Electrochim. Acta 43 (1998) 3657-3663.

[200] J. H. Choi, K. W. Park, I. S. Park, W. H. Nam, Y. E. Sung. Methanol electro-oxidation and direct methanol fuel cell using Pt/Rh and Pt/Ru/Rh alloy catalysts. Electrochim. Acta 50 (2004) 787-790.

[201] S. Sen Gupta, J. Datta. A comparative study on ethanol oxidation behavior at Pt and PtRh electrodeposits. J. Electroanal. Chem. 594 (2006) 65-72.

[202] L. X. Yang, R. G. Allen, K. Scott, P. Christenson, S. Roy. A comparative study of PtRu and PtRuSn thermally formed on titanium mesh for methanol electro-oxidation. J. Power Sources 137 (2004) 257-263.

[203] A. S. Arico, A. K. Shukla, H. Kim, S. Park, M. Min, V. Antonucci. An XPS study on oxidation states of Pt and its alloys with Co and Cr and its relevance to electroreduction of oxygen. Appl. Surf. Sci. 172 (2001) 33-40.

[204] E. Antolini, J. R. C. Salgado, E. R. Gonzalez. The methanol oxidation reaction on

platinum alloys with the first row transition metals - The case of Pt-Co and -Ni alloy electrocatalysts for DMFCs: A short review. Appl. Catal. B Environ. 63 (2006) 137-149.

[205] V. Neburchilov, H. J. Wang, J. J. Zhang. Low Pt content Pt-Ru-Ir-Sn quaternary catalysts for anodic methanol oxidation in DMFC. Electrochem. Commun. 9 (2007) 1788-1792.

[206] E. Antolini. Platinum-based ternary catalysts for low temperature fuel cells Part I. Preparation methods and structural characteristics. Appl. Catal. B Environ. 74 (2007) 324-336.

[207] E. Antolini. Platinum-based ternary catalysts for low temperature fuel cells Part II. Electrochemical properties. Appl. Catal. B Environ. 74 (2007) 337-350.

[208] K. W. Park, J. H. Choi, S. A. Lee, C. Pak, H. Chang, Y. E. Sung. PtRuRhNi nanoparticle electrocatalyst for methanol electrooxidation in direct methanol fuel cell. J. Catal. 224 (2004) 236-242.

[209] A. S. Arico, P. Creti, N. Giordano, V. Antonucci, P. L. Antonucci, A. Chuvilin. Chemical and morphological characterization of a direct methanol fuel cell based on a quaternary Pt-Ru-Sn-W/C anode. J. Appl. Electrochem. 26 (1996) 959.

[210] A. S. Arico, A. K. Shukla, K. M. El-Khatib, P. Creti, V. Antonucci. Effect of carbon-supported and unsupported Pt-Ru anodes on the performance of solid-polymer-electrolyte direct methanol fuel cells. J. Appl. Electrochem. 29 (1999) 671-676.

[211] J. H. Nam, Y. Y. Jang, Y. U. Kwon, J. D. Nam. Direct methanol fuel cell Pt-carbon catalysts by using SBA-15 nanoporous templates. Electrochem. Commun. 6 (2004) 737-741.

[212] A. K. Shukla, R. K. Raman, N. A. Choudhury, K. R. Priolkar, P. R. Sarode, S. Emura, R. Kumashiro. Carbon-supported Pt-Fe alloy as a methanol-resistant oxygen-reduction catalyst for direct methanol fuel cells. J. Electroanal. Chem. 563 (2004) 181-190.

[213] J. R. C. Salgado, E. Antolini, E. R. Gonzalez. Carbon supported Pt-Co alloys electrocatalysts for as methanol-resistant oxygen-reduction direct methanol fuel cells. Appl. Catal. B Environ. 57 (2005) 283-290.

[214] J. H. Zeng, J. Y. Lee, W. J. Zhou. A more active Pt/carbon DMFC catalyst by simple reversal of the mixing sequence in preparation. J. Power Sources 159 (2006) 509-513.

[215] K. P. De Jong, J. W. Geus. Carbon nanofibers: Catalytic synthesis and applications. Cat. Rev. - Sci. Eng. 42 (2000) 481-510.

[216] J. Guo, G. Sun, Q. Wang, G. Wang, Z. Zhou, S. Tang, L. Jiang, B. Zhou, Q. Xin. Carbon nanofibers supported Pt–Ru electrocatalysts for direct methanol fuel cells. Carbon 44 (2006) 152-157.

[217] C. W. Yang, X. G. Hu, D. L. Wang, C. S. Dai, L. Zhang, H. B. Jin, S. Agathopoulos. Ultrasonically treated multi-walled carbon nanotubes (MWCNTs) as PtRu catalyst supports for methanol electrooxidation. J. Power Sources 160 (2006) 187-193.

[218] N. Jha, A. L. M. Reddy, M. M. Shaijumon, N. Rajalakshmi, S. Ramaprabhu. Pt-Ru/multi-walled carbon nanotubes as electrocatalysts for direct methanol fuel cell. Int. J. Hydrogen Energy 33 (2008) 427-433.

[219] R. Q. Yu, L. W. Chen, Q. P. Liu, J. Y. Lin, K. L. Tan, S. C. Ng, H. S. O. Chan, G. Q. Xu, T. S. A. Hor. Platinum deposition on carbon nanotubes via chemical modification. Chem. Mater. 10 (1998) 718-722.

[220] N. Rajalakshmi, H. Ryu, M. M. Shaijumon, S. Ramaprabhu. Performance of polymer electrolyte membrane fuel cells with carbon nanotubes as oxygen reduction catalyst support material. J. Power Sources 140 (2005) 250-257.

[221] Y. Y. Mu, H. P. Liang, J. S. Hu, L. Jiang, L. J. Wan. Controllable Pt nanoparticle deposition on carbon nanotubes as an anode catalyst for direct methanol fuel cells. J. Phys. Chem. B 109 (2005) 22212-22216.

[222] W. Z. Li, C. H. Liang, W. J. Zhou, J. S. Qiu, Z. H. Zhou, G. Q. Sun, Q. Xin. Preparation and characterization of multiwalled carbon nanotube-supported platinum for cathode catalysts of direct methanol fuel cells. J. Phys. Chem. B 107 (2003) 6292-6299.

[223] E. S. Steigerwalt, G. A. Deluga, D. E. Cliffel, C. M. Lukehart. A Pt-Ru/graphitic carbon nanofiber nanocomposite exhibiting high relative performance as a direct-methanol fuel cell anode catalyst. J. Phys. Chem. B 105 (2001) 8097-8101.

[224] Z. B. He, J. H. Chen, D. Y. Liu, H. H. Zhou, Y. F. Kuang. Electrodeposition of Pt-Ru nanoparticles on carbon nanotubes and their electrocatalytic properties for methanol electrooxidation. Diamond Relat. Mater. 13 (2004) 1764-1770.

[225] H. Tang, J. H. Chen, S. Z. Yao, L. H. Nie, Y. F. Kuang, Z. P. Huang, D. Z. Wang, Z. F. Ren. Deposition and electrocatalytic properties of platinum on well-aligned carbon nanotube (CNT) arrays for methanol oxidation. Mater. Chem. Phys. 92 (2005) 548-553.

[226] C. C. Chien, K. T. Jeng. Effective preparation of carbon nanotube-supported Pt-Ru electrocatalysts. Mater. Chem. Phys. 99 (2006) 80-87.

[227] J. H. Wee, K. Y. Lee, S. H. Kim. Fabrication methods for low-Pt-loading electrocatalysts in proton exchange membrane fuel cell systems. J. Power Sources 165 (2007)

667-677.

[228] A. Rasheed, J. Y. Howe, M. D. Dadmun, P. F. Britt. The efficiency of the oxidation of carbon nanofibers with various oxidizing agents. Carbon 45 (2007) 1072-1080.

[229] C. Wang, M. Waje, X. Wang, J. M. Tang, R. C. Haddon, Y. S. Yan. Proton exchange membrane fuel cells with carbon nanotube based electrodes. Nano Lett. 4 (2004) 345-348.

[230] M. Y. Li, G. Y. Han, B. S. Yang. Fabrication of the catalytic electrodes for methanol oxidation on electrospinning-derived carbon fibrous mats. Electrochem. Commun. 10 (2008) 880-883.

[231] Z. Lin, L. Ji, X. Zhang. Electrodeposition of platinum nanoparticles onto carbon nanofibers for electrocatalytic oxidation of methanol. Mater. Lett. 63 (2009) 2115-2118.

[232] M. A. Correa-Duarte, N. Sobal, L. M. Liz-Marzan, M. Giersig. Linear assemblies of silica-coated gold nanoparticles using carbon nanotubes as templates. Adv. Mater. 16 (2004) 2179.

[233] Y. Y. Ou, M. H. Huang. High-density assembly of gold nanoparticles on multiwalled carbon nanotubes using 1-pyrenemethylamine as interlinker. J. Phys. Chem. B 110 (2006) 2031-2036.

[234] L. Cao, F. Scheib, C. Roth, F. Schweiger, C. Cremers, U. Stimming, H. Fuess, L. Chen, W. Zhu, X. Qiu. Novel Nanocomposite Pt/RuO2·xH2O/Carbon Nanotube Catalysts for Direct Methanol Fuel Cells. Angew. Chem. Int. Ed. 45 (2006) 5315-5319.

[235] N. T. Xuyen, H. K. Jeong, G. Kim, K. P. So, K. H. An, Y. H. Lee. Hydrolysis-induced immobilization of Pt(acac)(2) on polyimide-based carbon nanofiber mat and formation of Pt nanoparticles. J. Mater. Chem. 19 (2009) 1283-1288.

[236] Z. Lin, L. Ji, M. D. Woodroof, Y. Yao, W. Krause, X. Zhang. Synthesis and Electrocatalysis of Carbon Nanofiber-Supported Platinum by 1-AP Functionalization and Polyol Processing Technique. J. Phys. Chem. C (2010).

[237] W. X. Chen, J. Y. Lee, Z. L. Liu. Microwave-assisted synthesis of carbon supported Pt nanoparticles for fuel cell applications. Chem. Commun. (2002) 2588-2589.

[238] Z. L. Liu, J. Y. Lee, W. X. Chen, M. Han, L. M. Gan. Physical and electrochemical characterizations of microwave-assisted polyol preparation of carbon-supported PtRu nanoparticles. Langmuir 20 (2004) 181-187.

[239] X. Li, W. X. Chen, J. Zhao, W. Xing, Z. D. Xu. Microwave polyol synthesis of Pt/CNTs catalysts: Effects of pH on particle size and electrocatalytic activity for methanol

electrooxidization. Carbon 43 (2005) 2168-2174.

[240] Z. L. Liu, L. M. Gan, L. Hong, W. X. Chen, J. Y. Lee. Carbon-supported Pt nanoparticles as catalysts for proton exchange membrane fuel cells. J. Power Sources 139 (2005) 73-78.

[241] W. X. Chen, J. Zhao, J. Y. Lee, Z. L. Liu. Microwave heated polyol synthesis of carbon nanotubes supported Pt nanoparticles for methanol electrooxidation. Mater. Chem. Phys. 91 (2005) 124-129.

[242] E. S. Steigerwalt, G. A. Deluga, C. M. Lukehart. Rapid preparation of Pt-Ru/graphitic carbon nanofiber nanocomposites as DMFC anode catalysts using microwave processing. J. Nanosci. Nanotechnol. 3 (2003) 247-251.

[243] M. Tsuji, M. Kubokawa, R. Yano, N. Miyamae, T. Tsuji, M. S. Jun, S. Hong, S. Lim, S. H. Yoon, I. Mochida. Fast preparation of PtRu catalysts supported on carbon nanofibers by the microwave-polyol method and their application to fuel cells. Langmuir 23 (2007) 387-390.

[244] T. Yoshitake, H. Kimura, S. Kuroshima, S. Watanabe, Y. Shimakawa, T. Manako, S. Nakamura, Y. Kubo. Small direct methanol fuel cell pack for portable applications. Electrochemistry 70 (2002) 966-968.

[245] T. Yoshitake, Y. Shimakawa, S. Kuroshima, H. Kimura, T. Ichihashi, Y. Kubo, D. Kasuya, K. Takahashi, F. Kokai, M. Yudasaka, S. Iijima. Preparation of fine platinum catalyst supported on single-wall carbon nanohorns for fuel cell application. Physica B 323 (2002) 124-126.

[246] K. Sasaki, H. Ujiie, T. Higa, T. Hori, N. Shinya, T. Uchida. Rabbit aneurysm model mediated by the application of elastase. Neurol. Med. Chir. 44 (2004) 467-473.

[247] W. Z. Li, C. H. Liang, W. J. Zhou, J. S. Qiu, H. Q. Li, G. Q. Sun, Q. Xin. Homogeneous and controllable Pt particles deposited on multi-wall carbon nanotubes as cathode catalyst for direct methanol fuel cells. Carbon 42 (2004) 436-439.

[248] S. Hirano, J. Kim, S. Srinivasan. High performance proton exchange membrane fuel cells with sputter-deposited Pt layer electrodes. Electrochim. Acta 42 (1997) 1587-1593.

[249] C. L. Lee, C. C. Wan, Y. Y. Wang. Synthesis of metal nanoparticles via self-regulated reduction by an alcohol surfactant. Adv. Funct. Mater. 11 (2001) 344-347.

[250] L. Zhang, B. Cheng, E. T. Samulski. In situ fabrication of dispersed, crystalline platinum nanoparticles embedded in carbon nanofibers. Chem. Phys. Lett. 398 (2004) 505-510.

[251] C. L. Lee, Y. C. Ju, P. T. Chou, Y. C. Huang, L. C. Kuo, J. C. Oung. Preparation of Pt nanoparticles on carbon nanotubes and graphite nanofibers via self-regulated reduction of surfactants and their application as electrochemical catalyst. Electrochem. Commun. 7 (2005) 453.

[252] S. D. Oh, B. K. So, S. H. Choi, A. Gopalan, K. P. Lee, K. R. Yoon, I. S. Choi. Dispersing of Ag, Pd, and Pt-Ru alloy nanoparticles on single-walled carbon nanotubes by gamma-irradiation. Mater. Lett. 59 (2005) 1121-1124.

[253] N. Wakabayashi, H. Uchida, M. Watanabe. Temperature-dependence of methanol oxidation rates at PtRu and Pt electrodes. Electrochem. Solid-State Lett. 5 (2002) E62-E65.

[254] K. Lee, J. Zhang, H. Wang, D. P. Wilkinson. Progress in the synthesis of carbon nanotube- and nanofiber-supported Pt electrocatalysts for PEM fuel cell catalysis. J. Appl. Electrochem. 36 (2006) 507–522.

[255] J. H. Chen, W. Z. Li, D. Z. Wang, S. X. Yang, J. G. Wen, Z. F. Ren. Electrochemical characterization of carbon nanotubes as electrode in electrochemical double-layer capacitors. Carbon 40 (2002) 1193-1197.

[256] G. L. Che, B. B. Lakshmi, E. R. Fisher, C. R. Martin. Carbon nanotubule membranes for electrochemical energy storage and production. Nature 393 (1998) 346-349.

[257] S. H. Joo, S. J. Choi, I. Oh, J. Kwak, Z. Liu, O. Terasaki, R. Ryoo. Ordered nanoporous arrays of carbon supporting high dispersions of platinum nanoparticles. Nature 412 (2001) 169-172.

[258] A. Rasheed, J. Y. Howe, M. D. Dadmun, P. F. Britt. The efficiency of the oxidation of carbon nanofibers with various oxidizing agents. Carbon 45 (2007) 1072–1080.

[259] H. Jaegfeldt, T. Kuwana, G. Johansson. Electrochemical Stability of Catechols with a Pyrene Side-Chain Strongly Adsorbed on Graphite-Electrodes for Catalytic-Oxidation of Dihydronicotinamide Adenine-Dinucleotide. JACS 105 (1983) 1805-1814.

[260] S. Y. Wang, X. Wang, S. P. Jiang. PtRu nanoparticles supported on 1-aminopyrene-functionalized multiwalled carbon nanotubes and their electrocatalytic activity for methanol oxidation. Langmuir 24 (2008) 10505-10512.

[261] A. C. Ferrari, J. C. Meyer, V. Scardaci, C. Casiraghi, M. Lazzeri, F. Mauri, S. Piscanec, D. Jiang, K. S. Novoselov, S. Roth, A. K. Geim. Raman spectrum of graphene and graphene layers. Phys. Rev. Lett. 97 (2006).

[262] M. S. Dresselhaus, G. Dresselhaus, R. Saito, A. Jorio. Raman spectroscopy of carbon nanotubes. Phys. Rep. 409 (2005) 47-99.

[263] S. L. Knupp, W. Z. Li, O. Paschos, T. M. Murray, J. Snyder, P. Haldar. The effect of experimental parameters on the synthesis of carbon nanotube/nanofiber supported platinum by polyol processing techniques. Carbon 46 (2008) 1276-1284.

[264] D. Pletcher. Electrocatalysis - Present and Future. J. Appl. Electrochem. 14 (1984) 403-415.

[265] P. N. Ross. Characterization of Alloy Electrocatalysts for Direct Oxidation of Methanol - New Methods. Electrochim. Acta 36 (1991) 2053-2062.

[266] Z. B. He, J. H. Chen, D. Y. Liu, H. Tang, W. Deng, W. F. Kuang. Deposition and electrocatalytic properties of platinum nanoparticals on carbon nanotubes for methanol electrooxidation. Mater. Chem. Phys. 85 (2004) 396-401.

[267] K. Shimazu, D. Weisshaar, T. Kuwana. Electrochemical dispersion of Pt microparticles on glassy carbon electrodes. J. Electroanal. Chem. 223 (1987) 223-234.

[268] B. K. Balan, S. M. Unni, S. Kurungot. Carbon Nanofiber with Selectively Decorated Pt Both on Inner and Outer Walls as an Efficient Electrocatalyst for Fuel Cell Applications. J. Phys. Chem. C 113 (2009) 17572-17578.

[269] Z. P. Guo, D. M. Han, D. Wexler, R. Zeng, H. K. Liu. Polyoxometallate-stabilized platinum catalysts on multi-walled carbon nanotubes for fuel cell applications. Electrochim. Acta 53 (2008) 6410-6416.

[270] A. D. Taylor, R. C. Sekol, J. M. Kizuka, S. D'Cunha, C. M. Comisar. Fuel cell performance and characterization of 1-D carbon-supported platinum nanocomposites synthesized in supercritical fluids. J. Catal. 259 (2008) 5-16.

[271] X. Wang, W. Z. Li, Z. W. Chen, M. Waje, Y. S. Yan. Durability investigation of carbon nanotube as catalyst support for proton exchange membrane fuel cell. J. Power Sources 158 (2006) 154-159.

[272] F. L. Li, B. L. Zhang, S. J. Dong, E. K. Wang. A novel method of electrodepositing highly dispersed nano palladium particles on glassy carbon electrode. Electrochim. Acta 42 (1997) 2563-2568.

[273] K. W. Park, J. H. Choi, B. K. Kwon, S. A. Lee, Y. E. Sung, H. Y. Ha, S. A. Hong, H. Kim, A. Wieckowski. Chemical and electronic effects of Ni in Pt/Ni and Pt/Ru/Ni alloy nanoparticles in methanol electrooxidation. J. Phys. Chem. B 106 (2002) 1869-1877.

[274] M. C. Tsai, T. K. Yeh, C. H. Tsai. An improved electrodeposition technique for preparing platinum and platinum-ruthenium nanoparticles on carbon nanotubes directly grown on carbon cloth for methanol oxidation. Electrochem. Commun. 8 (2006) 1445-1452.

[275] S. Hrapovic, Y. L. Liu, K. B. Male, J. H. T. Luong. Electrochemical biosensing platforms using platinum nanoparticles and carbon nanotubes. Anal. Chem. 76 (2004) 1083-1088.

[276] N. M. Rodriguez, A. Chambers, R. T. K. Baker. Catalytic Engineering of Carbon Nanostructures. Langmuir 11 (1995) 3862-3866.

[277] M. Li, G. Han, B. Yang. Fabrication of the catalytic electrodes for methanol oxidation on electrospinning-derived carbon fibrous mats. Electrochem. Commun. 10 (2008) 880–883.

[278] M. M. E. Duarte, A. S. Pilla, J. M. Sieben, C. E. Mayer. Platinum particles electrodeposition on carbon substrates. Electrochem. Commun. 8 (2006) 159-164.

[279] T. M. Gur, R. A. Huggins. Direct Electrochemical Conversion of Carbon to Electrical Energy in a High-Temperature Fuel-Cell. J. Electrochem. Soc. 139 (1992) L95-L97.

[280] R. S. Morris, B. G. Dixon, T. Gennett, R. Raffaelle, M. J. Heben. High-energy, rechargeable Li-ion battery based on carbon nanotube technology. J. Power Sources 138 (2004) 277-280.

[281] S. L. Jain, B. Lakeman, K. D. Pointon, J. T. S. Irvine. Carbon-air fuel cell development to satisfy our energy demands. Ionics 13 (2007) 413-416.

[282] Z. Z. Li, X. L. Cui, X. S. Zhang, Q. F. Wang, Y. Y. Shao, Y. H. Lin. Pt/Carbon Nanofiber Nanocomposites as Electrocatalysts for Direct Methanol Fuel Cells: Prominent Effects of Carbon Nanofiber Nanostructures. J. Nanosci. Nanotechnol. 9 (2009) 2316-2323.

[283] E. Lafuente, E. Munoz, A. M. Benito, W. K. Maser, M. T. Martinez, F. Alcaide, L. Ganborena, I. Cendoya, O. Miguel, J. Rodriguez, E. P. Urriolabeitia, R. Navarro. Single-walled carbon nanotube-supported platinum nanoparticles as fuel cell electrocatalysts. J. Mater. Res. 21 (2006) 2841-2846.

[284] V. Selvaraj, M. Alagar. Ethylene glycol oxidation on Pt and Pt-Ru nanoparticle decorated polythiophene/multiwalled carbon nanotube composites for fuel cell applications. Nanotechnology 19 (2008) -.

[285] Y. B. Lee, C. H. Lee, D. S. Lim. The electrical and corrosion properties of carbon nanotube coated 304 stainless steel/polymer composite as PEM fuel cell bipolar plates. Int. J. Hydrogen Energy 34 (2009) 9781-9787.

[286] Y. Show, K. Takahashi. Stainless steel bipolar plate coated with carbon nanotube (CNT)/polytetrafluoroethylene (PTFE) composite film for proton exchange membrane fuel cell (PEMFC). J. Power Sources 190 (2009) 322-325.

[287] H. Tang, J. H. Chen, L. H. Nie, D. Y. Liu, W. Deng, Y. F. Kuang, S. Z. Yao. High dispersion and electrocatalytic properties of platinum nanoparticles on graphitic carbon nanofibers (GCNFs). J. Colloid Interface Sci. 269 (2004) 26-31.

[288] L. Cao, F. Scheiba, C. Roth, F. Schweiger, C. Cremers, U. Stimming, H. Fuess, L. Q. Chen, W. T. Zhu, X. P. Qiu. Novel nanocomposite Pt/RuO2 center dot xH(2)O/carbon nanotube catalysts for direct methanol fuel cells. Angew. Chem. Int. Ed. 45 (2006) 5315-5319.

[289] J. Luo, L. Wang, D. Mott, P. N. Njoki, Y. Lin, T. He, Z. Xu, B. N. Wanjana, I. I. S. Lim, C. J. Zhong. Core/Shell Nanoparticles as Electrocatalysts for Fuel Cell Reactions. Adv. Mater. 20 (2008) 4342-4347.

[290] M. S. Saha, R. Y. Li, X. L. Sun. Composite of Pt-Ru supported SnO2 nanowires grown on carbon paper for electrocatalytic oxidation of methanol. Electrochem. Commun. 9 (2007) 2229-2234.

[291] Z. H. Wen, J. Liu, J. H. Li. Core/shell Pt/C nanoparticles embedded in mesoporous carbon as a methanol-tolerant cathode catalyst in direct methanol fuel cells. Adv. Mater. 20 (2008) 743.

[292] E. Peled, T. Duvdevani, A. Aharon, A. Melman. New fuels as alternatives to methanol for direct oxidation fuel cells. Electrochem. Solid-State Lett. 4 (2001) A38-A41.

[293] G. K. S. Prakash. Low crossover membrane for liquid feed direct oxidation methanol fuel cells. Abstracts of Papers of the American Chemical Society 226 (2003) U524-U524.

[294] E. Vilar, R. A. Dougal. Study of pulsed-current loading of direct methanol fuel cells using a new time-domain model based on bi-functional methanol oxidation kinetics. J. Power Sources 169 (2007) 276-287.

[295] W. M. Wang, D. Zheng, C. Du, Z. Q. Zou, X. G. Zhang, B. J. Xia, H. Yang, D. L. Akins. Carbon-supported Pd-Co bimetallic nanoparticles as electrocatalysts for the oxygen reduction reaction. J. Power Sources 167 (2007) 243-249.

[296] X. W. Li, Y. Zhu, Z. Q. Zou, M. Y. Zhao, Z. L. Li, Q. Zhou, D. L. Akins, H. Yang. Simple Complexing-Reduction Synthesis of Pd-Pt/C Alloy Electrocatalysts for the Oxygen Reduction Reaction. J. Electrochem. Soc. 156 (2009) B1107-B1111.

[297] T. Lopes, E. Antolini, E. R. Gonzalez. Carbon supported Pt-Pd alloy as an ethanol tolerant oxygen reduction electrocatalyst for direct ethanol fuel cells. Int. J. Hydrogen Energy 33 (2008) 5563-5570.

[298] D. Morales-Acosta, L. G. Arriaga, L. Alvarez-Contreras, S. F. Luna, F. J. R. Varela.

Evaluation of Pt40Pd60/MWCNT electrocatalyst as ethylene glycol-tolerant oxygen reduction cathodes. Electrochem. Commun. 11 (2009) 1414-1417.

[299] O. Outiki, E. Lamypitara, J. Barbier. Platinum-Palladium Catalysts for Fuel-Cell Oxygen Electrodes. React. Kinet. Catal. Lett. 23 (1983) 213-220.

[300] W. M. Wang, Q. H. Huang, J. Y. Liu, Z. Q. Zou, Z. L. Li, H. Yang. One-step synthesis of carbon-supported Pd-Pt alloy electrocatalysts for methanol tolerant oxygen reduction. Electrochem. Commun. 10 (2008) 1396-1399.

[301] L. H. Jiang, A. Hsu, D. Chu, R. R. Chen. Oxygen reduction on carbon supported Pt and PtRu catalysts in alkaline solutions. J. Electroanal. Chem. 629 (2009) 87-93.

[302] A. S. Arico, P. Creti, N. Giordano, V. Antonucci, P. L. Antonucci, A. Chuvilin. Chemical and morphological characterization of a direct methanol fuel cell based on a quaternary Pt-Ru-Sn-W/C anode. J. Appl Electrochem 26 (1996) 959-967.

[303] C. Kim, K. S. Yang. Electrochemical properties of carbon nanofiber web as an electrode for supercapacitor prepared by electrospinning. Appl. Phys. Lett. 83 (2003) 1216-1218.

[304] A. Guha. Platinum/carbon nanofiber electrodes for polymer electrolyte membrane (PEM) fuel cells. Abstracts of Papers of the American Chemical Society 228 (2004) U462-U462.

[305] E. Wallnofer, M. Perchthaler, V. Hacker, G. Squadrito. Optimisation of carbon nanofiber based electrodes for polymer electrolyte membrane fuel cells prepared by a sedimentation method. J. Power Sources 188 (2009) 192-198.

[306] Z. Lin, L. W. Ji, X. W. Zhang. Electrodeposition of platinum nanoparticles onto carbon nanofibers for electrocatalytic oxidation of methanol. Mater. Lett. 63 (2009) 2115-2118.

[307] I. Becerik, S. Suzer, F. Kadirgan. Platinum-palladium loaded polypyrrole film electrodes for the electrooxidation of D-glucose in neutral media. J. Electroanal. Chem. 476 (1999) 171-176.

[308] E. Budevski, G. Staikov, W. J. Lorenz, *Electrochemical Phase Formation and Growth*, 1996.